UNIVERSIDADE DE LISBOA

INSTITUTO SUPERIOR TÉCNICO

Strategies to integrate and intensify the manufacturing of biological products

Diogo Filipe Frazão Ferreira Faria

Supervisor: Doctor Ana Margarida Nunes da Mata Pires de Azevedo

Co-supervisor: Doctor Maria Raquel Murias dos Santos Aires Barros

Thesis approved in public session to obtain the PhD degree in

Biotechnology and Biosciences

Jury final classification: Pass with Distinction

2024

UNIVERSIDADE DE LISBOA

INSTITUTO SUPERIOR TÉCNICO

Strategies to integrate and intensify the manufacturing of biological products

Diogo Filipe Frazão Ferreira Faria

Supervisor: Doctor Ana Margarida Nunes da Mata Pires de Azevedo

Co-supervisor: Doctor Maria Raquel Murias dos Santos Aires Barros

Thesis approved in public session to obtain the PhD degree in Biotechnology and Biosciences

Jury final classification: Pass with Distinction

Jury:

Chairperson: Doctor Arsénio do Carmo Sales Mendes Fialho, Instituto Superior Técnico, Universidade de Lisboa

Members of the Committe:

Doctor Ana Margarida Nunes da Mata Pires de Azevedo, Instituto Superior Técnico, Universidade de Lisboa

Doctor Ana Cristina Mendes Dias Cabral, Faculdade de Ciências, Unversidade da Beira Interior

Doctor Maria Ângela Cabral Garcia Taipa Meneses de Oliveira, Instituto Superior Técnico, Universidade de Lisboa

Doctor António Manuel Azevedo Ferreira, Faculdade de Engenharia, Universidade do Porto

Doctor Ana Rita da Silva Santos, Instituto Superior Técnico, Universidade de Lisboa

Funding Institution: Fundação para a Ciência e Tecnologia

2024

RESUMO

A indústria biotecnológica tem baseado a sua produção em processos descontínuos, normalmente associados a baixas produtividades. Neste sentido, uma mudança para um processamento contínuo irá permitir a intensificação de processo, trazendo fortes vantagens.

Extração com duas fases aquosas e precipitação são processos de baixo custo que têm sido estudados em modo descontínuo, carecendo de uma alternativa eficiente para processamento contínuo. O reator de fluxo oscilatório (RFO) é um tipo de reator tubular que tem sido usado em vários processos da industria química. Uma das características mais importantes deste tipo de reator é a mistura uniforme que é proporcionada pela combinação de restrições periodicamente espaçadas e pelo movimento oscilatório do fluido, tornando-o a resposta para um processo com custo mais competitivo. Neste trabalho, a partição de uma enzima industrial comercial – α-amilase – em diferentes sistemas polietilenoglicol (PEG)/fosfato foi estudada em modo descontínuo, e as composições que apresentavam maior rendimento de partição para a fase superior foram transferidas para este reator, onde diferentes condições de frequência e amplitude de oscilação e fluxo de massa total foram avaliadas. Este reactor foi igualmente usado na precipitação de anticorpos com PEG/$ZnCl_2$ a partir de uma mistura artificial com soro fetal bovino, mimetizando o sobrenadante de células produtoras de anticorpos. A precipitação foi primeiro otimizada em descontínuo e posteriormente implementada no reator em operação contínua

Com a expansão do mercado biofarmacêutico, torna-se necessário melhorar os processos que levam a produtos de alta pureza. Para a obtenção da imunoglobulina A secretora (sIgA), foram construídos dois processos de cromatografia de afinidade, utilizando duas resinas cromatográficas diferentes, com vista ao desenvolvimento de um processo de purificação eficiente para este biofármaco inovador, a partir dum sobrenadante clarificado de células de ovário de hamster Chinês.

Palavras-chave: Processamento a jusante; Extração em duas fases aquosas; Precipitação; Reator de fluxo oscilatório; Cromatografia

ABSTRACT

The biotechnology industry has been based on batch processing, which is normally associated with low productivities, but moving to continuous processing enables process intensification and brings strong advantages.

Aqueous two-phase extraction and precipitation are low-cost unit operations that have been widely studied in batchwise mode, but they lack an efficient alternative for continuous processing. An oscillatory flow reactor (OFR) is a tubular reactor that has been used in multiple chemical engineering processes. One of the most important features of this reactor is the uniform mixing that is provided by the combination of periodically spaced restrictions and the oscillatory motion of the fluid, making it the answer for a more cost-competitive process. In this work, the partition of a commercial industrial enzyme – α-amylase – in different polyethylene glycol (PEG)/phosphate systems was studied in batch, and the compositions presenting the highest yield of partition to the top phase were transferred to this reactor, where different conditions for frequency and amplitude of oscillation, and total mass flow were evaluated. It was performed PEG/zinc chloride ($ZnCl_2$) precipitation of antibodies from an artificial mixture with fetal bovine serum, mimicking the supernatant of antibody-producing cells. PEG/$ZnCl_2$ precipitation was first optimized in batch and further implemented in the reactor under continuous operation, where the influence of mixing intensity was investigated.

With the expansion of the biopharmaceuticals market, it is important to improve the processes that lead to high purity products. To obtain secretory immunoglobulin A (sIgA), two affinity chromatography processes, using Capture Select IgA and Capture Select IgA-CH1 resins, were built to verify if it would be possible to develop an efficient purification of this innovative biopharmaceutical from clarified Chinese hamster ovary cells supernatant.

Keywords: Downstream processing; Aqueous two-phase extraction; Precipitation; Oscillatory flow reactor; Chromatography

ACKNOWLEDGMENTS

O meu primeiro agradecimento vai para a Professora Ana Azevedo e para a Professora Raquel Aires Barros por todo o apoio ao longo do projecto, todas as reuniões de discussões de resultados, todos os encontros no laboratório para discutir a melhor forma de levar a bom porto as minhas experiências. Também agradecer por me terem agarrado a este projecto quando eu estava mais desmotivado e pronto a desistir.

I would also like to thank to Professor Alois Jungbauer for welcoming in Vienna in his group, and a special thanks to all its members, the ones that helped me to perform my work – Narges, Tomas, Nico and David – and specially to the last two that also assisted me in the hard times in the cold capital city of Austria, being always available for some fun.

Gostaria também de agradecer ao António Ferreira. Ele é a mente brilhante por trás da ideia de usar o reactor de fluxo oscilatório no meu trabalho. Recebeu-me no seu laboratório, ensinou-me tudo o que havia a saber para trabalhar autonomamente com esse equipamento e esteve sempre presente, quer para arranjá-lo quando foi preciso, quer para discutir resultados e delinear algumas estratégias.

Queria também agradecer ao programa BIOTECnico, na pessoa da Professora Isabel Sá Correia, por me ter aceitado no programa e ter dado oportunidade de navegar neste desafio que foi o doutoramento. Um obrigado também ao Professor Miguel Prazeres que foi membro da minha Comissão de Acompanhamento de Tese e por ter demonstrado sempre abertura para discutir a ciência por trás de tudo isto.

Gostaria também de agradecer ao iBB por me ter recebido ao longo de 4 anos e 3 meses e a todos os que se cruzaram comigo: André, Rita, as duas Sara Rosa, Maria João, Jorge, Ricardo, Cristana, Alexandra, Miguel, Cláudia, Mafalda e Filipa. Vocês foram sempre o conforto daquela experiência falhada e ponto de lucidez em dias em que o azar parecia não ter fim.

Queria agrecer à Mariana, ao Rui, ao Tiago e ao José. Este grupo de 4 pessoas, maioritariamente via internet, foi muito importante nos desabafos sobre a vida de cientista mas, a dada altura,

sobre a vida fora do país natal, longe da família, que me fez muitas vezes levantar a cabeça em vez de a baixar.

Gostaria também agradecer aos meus amigos que me ajudaram a passar pelos bons e os maus momentos que um doutoramento nos proporciona. Primeiramente, um muito obrigado ao Ricardo Carvalho, ao Cláudio Pedroso, ao Gonçalo Gonçalves e ao Miguel Runa por terem estado sempre lá quando era preciso e me terem feito rir quando eu mais precisava. Um grande obrigado também ao João Machado, João Santos, João Passos, Gonçalo Santos, Cláudio Runa, João Eusébio e Cláudio Costa que também tiveram um papel importante.

Um agradecimento especial também aos amigos que ganhei na faculdade: Sofia, Miguel e Catarina. Aquelas tardes de piscina e os jantares (mais esporádicos do que deviam) eram um verdadeiro bálsamo para a minha saúde mental.

Queria também agradecer à minha família. Ao meu pai e à minha mãe que são os responsáveis por tudo isto, sempre a apoiar o filho para que ele pudesse continuar a estudar. Um obrigado à minha irmã que também sempre foi uma fonte de apoio incondicional.

Um agradecimento especial à família que entretanto foi adicionada à minha vida. Obrigado às minhas sobrinhas, Margarida e Matilde, os seus sorrisos foram sempre capazes de alegrar mais o dia, e também aos seus pais, João e Catarina, que estiveram lá sempre para tudo.

Finalmente, um agradecimento à mais importante. Um obrigado não é suficiente para expressar o que devo à Inês. Apoiou-me sempre neste percurso, mesmo quando me levou a estar durante 10 meses a mais de 2000 km de distância. Esteve sempre lá para os momentos de vitórias, mas também nos momentos de derrota. Esta tese também é tua.

SCOPE AND OUTLINE

This thesis was developed in the framework of BIOTECnico PhD program at Institute for Bioengineering and Biosciences in Instituto Superior Técnico (Lisbon, Portugal), and at Professor Alois Jungbauer's laboratory in Department of Biotechnology, Institute of Bioprocess Science and Engineering, University of Natural Resources and Life Sciences (Vienna, Austria). During the entire work, there was also a collaboration with the Laboratory for Process Engineering, Environment, Biotechnology and Energy (LEPABE) and the Associate Laboratory in Chemical Engineering (ALiCE) from the Faculty of Engineering (Porto, Portugal).

The goals of this project were i) to develop two continuous processes – aqueous two-phase extraction (ATPE) and precipitation – for the purification of two different biomolecules – industrial enzymes and human antibodies, respectively – using an oscillatory flow reactor (OFR), and ii) to build an affinity chromatography process able to purify an innovative biopharmaceutical – secretory immunoglobulin A (sIgA) – from a clarified CHO cell supernatant.

Chapter 1 presents a general introduction on two main topics. Firstly, it focuses the advantages of shifting the operation mode from batch to continuous, and how simple operations as aqueous two-phase extraction and precipitation can be useful in continuous downstream, despite of lacking an efficient process for both, and how OFR can solve this breach. Secondly, it is presented how chromatography is still very important in the purification of biopharmaceuticals and how the process can be designed using distinctive tools as computational models.

The following three chapters present the research work carried out during this thesis. Chapter 2 presents the development of a proof of concept of a process of continuous ATPE using an OFR. For that purpose, the partition of a commercial enzyme – α-amylase from *Aspergillus oryzae* – in different polyethylene glycol (PEG)/phosphate systems was studied in batch. The compositions presenting the highest yield of partition to the top phase were transferred to the oscillatory flow plate reactor with 2D smooth periodic constrictions, and the continuous ATPE was further optimized regarding the operating conditions of the reactor (flow rate, oscillation frequency and amplitude). In the end, a fully continuous ATPE process (with continuous separation of the

phases) of the pure enzyme was evaluated, as well as a process of extraction of the α-amylase from a *S. cerevisiae* cellular broth.

Chapter 3 shows the construction of a process for the continuous precipitation of proteins with an OFR using human serum antibody as model protein. To do so, the effect of different precipitants was studied in batch, namely PEG and zinc chloride ($ZnCl_2$), which have already been reported in antibody precipitation, and sodium chloride (NaCl) which has been described to precipitate proteins by salting-out. Using the optimal condition determined in batch, continuous precipitation was implemented in the oscillatory flow and further optimized regarding the operating conditions of the reactor (flow rate, oscillation frequency and amplitude).

Chapter 4 exploits the possibility of developing a purification platform for recombinant secretory immunoglobulin A (sIgA) from a Chinese hamster ovarian (CHO) cells supernatants, using two different affinity chromatography resins – Capture IgA and Capture IgA-CH1. To further optimize this process, the breakthrough during loading was fitted with a model to characterize diffusional behavior. The hydrodynamic size and isoelectric point of purified sIgA were determined, as well as the pore size of the used resins. An economic feasibility analysis was carried out and compared to a protein A purification process for immunoglobulin G (IgG). Lastly, a macroporous resin structure is proposed and simulated to show the potential improvement in productivity.

Finally, Chapter 5 presents the final remarks of this thesis, summing the conclusions and raising possible future challenges.

LIST OF ABBREVIATIONS

% v/v	Percentage volume on volume
% w/v	Percentage weight on volume
% w/w	Percentage weight on weight
2D	Two-dimensional
ANOVA	Analysis of variance
ATPE	Aqueous two-phase extraction
ATPS	Aqueous two-phase system
BBD	Box-Behnken design
BCA	Bicinchoninic acid
BGG	Bovine gamma globulin
BSA	Bovine serum albumin
BTC	Breakthrough curves
c	Concentration (Chapter 3)
c	Pore fluid concentration (Chapter 4)
C	External bulk fluid concentration
CCD	Central Composite Design
CD	Circular dichroism
CDR	Complementary-determining regions
CHO	Chinese hamster ovary
$\mathbf{C_{out}}$	Concentration at the outlet of the column
CPC	Centrifugal partition chromatography
CQA	Critical Quality Attribute
CSA	Capture Select IgA
CSH	Capture Select IgA-CH1
CSTR	Continuous stirred tank reactor

CTR	Continuous tubular reactor
CV	Column volumes
d	Diameter of the constriction
d_l	Path length
D	Diameter of the tube
D_0	Diffusivity in the mobile phase
DAD	Diode array detector
$DBC_{10\%}$	Dynamic binding capacity at 10% breakthrough
De	Effective pore diffusivity
DIgA	Dimeric Immunoglobulin A
D_L	bed or total porosity
DLS	Dynamic Light Scattering
DNA	Deoxyribonucleic Acid
DNS	3,5-Dinitrosalicylic acid
DoE	Desing of Experiments
D_p	Pore diffusion coefficient
Ds	Solid diffusion coefficient
DTT	Dithiothreitol
EBC	Equilibrium binding capacity
ELISA	Enzyme-Linked Immunosorbent Assay
f	Oscillation frequency
FBS	Fetal bovine serum
F_m	Total mass flow rate
HC	Heavy chain
HCP	Host cell proteins
HIC	Hydrophobic interaction chromatography
IEC	Ion-exchange chromatography

IgA	Immunoglobulin A
IgG	Immunoglobulin G
IL	Ionic liquid
iSEC	Inverse size exclusion chromatography
JC	Connection chain
k_B	Boltzmann constant
K_D	Distribution coefficient
K_p	Hindrance parameter for pore diffusion (Chapter 4)
K_p	Partition Coefficient (Chapter 2)
L	Length of the column
L/u	Residence time
LC	Light chain
mAb	Monoclonal antibody
mIgA	Monomeric immunoglobulin A
MMC	Mixed-mode chromatography
MRE	Mean residue ellipticity
MRW	Mean residue weight
MW	Molecular Weight
n_{pore}	Number of transfer units for the pore diffusion
n_{film}	Number of transfer units for the solid diffusion
OFR	Oscillatory flow reactor
OV	Maximum oscillatory velocity
PAT	Process analytical technology
pDNA	Plasmidic DNA
PEG	Polyethylene glycol
pI	Isoelectric point
Pr	Productivity

ProA	Protein A
Q	Total net flow rate
q_m	Maximum binding capacity
Re_n	Net flow Reynolds number
Re_o	Oscillatory Reynolds number
R_g	Radius of gyration
R_h	Hydrodynamic radius
RI	Refractive index
r_m	Radius of the injected molecule
RO	Reverse osmosis
r_p	Radius of the beads
RPC	Reversed phase chromatography
RU	Resin utilization
SC	Secretory component
SDS-PAGE	Sodium dodecyl sulfate-polyacrylamide gel electrophoresis
SEC	Size exclusion chromatography
sIgA	Secretory immunoglobulin A
SPC	Smooth periodic constrictions
SSF	Solid-state fermentation
St	Strouhal number
T	Absolute temperature
t	process time
TEMED	N,N,N',N'tetramethylethylenediamine
TFF	Tangential flow filtration
TLL	Tie-line length
$t_{load10\%}$	Required time to reach 10% breakthrough
t_{rest}	Combination of all process time intervals (except loading)

Tris-HCl	Tris(hydroxymethyl)aminomethane – hydrochloric acid
U	Enzyme activity unit
u	Net flow velocity
UPLC	Ultra Performance Liquid Chromatography
V	Volume between constrictions
$\mathbf{V_0}$	Void volume
$\mathbf{V_c}$	Column volume
$\mathbf{V_R}$	Retention volume of a molecule migrating through the column (Chapter 4)
$\mathbf{V_R}$	Volume Ratio (Chapter 2)
$\mathbf{x_0}$	Oscillation amplitude
$\mathbf{Y_{top}}$	Yield of the partition to the top phase
z	Axial bed length coordinate
ε	Void fraction of a packed column
$\mathbf{\varepsilon_b}$	Bed or total porosity
$\mathbf{\varepsilon_p}$	Porosity of the particles
θ	Measured ellipticity
$\mathbf{\lambda_m}$	Ratio of the solute molecule radius to the pore radius
μ	Dynamic viscosity
$\mathbf{\mu_{bot}}$	Viscosity of the bottom phase
$\mathbf{\mu_s}$	Viscosity of the aqueous two-phase system
$\mathbf{\mu_{top}}$	Viscosity of the top phase
ρ	Fluid density
τ	Residence time (Chapters 2 and 3)
τ	Tortuosity factor for intraparticle diffusion (Chapter 4)
$\mathbf{\tau_1}$	Dimensionless time
Ψ	Velocity ratio

INDEX

Contents

Chapter 1 – Intensification of bioprocesses: a needed revolution

*Part of this chapter has been published as: Ferreira-Faria, D., Aires-Barros, M. R., & Azevedo, A. M. (2020). Continuous aqueous two-phase extraction: From microfluidics to integrated biomanufacturing. Fluid Phase Equilibria, 508, 112438.

1.1. Integrated Continuous Biomanufacturing

The biotechnology industry has been based on batch processing: each unit operation is done in sequence, with its outflow collected in a large container before moving to the next one [1]. This mode of operation facilitates the construction and the optimization of the single unit operations and eases off-line measurements of the product quality before the following processes [1]. However, batchwise biomanufacturing is normally associated with low productivities and does not reach the total potential of the reprogrammed cells generated by modern biotechnology [2].

A shift to continuous mode is normally an indicator of a maturing industry, as can be seen in multiple industries like cars, casting, chemicals, food, petrochemicals, etc. Moving to continuous processing enables the process intensification and brings some strong advantages: i) considerable reductions in capital costs and facility size; ii) significant increases in productivity (all equipment is used permanently); iii) greater flexibility (the facility is used more efficiently); iv) enhanced product quality due to higher uniformity in process time [1,3].

A common bioprocessing is divided into two main sections: upstream and downstream. While the former is the process from the cell isolation, cultivation and expansion until a final harvest, the latter describes the branch of the bioprocess where the cell mass from the downstream is processed until reaching desired purity and quality. The increasing interest for the shift from batch to continuous in biomanufacturing can be verified by the increase of publication with the topics “continuous upstream” and “continuous downstream”: in both cases, this number increased more than 7-fold since 1991 (Figure 1.1.). Additionally, there are several examples from the literature on biomanufacturing using hybrid systems – continuous upstream/batch downstream; batch upstream/continuous downstream; continuous upstream and capture/batch downstream.

All this progress has contributed to getting closer to the ultimate goal: the achievement of the fully integrated continuous process (Figure 1.2.)

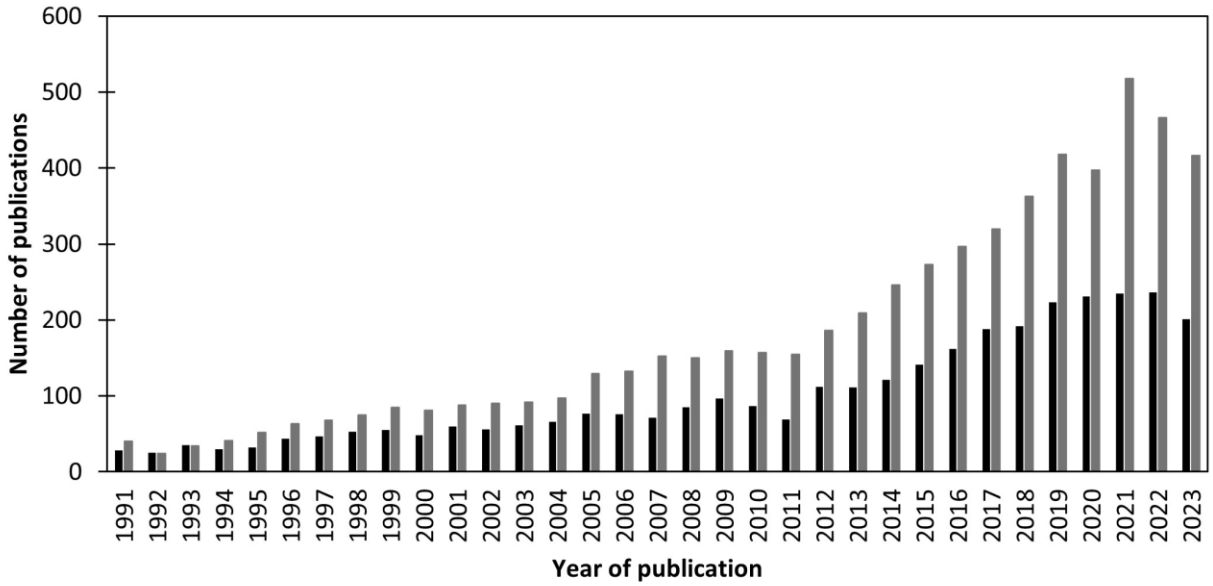

Figure 1.1. Published papers with the topic either "continuous upstream" (grey) or "continuous downstream" (black). Source: https:// www.webofscience.com.

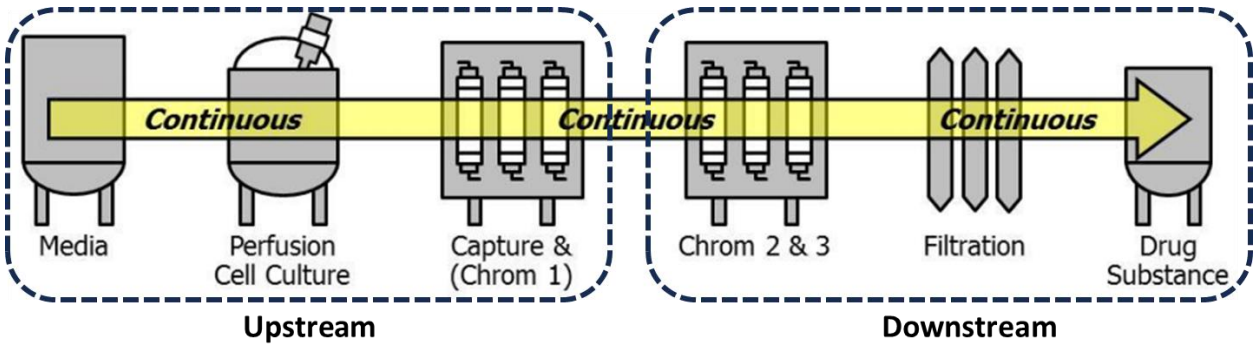

Figure 1.2. Schematic illustration of and end-to-end continuous bioprocessing. Adapted from [3].

1.1.2. Continuous Upstream

Since the 1950s, together with batch, fed-batch has also been used as standard design of upstream bioprocessing due to advantages as simple structure and design, easy scale-up and high flexibility for the production of different molecules [2]. However, there are two major drawbacks in using both modes: i) limited productivity due to high downtime between batches and inability of consistency in the overall production rate; ii) reduced ability in achieving the true conversion potential the organisms engineered by modern biotechnology [2].

In the past few years, continuous upstream has been extensively studied (Figure 1.1.), demonstrating that can increase productivity and reduce the capital investment and biomanufacturing cost. However, this mode of operation has its own challenges: i) contamination risk, due to the long process times (several weeks or months); ii) genetic instability, since the cellular evolution during the process can imply a higher cell growth, but a lower production of the biomolecule of interest, caused by plasmid loss or mutations: iii) lack of efficient tools for continuous upstream study; iv) disconnection between bioproduct formation and recovery, since the latter is not always designed to handle concentration and flow variations[2].

These challenges have been tackled using some strategies as contamination-risk control, enhancement of the genetic stability of the production strain, dissociation of the cell growth from the production of the biomolecule using multistage continuous fermentation and usage of mathematical models to accelerate the development of continuous upstream processes and, in the future, the application of artificial intelligence and machine learning can be answer for a more efficient design of the processes [2,4].

1.1.3. Continuous Downstream

Similarly with the case of the upstream, downstream process is based on batch operations, but, in the last 30 years, the interest in continuous downstream processing has been growing, which can be seen in the increasing number of publications about that topic (Figure 1.1.). As in the case presented in the case of the upstream, a continuous downstream processing presents numerous

Table 1.1. Examples of continuous operations in each stage of downstream processing.

Stage	Type of Operation	Examples	References
Clarification	Centrifugation	Disc centrifuge	[5]
	Filtration	Tangential Flow Filtration	[6]
		Alternating Tangential Flow Filtration	[6]
		Diafiltration	[7]
		Membrane Cascades	[8]
	Homogenization	High-pressure homogenizers	[9]
	Cell Lysis	Alkaline Lysis	[10]
		Thermal Lysis	[11]
Primary Capture	Chromatography	Periodic Counter-Current Chromatography	[12]
		Multicolumn Countercurrent Solvent Gradient Purification	[13]
		Continuous Countercurrent Tangential Chromatography	[14]
	Aqueous Two-Phase Extraction	Mixer-Settler	[15]
		Spray Column	[16]
		Perforated Rotating Disk Contactor	[17]
		Pulsed Cap Column	[18]
		Centrifugal Partition Chromatography	[19]
	Precipitation	Continuous Stirred Tank Reactor	[1]
		Continuous Tubular Reactor	[20]
Polishing	Chromatography	Flow-Through Chromatography	[21]
		Simulated Moving Bed	[22]
		Annular Chromatography	[23]
		Radial Flow Chromatography	[24]
	Crystallization	Continuous Tubular Reactor	[25]
	Filtration	High performance tangential flow filtration	[26]
Formulation	Filtration	Single-Pass Tangential Flow Filtration	[27]
		Cascade Diafiltration	[28]

advantages, comparing with the batch mode: i) reductions in the costs of equipment and facility size; ii) enhancement of the productivity (all equipment is used continuously): iii) increment in the flexibility of the process, since the facility is used in a more efficient way; iv) improvement in the quality of the product, due to higher uniformity during the bioprocess [1].

Downstream processing of biological can be divided into four main stages: i) clarification; ii) primary capture; iii) polishing and iv) formulation. Table 1.1. presents different types of operations for the different stages of the downstream.

On the one hand, filtration dominates clarification – separation of the cells and the product of interest – and formulation – final preparation of the drug to be consumed by the patients. On the other hand, chromatography is the most used method for primary capture and polishing – further purification of the product of interest. The latter happens for impactful advantages of chromatography: i) high removal of host cell proteins and DNA; ii) superior robustness to little variations in the characteristics of the feed and the product; iii) significant volume reduction; iv) in many cases, no previous adjustment in pH or salt concentration [1]. However, although multiple continuous methods have been created in the last years, chromatography is intrinsically a batch process (the column is loaded, washed and eluted in sequence), which presents an engineering problem, and, principally in the case of affinity chromatography, some resins are very expensive. In the last years, the evolution of the upstream (batch and continuous) allowed the achievement of high product titers enabling the use of non-chromatography methods, as aqueous two-phase extraction (ATPE) and precipitation, that are cheaper and more flexible to be integrated in a full continuous bioprocess [1].

1.1.4. Continuous Aqueous Two-Phase Extraction

Aqueous two-phase systems (ATPS) are spontaneously formed when two hydrophilic solutes are mixed above a critical concentration. These species can be two polymers (e.g. polyethylene glycol and dextran); a polymer and a kosmotropic salt (e.g. phosphate, sulphate, citrate); an alcohol (e.g. methanol, ethanol, 1-propanol) and a salt; a surfactant (e.g. Triton X-100) and a polymer/salt

to create micelles; and ionic liquids (IL) as the phase-forming component in the previous systems. ATPS have been used, since the early 1960s [29–31] in the separation and concentration of countless biological products, including cell constituents like plasma membranes [32–34] and extracellular vesicles [35,36] different types of cells, from erythrocytes [37–40] and leucocytes [41] to stem cells [42–44], and microorganisms [45]; viral particles [46–48] and bacteriophages [49]; proteins [50–57], nucleic acids [58–60] and low molecular weight compounds [61]. The wide range of usage for the recovery and purification of biological product arises from their numerous advantages: i) reaching the equilibrium very fast; ii) high biocompatibility since the majority of the system is water; iii) low cost; iv) recycling of phase forming components; v) easy to scale up and vi) prone to process integration. However, despite all these key strengths, few studies are using large scale ATPS [62–66] and even fewer industrial applications.

ATPS are typically studied at bench scale and in batch mode, which is easier to implement, validate and operate, reasons why the biotechnological industry is currently dominated by batchwise mode unit operations. However, a new era is approaching where decreasing buffer consumption, reducing process time, plant footprint and costs, and increasing process yields are mandatory. All these improvements can only be implemented through process integration and continuous manufacturing. Considering all the advantages already mentioned, ATPE can be successfully adapted to continuous mode, becoming a valuable tool in the biotechnological industry of the future.

The batch extraction processes can be divided into 5 main stages: i) preparation of the stocks and the sample; ii) mixing of the solutions; iii) phase separation; iv) recovery of the phase of interest and removal and/or recycling of the other; and in some cases, v) back or multi extraction. In the case of the continuous ATPE, stages ii) to v) must occur in the same place and, therefore, the device used must allow multiple entrances, promote the mixing and the settling of the two phases and, in the end, the exit of the phases.

Regarding the broad features of such devices, there is no specific equipment for continuous ATPE. Until today, the two most used are mixer-settlers and extraction columns (Figure 1.3.).

The mixer-settlers (Figure 1.3.-I) have been widely used for continuous ATPE, because of their easiness of assembling and the possibility of studying each stage of mixing, coalescence, and separation, individually. However, it is very difficult to achieve a fully hydrodynamic characterization of the system [15].

The most used types of devices in continuous ATPE are spray columns (Figure 1.3.-II), perforated rotating disk contactor (Figure 1.3.-III) and pulsed cap columns (Figure 1.3.-IV).

Spray columns (Figure 1.3.-II) have been widely used to study the continuous separation or purification of biological products, including the characterization of the partition of bovine serum albumin (BSA) in PEG/Reppal PES 100 [16], the measurement of mass transfer coefficients for amyloglucosidase and β-galactosidase in PEG 4000/sodium sulfate system [67], the separation of xylanase and BSA in PEG 4000/K_2HPO_4 systems [68], among others. In this type of equipment, one of the phases is the continuous phase and the other is the dispersed phase, which typically contains the biological product to be separated and is continuously dispersed by a spray nozzle into small droplets that rise (Figure 1.3.-II) or descend through the continuous phase [16,68].

The advantages of using spray columns arise from their simplicity of construction and low operation and maintenance costs, however, the major drawbacks of this type of columns are the higher time to reach steady-state compared to mixer-settlers – minutes [68] *versus* few seconds [69], respectively – and the axial dispersion or back-mixing. The latter occurs when the flow rate is above a critical value, not allowing the development of drops but the formation of a liquid jet, which diminishes the mass transfer [16,68].

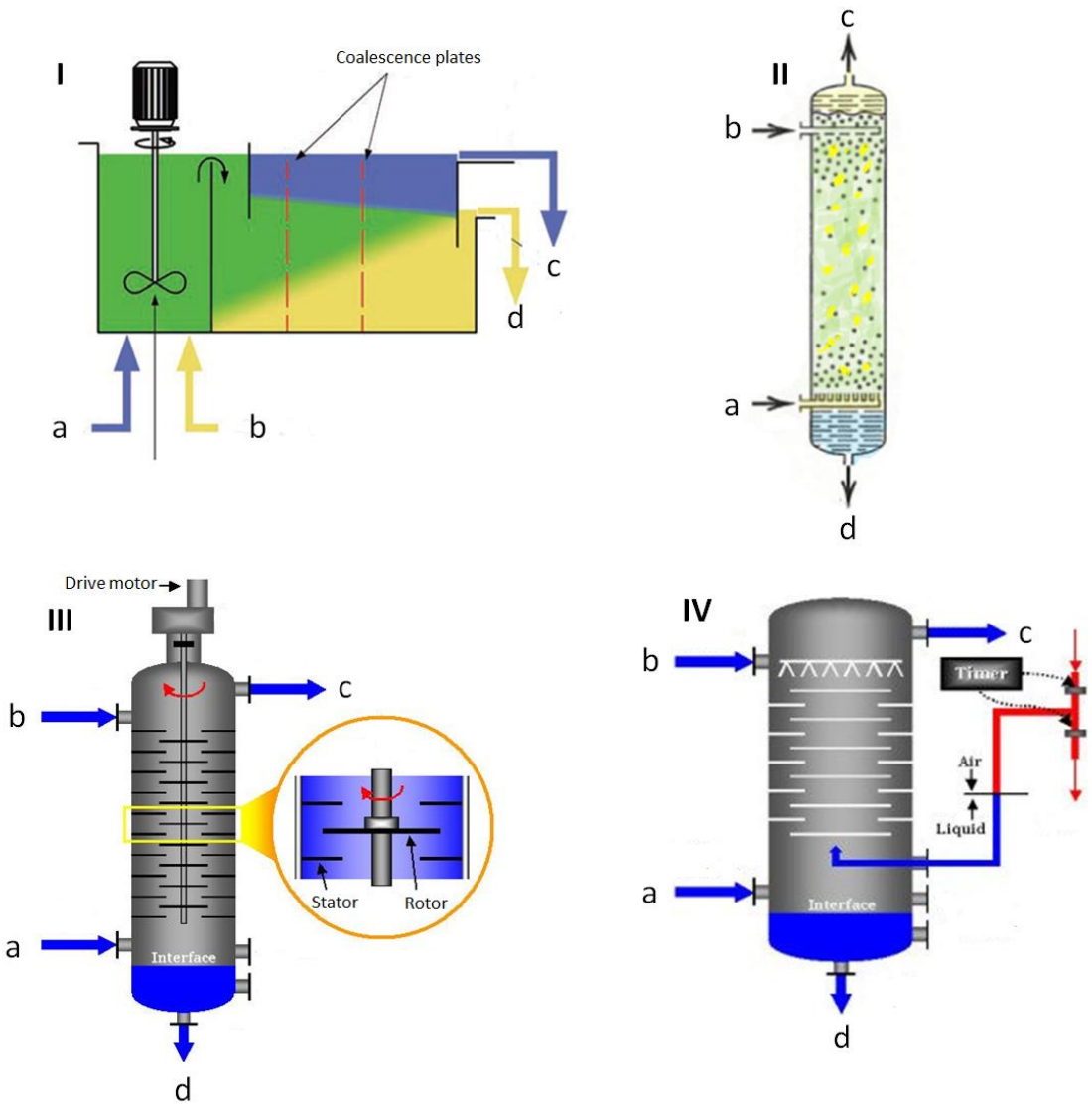

Figure 1.3. Main devices used in continuous ATPE: I – mixer-settler; II – spray column; III – perforated rotating disk contactor; IV – pulsed cap column; a – inlet of lighter component solution; b – inlet of heavier component solution; c – outlet of top phase; d – outlet of bottom phase.

The perforated rotating disk contactor (Figure 1.3.-III) is another type of column used for continuous extraction. It is composed of a cylindrical tube with spaced stators and perforated rotating disks [70]. The operational flexibility, high efficiency, and mass transfer rates make this

type of equipment very appropriate for continuous operation, as in the case of the ATPE of proteins such as cutinase [17], albumin [17,70] and trypsin [71]. The major drawback in this type of equipment is the occurrence of flooding, which happens when flow rates of both phases are higher than a certain value and the coalescence is not allowed and affects negatively the entire process since one of the phases is recovered together with the product of interest in the other phase [72]. Besides the flows of the different phases of the ATPS *per se*, the rotational speed of the disks can be the reason for the flooding phenomenon, however, the relation between both is not known [70,72].

Another type of column used is the pulsed columns (Figure 1.3.-IV), where the agitation is produced by the movement of the cap up and down, being an efficient and gentle way of producing mixing, diminishing the possibility of protein denaturation. Another strength of this type of device is that the caps increase the contact time between the phases and produce a uniform dispersion of drops inside the column, improving mass transfer [73]. Despite all these advantages, this type of equipment has not been presented as completely suitable for continuous ATPE. In Bim & Franco, 2000, the usage of pulsed column showed that xylanase from *Bacillus pumilus* had an equal partition in the top and bottom phases for the system 22% (w/w) PEG 6000 – 10% (w/w) K_2HPO_4 – 12% (w/w) NaCl, while in batch mode a partition coefficient of 46.9 was obtained [18]. Still, in Rabelo & Tambourgi, 2003, the percentages of recovery in the salt phase in the cases of cytochrome b5 and ascorbic oxidoreductase were similar in both batch and continuous mode [73].

Apart from these most well-known examples of operations, there is one more that must be appointed, given its applicability in continuous ATPE: centrifugal partition chromatography (CPC). In this technique, the rotation of the disks results in a strong centrifugal force that causes the decantation in each cell, retaining the liquid stationary phase against the flow of the liquid mobile phase (Figure 1.4.) [74]. The mobile phase can be pumped from cell to cell, flowing in the centrifugal direction if it is denser – descending mode – or in the centripetal direction whether it is less dense – ascending mode [74].

CPC has been used in continuous and semi-continuous ATPE for the purification of some biomolecules: Dellanay and co-workers, using a 12.5% (w/w) PEG 1000 – 12.5% (w/w) K_2HPO_4, were capable to achieve a good separation between lysozyme and myoglobin, despite the loss of stationary phase (top phase of the system) [75]; Oiemeier and co-workers demonstrated that CPC can be used to perform high throughput screening and the best system has shown an increase in host cell proteins (HCP) clearance in the purification of monoclonal antibodies (mAbs) from CHO cell culture, using numerous PEG-phosphate system [76]; the same group was able to recover 93% of the mAbs, reducing the HCP content by 99.4%, using precipitation with PEG 4000 after CPC with PEG – citrate systems [77].

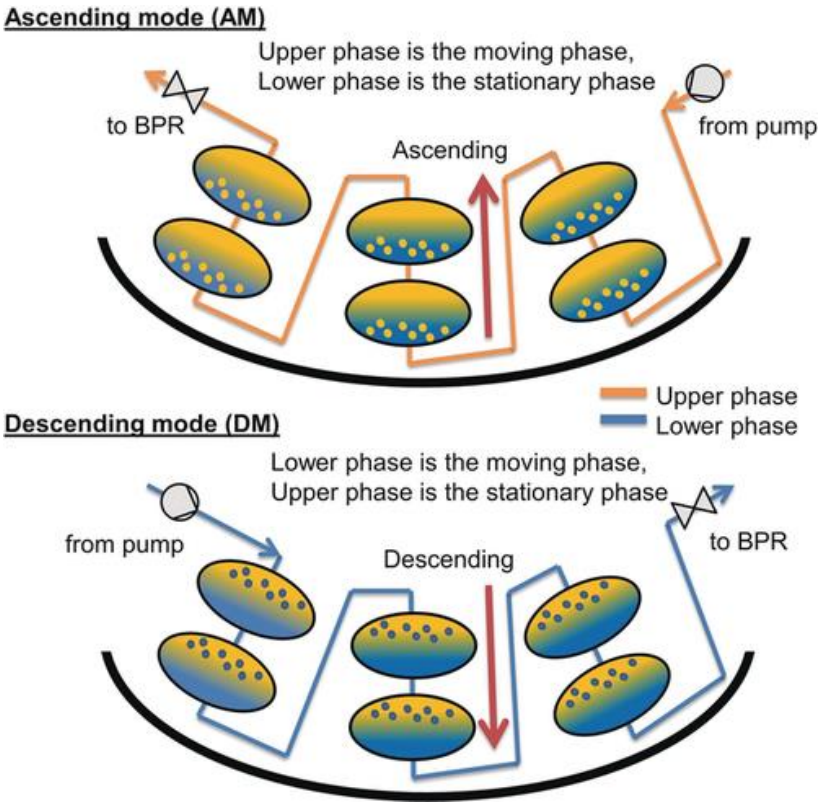

Figure 1.4. Working principle of ascending mode and descending mode CPC devices. Adapted from [19].

Although this technique can be applied successfully in ATPE, some processes were not done in full continuous mode, but in semi-continuous, with a constant inflow or outflow, but not both [54,56], which are a challenge to the integration of the processes.

1.1.5. Continuous Precipitation

Precipitation has been widely used in the last years in the purification of low value and blood fractionation products and, lately, it has been utilized for the downstream processing of some biopharmaceuticals, such as antibodies. Precipitation is an operation with impactful advantages: i) low cost; ii) high robustness; iii) characteristic high yield and purity of the product of interest; iv) easy scalability. These advantages, allied with increasing higher titers of bioproducts, make precipitation a good method for the downstream of biomolecules (and proteins, in particular) [20].

Precipitation consists of changing the state of the proteins from soluble to insoluble by disrupting the interaction between the protein surface and the solution molecules [79]. It is composed by three main steps: i) nucleation, where submicron-sized particles are formed after the addition of the precipitant agent; ii) growth, characterized by the increase of the particles dimension due to Brownian diffusion; iii) agglomeration, where collision between particles is responsible for a size increment until reaching a stable level [79].

That disruption can be induced by modifications in physical characteristics of the solution (temperature, for example) or, in the case of biomolecules (namely antibodies) the addition of precipitation agents as salts, organic solvents, non-ionic solvents or metal ions.

In the case of salt precipitation, it is achieved using high concentration of kosmotropic salts that will promote a mechanism called “salting-out”. The high number of ions will disturb the interaction between the hydrophilic regions of the protein and the molecules of water, leading to a loss of entropy, hence, to minimize this reduction, the protein aggregates and precipitates [80]. There are two predominant salts in protein precipitation: ammonium sulfate $(NH_4)_2SO_4$) and calcium chloride ($CaCl_2$). While in the former case, its high solubility allows to form a concentrated

solution that avoids proteolysis and bacterial and bacteria growth, in the latter, this salt is able to precipitate high molecular weight impurities: the ion Ca^{2+} interacts with the phosphate backbone of the DNA forming an insoluble calcium phosphate , co-precipitating high molecular weight proteins as well [81].

The precipitation with organic solvents occurs due to the addition of water-miscible solvent. The polar groups of this compound will interact with the polar groups of the protein, competing with the water, and its hydrophobic groups can disturb the interaction between the hydrophobic residues of the protein, both mechanisms will be responsible for the precipitation of the protein [82]. Ethanol is the most widely used organic solvent in downstream of biopharmaceuticals, for example, the fractionation of human plasma into functional protein as albumins and immunoglobulins is done using cold ethanol precipitation. Lately, this method has been combined with $CaCl_2$ precipitation for the precipitation of monoclonal antibodies, achieving high yields and purities. However, the low temperatures used to perform this method – to not denature the protein – increase the cost of the process.

In the case of precipitation using non-ionic solvents, the most widely used precipitant is polyethylene glycol (PEG). This type of precipitation can occur at room temperature, presents a fast kinetics and it has no denaturing effect on the proteins [83]. There are two theories for the mechanism responsible for the precipitation induced by PEG:

– Excluded volume theory: PEG molecules occupy the regions where the protein was in the solvent (steric exclusion) and the concentration of protein increases in the remaining volume, precipitating when the solubility limit is attained [84].

– Attractive depletion theory: PEG molecules are sterically excluded from the protein surface, creating a depletion zone. When two protein molecules get close to each other, their depletion zones overlap, creating an osmotic pressure that favors protein aggregation [85].

PEG-induced precipitation has as major disadvantages the low selectivity and the increment of the viscosity of the solution, which can cause problems in a possible membrane process after the precipitation, since decreases the flux, increasing the pressure [86].

Finaly, in the case of the precipitation using metal ions, zinc chloride ($ZnCl_2$) is the compound at hand. The Zn^{2+} forms relatively stable complexes with histidine and cysteine residues on the surface of the proteins, mainly antibodies, through imidazole and thiol groups, respectively [87]. The precipitation occurs not only because this binding to the exposed amino acids reduces the protein solubility by modifying its isoelectric point (pI) – pH of a solution at which the net charge of the protein is zero – but also because of the crosslink between the different complexes formed between the metal ions and the proteins [88,89].

Considering all the advantages already mentioned, precipitation can be successfully adapted to continuous mode, becoming a valuable tool in the biotechnological industry of the future.

In the recent years, continuous precipitation has been done using continuous stirred tank reactors (CSTR) or continuous tubular reactor (CTR) (Figure 1.5. A and B, respectively) [90].

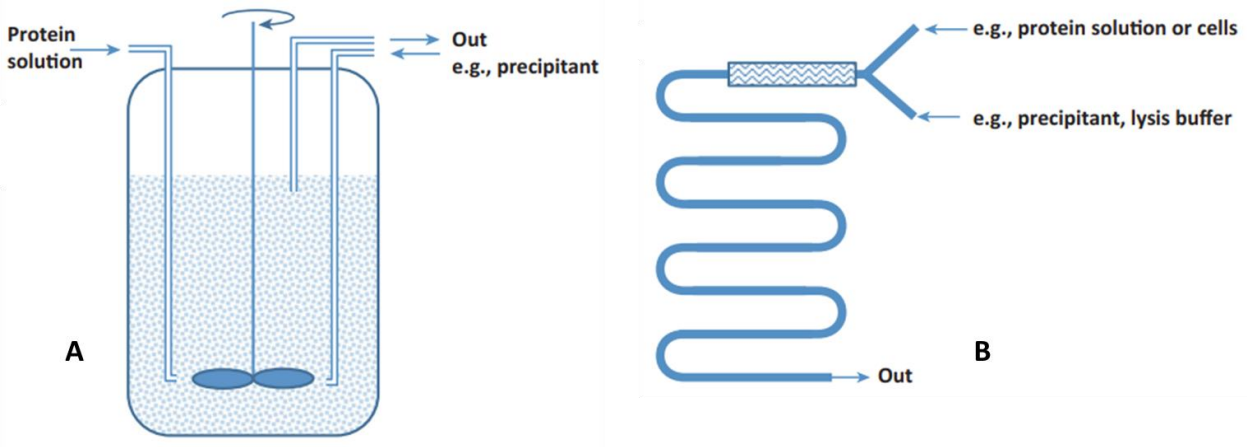

Figure 1.5. Schematic representation of (A) Continuous Stirred Tank Reactor (CSTR) and (B) Continuous Tubular Reactor (CTR) used for continuous precipitation. Adapted from [90].

In the CSTR, a stirred tank is continuously fed (feed and precipitant) and the output (precipitated protein) is withdrawn at the same rate [90]. In this type of reactor, the rate of precipitation can be monitored better than in a batch reactor, but at the industrial scale, CSTRs are often associated with problems regarding shear forces and low mixing efficiency [91], reason why they are more often used for research purposes [90].

In the CTR, the protein solution and the precipitant are mixed by a static mixer and precipitation occurs through the tube [90]. This type of reactor has as main advantage the simple design, very suitable for continuous operations, however, the high flow rates needed to produce stable flocks determines long CTR, since the reactor size is controlled by the time to reach the equilibrium, and, hence, higher working volumes [90].

1.1.6. Oscillatory flow reactor: one answer for continuous downstream?

Oscillatory flow reactor (OFR) (Figure 1.6.) is a type of tubular/channel reactor provided with periodic constrictions (or baffles) operating under oscillatory flow mixing [92]. The liquid or multiphase fluid is typically oscillated in the axial direction using diaphragms, bellows or piston, at one end or both ends of the tube, developing an efficient mixing mechanism where fluid moves from the walls to the centre of the tube (Figure 1.7.) with an intensity controlled by the oscillation frequency (f) and amplitude (x_0) [92].

a) b)

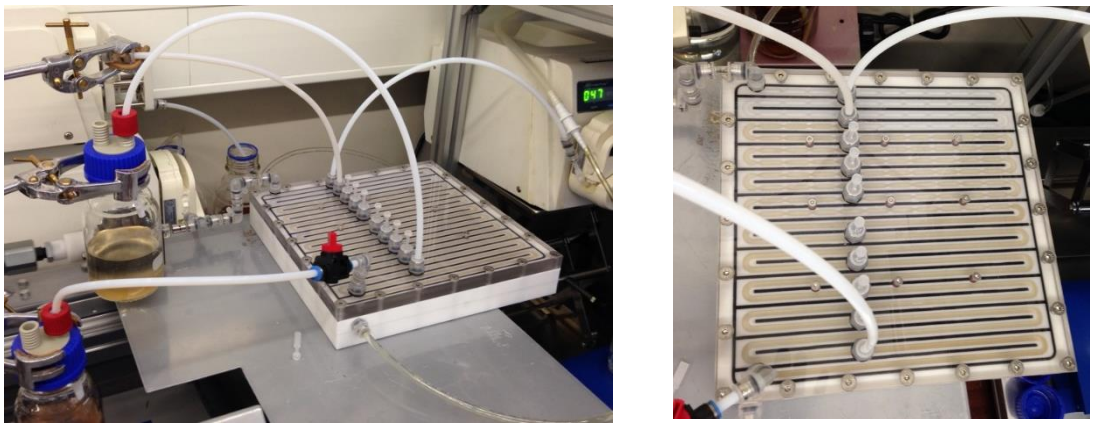

Figure 1.6. Continuous ATPE apparatus (a) and oscillatory flow reactor detail (b).

OFR has some general advantages comparing with a conventional tubular reactor. In a CTR, the mixing relies on high net velocity in order to achieve a high enough Reynolds number, resulting in excessive tube lengths, because of the long residence times [92]. In the OFR, the periodical oscillation makes the fluid interact with the restrictions, creating strong vortices (Figure 1.7.) and allowing lower net flow velocity, shorter tube lengths and, hence, lower working volumes. Additionally, it is possible to operate under plug-flow conditions, which means that the residence time is the same in all the fluid inside the reactor [92]. Other advantages of this type of reactor are enhanced heat and mass transfer capabilities, linear scalability, minimal concentration gradients and easy implementation of process analytical technology (PAT) [92].

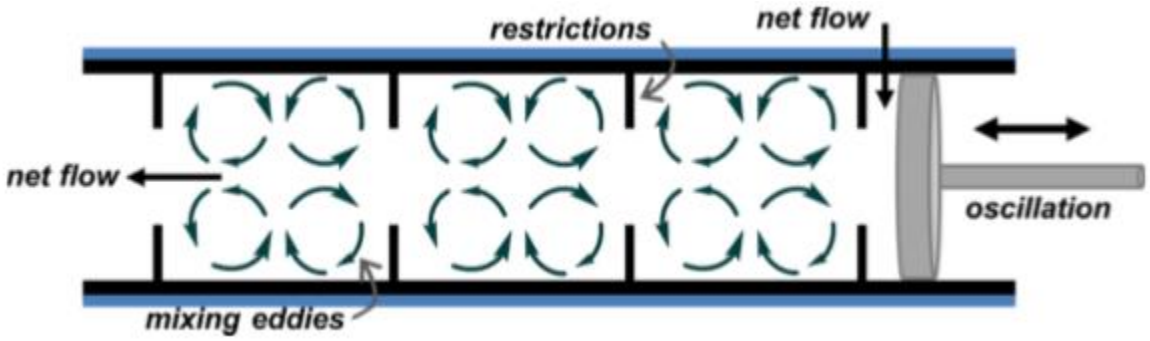

Figure 1.7. Scheme of the fluid mixing interaction with the spaced restrictions in the OFR. The circular arrows represent idealized fluid flow conditions. Adapted from McGlone *et al*., [92].

Regarding all these advantages, OFR has been used in multiple processes and it has been proved to be efficient in heat [93] and mass transfer [94], liquid-liquid reaction [95], polymerization [96,97], flocculation [98] and crystallization [99,100]. This type of equipment has not been often used for continuous ATPE, but there is one example in the literature where this reactor was used for the extraction of glucose-6-phosphate dehydrogenase, using aqueous two-phase micellar system [101], that highlights the suitable characteristics of this equipment for ATPE. OFR was also used in the precipitation, both in batch and in continuous mode, of the hydroxyapatite [102,103], exhibiting also the appropriateness for this type of purification process.

OFR apparatus used in continuous ATPE has two regions (Chapter 2, Figure 2.1.): one with restrictions and another without them. In the first region, the mixing of the different solutions takes place, due to the oscillatory effect explained previously; in the second, the settling – separation of the phases – occurs. This apparatus presents some advantages when compared with the type of reactors used for continuous ATPE (mixer-settlers and columns): separation of mixing and settling process in two different regions avoid bottlenecks present in columns, as flooding and emulsification; the additional inlets and outlets contribute to versatility of the reactor, that cannot be found in the mixer-settlers and columns; the plug flow conditions are well-established and the hydrodynamic characterization of the system is well-known; the oscillatory flow allows lower net flow velocity and, hence, lower working volumes and less time to reach steady state. With all these advantages, OFR can be the answer for an efficient continuous ATPE.

OFR apparatus used in continuous precipitation has the same two regions (Chapter 3, Figure 3.1.), but the one without restrictions is much smaller, since in this case, there is no need of a region for separation of the phases.

1.2. Novel Biopharmaceuticals

With the improvement in our understanding of the diversity and complexity of human diseases, there is an expansion of the nature of the biopharmaceutical drug candidates to be commercialized [104]. These novel biopharmaceuticals need high purity levels and, despite the increasing attention in nonchromatographic techniques and some engineering problems in building fully continuous chromatographic processes, packed-bed chromatography is still the dominant technique for (batch) biopharmaceutical purification due to its high separation efficiencies, that allows high yield processes and high purity products [104,105].

1.2.1. Optimization for chromatography of biopharmaceuticals

There are a various types of chromatography based on the principle of separation: i) size exclusion chromatography (SEC) operates based on differences in molecular sizes; ii) ion exchange chromatography (IEC) performs the separation based on differences in the charges; iii) hydrophobic interaction chromatography (HIC) and reversed-phase chromatography (RPC) exploits the differences in the surface hydrophobicity and iv) mixed-mode chromatography (MMC) uses combinations of all these differences [105].

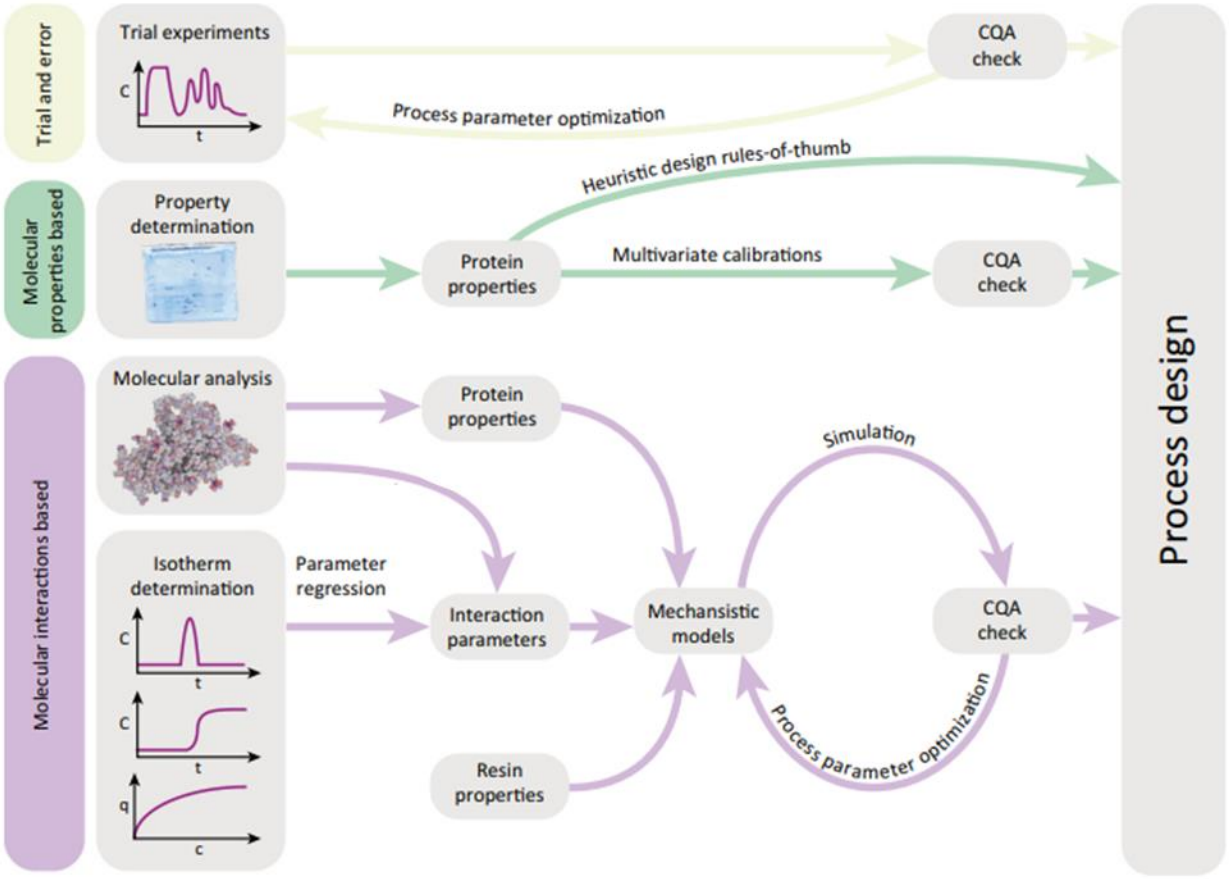

Figure 1.8. Schematic representation of the different process-development approaches that can be applied for chromatography of biopharmaceuticals. Adapted from [105].

After knowing the principle of separation and, hence, the type of chromatography to use, there are three ways to build the process design (Figure 1.8.).

The first one is more rudimentary: using a trial-and-error approach until the critical quality attributes (CQAs) are met. This approach is quite obsolete because it can imply and large number of experiments, since it is a univariate analysis [105].

A second alternative is the molecular properties-based approach, which includes a first stage of determination of the protein properties, that can easily be determined using simple analytical methods without knowing the structure or the sequence of the protein [105]. In this case, there are two ways to achieve a process design: i) using heuristic design rules-of-thumb can produce a process focused on the best separation coefficients, which can lead to suboptimal process efficiency, due to lack of investigation [106]; ii) using a multivariate calibration based in the physical properties of the protein (molecular weight, pI and/or hydrophobicity) against data from other proteins, however, when the protein in question is very different from the calibration dataset the results are not great [107].

In recent years, a molecular interactions-based approach with the utilization of the mechanistic models appeared. These models are constructed with protein properties, but in this case, they are not acquired using only analytical methods, but also utilizing computational tools that can predict the protein structure using a large set of model proteins already known [105]. But, as name of this approach indicates, the mechanistic models are not fed only with information about the protein to be purified but also about the resin used in the chromatographic process and interaction between the two, that is achieved both by the structural information of the protein and the binding behavior, the latter can be easily achieved by running isotherm procedures [108]. The most known model is the general rate model, being too complicated because it considers dedicated parameters for all mass-transfer effects. On the contrary, pore or surface diffusion models are simpler because they only take into account the interactions inside the pores of the chromatographic matrix or along the its surface, respectively [105]. One disadvantage of using this approach is the high complexity that makes the models too complicated to solve. However, the development of quantum computing and artificial intelligence will be able to increase the ability of these models to design chromatography processes for all the innovative products that will be discovered.

1.3. References

[1] A.L. Zydney, Continuous downstream processing for high value biological products: a review, Biotechnol. Bioeng. 113 (2016) 465–475. doi:https://doi.org/10.1002/bit.25695.

[2] D. Xie, Continuous biomanufacturing with microbes—upstream progresses and challenges, Curr. Opin. Biotechnol. 78 (2022) 102793. doi:https://doi.org/10.1016/j.copbio.2022.102793.

[3] K.B. Konstantinov, C.L. Cooney, White paper on continuous bioprocessing May 20–21 2014 continuous manufacturing symposium, J. Pharm. Sci. 104 (2015) 813–820. doi:https://doi.org/10.1002/jps.24268.

[4] C.L. Gargalo, I. Udugama, K. Pontius, P.C. Lopez, R.F. Nielsen, A. Hasanzadeh, S.S. Mansouri, C. Bayer, H. Junicke, K. V Gernaey, Towards smart biomanufacturing: a perspective on recent developments in industrial measurement and monitoring technologies for bio-based production processes, J. Ind. Microbiol. Biotechnol. Off. J. Soc. Ind. Microbiol. Biotechnol. 47 (2020) 947–964. doi:https://doi.org/10.1007/s10295-020-02308-1.

[5] A.I. Clarkson, P. Lefevre, N.J. Titchener-Hooker, A study of process interactions between cell disruption and debris clarification stages in the recovery of yeast intracellular products, Biotechnol. Prog. 9 (1993) 462–467. doi:https://doi.org/10.1021/bp00023a004.

[6] M. Clincke, C. Mölleryd, P.K. Samani, E. Lindskog, E. Fäldt, K. Walsh, V. Chotteau, Very high density of Chinese hamster ovary cells in perfusion by alternating tangential flow or tangential flow filtration in WAVE bioreactor™—part II: Applications for antibody production and cryopreservation, Biotechnol. Prog. 29 (2013) 768–777. doi:https://doi.org/10.1002/btpr.1703.

[7] W.-S. Kim, I. Hirasawa, W.-S. Kim, Aging characteristics of protein precipitates produced by polyelectrolyte precipitation in turbulently agitated reactor, Chem. Eng. Sci. 57 (2002) 4077–4085. doi:https://doi.org/10.1016/S0009-2509(02)00319-6.

[8] E.Y. Chi, B.S. Kendrick, J.F. Carpenter, T.W. Randolph, Population balance modeling of aggregation kinetics of recombinant human interleukin-1 receptor antagonist, J. Pharm. Sci. 94 (2005) 2735–2748. doi:https://doi.org/10.1002/jps.20488.

[9] G.C. Barazzone, R. Carvalho Jr, S. Kraschowetz, A.L. Horta, C.R. Sargo, A.J. Silva, T.C. Zangirolami, C. Goulart, L.C.C. Leite, M.M. Tanizaki, Production and purification of recombinant fragment of pneumococcal surface protein A (PspA) in Escherichia coli, Procedia Vaccinol. 4 (2011) 27–35. doi:https://doi.org/10.1016/j.provac.2011.07.005.

[10] H. Chunsheng, Z. Qinglin, L. Yuxin, C. Xiaochen, W. Yanliang, Z. Tong, W. Zuze, A continuous cell alkaline lysis, neutralization, and clarification combination process for production of plasmid pUDK-HGF, Biotechnol. Appl. Biochem. 58 (2011) 162–165. doi:https://doi.org/10.1002/bab.23.

[11] K. Zhu, H. Jin, Z. He, Q. Zhu, B. Wang, A continuous method for the large-scale extraction of plasmid DNA by modified boiling lysis, Nat. Protoc. 1 (2006) 3088–3093. doi:https://doi.org/10.1038/nprot.2006.452.

[12] V. Warikoo, R. Godawat, K. Brower, S. Jain, D. Cummings, E. Simons, T. Johnson, J. Walther, M. Yu, B. Wright, Integrated continuous production of recombinant therapeutic proteins, Biotechnol. Bioeng. 109 (2012) 3018–3029. doi:https://doi.org/10.1002/bit.24584.

[13] L. Aumann, M. Morbidelli, A continuous multicolumn countercurrent solvent gradient purification (MCSGP) process, Biotechnol. Bioeng. 98 (2007) 1043–1055. doi:https://doi.org/10.1002/bit.21527.

[14] B. Napadensky, O. Shinkazh, A. Teella, A.L. Zydney, Continuous countercurrent tangential chromatography for monoclonal antibody purification, Sep. Sci. Technol. 48 (2013) 1289–1297. doi:https://doi.org/10.1080/01496395.2013.767837.

[15] S.L. Mistry, A. Kaul, J.C. Merchuk, J.A. Asenjo, Mathematical modelling and computer simulation of aqueous two-phase continuous protein extraction, J. Chromatogr. A. 741 (1996) 151–163. doi:https://doi.org/10.1016/0021-9673(96)00179-3.

[16] A. Venâncio, J.A. Teixeira, Protein mass transfer studies on a spray column using the PEG-Reppal PES 100 aqueous two-phase system, Bioprocess Eng. 13 (1995) 251–255. doi:https://doi.org/10.1007/BF00417636.

[17] A.L.F. Porto, L.A. Sarubbo, J.L. Lima-Filho, M.R. Aires-Barros, J.M.S. Cabral, E.B. Tambourgi, Hydrodynamics and mass transfer in aqueous two-phase protein extraction using a continuous perforated rotating disc contactor, Bioprocess Eng. 22 (2000) 215–218. doi:10.1007/s004490050722.

[18] M.A. Bim, T.T. Franco, Extraction in aqueous two-phase systems of alkaline xylanase produced by Bacillus pumilus and its application in kraft pulp bleaching, J. Chromatogr. B Biomed. Sci. Appl. 743 (2000) 349–356. doi:10.1016/S0378-4347(00)00223-1.

[19] R. Örkényi, J. Éles, F. Faigl, P. Vincze, A. Prechl, Z. Szakács, J. Kóti, I. Greiner, Continuous synthesis and purification by coupling a multistep flow reaction with centrifugal partition chromatography, Angew. Chemie Int. Ed. 56 (2017) 8742–8745.

[20] N. Hammerschmidt, B. Hintersteiner, N. Lingg, A. Jungbauer, Continuous precipitation of IgG from CHO cell culture supernatant in a tubular reactor, Biotechnol. J. 10 (2015) 1196–1205. doi:https://doi.org/10.1002/biot.201400608.

[21] J. Weaver, S.M. Husson, L. Murphy, S.R. Wickramasinghe, Anion exchange membrane adsorbers for flow-through polishing steps: part II. Virus, host cell protein, DNA clearance, and antibody recovery, Biotechnol. Bioeng. 110 (2013) 500–510. doi:https://doi.org/10.1002/bit.24724.

[22] A. Rajendran, G. Paredes, M. Mazzotti, Simulated moving bed chromatography for the separation of enantiomers, J. Chromatogr. A. 1216 (2009) 709–738. doi:https://doi.org/10.1016/j.chroma.2008.10.075.

[23] A. Uretschläger, A. Jungbauer, Preparative continuous annular chromatography (P-CAC), a review, Bioprocess Biosyst. Eng. 25 (2002) 129–140. doi:https://doi.org/10.1007/s00449-002-0282-0.

[24] P. Ghosh, K. Vahedipour, M. Lin, J.H. Vogel, C.A. Haynes, E. von Lieres, Zonal rate model for axial and radial flow membrane chromatography. Part I: Knowledge transfer across operating conditions and scales, Biotechnol. Bioeng. 110 (2013) 1129–1141. doi:https://doi.org/10.1002/bit.24771.

[25] A.J. Alvarez, A.S. Myerson, Continuous plug flow crystallization of pharmaceutical compounds, Cryst. Growth Des. 10 (2010) 2219–2228. doi:https://doi.org/10.1021/cg901496s.

[26] K. Ruanjaikaen, A.L. Zydney, Purification of singly PEGylated α-lactalbumin using charged ultrafiltration membranes, Biotechnol. Bioeng. 108 (2011) 822–829. doi:https://doi.org/10.1002/bit.22991.

[27] J. Dizon-Maspat, J. Bourret, A. D'Agostini, F. Li, Single pass tangential flow filtration to debottleneck downstream processing for therapeutic antibody production, Biotechnol. Bioeng. 109 (2012) 962–970. doi:https://doi.org/10.1002/bit.24377.

[28] L. Peeva, J. da Silva Burgal, I. Valtcheva, A.G. Livingston, Continuous purification of active pharmaceutical ingredients using multistage organic solvent nanofiltration membrane cascade, Chem. Eng. Sci. 116 (2014) 183–194. doi:https://doi.org/10.1016/j.ces.2014.04.022.

[29] S. Bengtsson, L. Philipson, P.-Å. Albertsson, Counter-current distribution of polio virus, Biochem. Biophys. Res. Commun. 9 (1962) 318–322. doi:10.1016/0006-291X(62)90047-5.

[30] P.Å. Albertsson, Fractionation of particles and macromolecules in aqueous two-phase systems, Biochem. Pharmacol. 5 (1961) 351–358. doi:10.1016/0006-2952(61)90028-4.

[31] T. Lif, Separation of ribonucleic acid components in aqueous polymer two-phase systems, Biochim. Biophys. Acta - Spec. Sect. Nucleic Acids Relat. Subj. 68 (1963) 1–8. doi:10.1016/0926-6550(63)90400-6.

[32] P. Navas, D. David Nowack, D. James Morré, Isolation of purified plasma membranes from cultured cells and hepatomas by two-phase partition and preparative free-flow electrophoresis, Cancer Res. 49 (1989) 2147–2156.

[33] D.M. Morré, D.J. Morre, Aqueous two-phase partition applied to the isolation of plasma membranes and Golgi apparatus from cultured mammalian cells, J. Chromatogr. B Biomed. Sci. Appl. 743 (2000) 377–387. doi:https://doi.org/10.1016/S0378-4347(00)00058-X.

[34] H. Everberg, R. Peterson, S. Rak, P. Tjerneld, C. Emanuelsson, Aqueous two-phase partitioning for proteomic monitoring of cell surface biomarkers in human peripheral blood mononuclear cells, J. Proteome Res. 5 (2006) 1168–1175. doi:https://doi.org/10.1021/pr050469z.

[35] J. Kim, H. Shin, J. Kim, J. Kim, J. Park, Isolation of high-purity extracellular vesicles by extracting proteins using aqueous two-phase system, PLoS One. 10 (2015). doi:https://doi.org/10.1371/journal.pone.0129760.

[36] H. Shin, C. Han, J.M. Labuz, J. Kim, J. Kim, S. Cho, Y.S. Gho, S. Takayama, J. Park, High-yield isolation of extracellular vesicles using aqueous two-phase system, Sci. Rep. 5 (2015). doi:https://doi.org/10.1038/srep13103.

[37] J.M. Van Alstine, D.E. Brooks, Cell membrane abnormality detected in erythrocytes from patients with multiple sclerosis by partition in two-polymer aqueous-phase systems., Clin. Chem. 30 (1984) 441–443. doi:https://doi.org/10.1093/clinchem/30.3.441.

[38] K.A. Sharp, M. Yalpani, S.J. Howard, D.E. Brooks, Synthesis and application of a poly(ethylene glycol)-antibody affinity ligand for cell separations in aqueous polymer two-phase systems, Anal. Biochem. 154 (1986) 110–117. doi:https://doi.org/10.1016/0003-2697(86)90503-8.

[39] P. Jimeno, A.I. Garcia-Perez, J. Luque, M. Pinilla, Changes in glycolytic enzyme activities in aging erythrocytes fractionated by counter-current distribution in aqueous polymer two-phase systems, Biochem. J. 279 (1991) 237–243. doi:https://doi.org/10.1042/bj2790237.

[40] M. Tsukamoto, S. Taira, S. Yamamura, Y. Morita, N. Nagatani, Y. Takamura, E. Tamiya, Cell separation by an aqueous two-phase system in a microfluidic device, Analyst. 134 (2009) 1994–1998. doi:https://doi.org/10.1039/B909597G.

[41] J.R. SooHoo, G.M. Walker, Microfluidic aqueous two phase system for leukocyte concentration from whole blood, Biomed. Microdevices. 11 (2009) 323–329. doi:https://doi.org/10.1007/s10544-008-9238-8.

[42] M. González-González, M. Rito-Palomares, Application of affinity aqueous two-phase systems for the fractionation of CD133+ stem cells from human umbilical cord blood, J. Mol. Recognit. 28 (2015) 142–147. doi:10.1002/jmr.2374.

[43] A.F. Sousa, P.Z. Andrade, R.M. Pirzgalska, T.M. Galhoz, A.M. Azevedo, C.L. da Silva, M. Raquel Aires-Barros, J.M.S. Cabral, A novel method for human hematopoietic stem/progenitor cell isolation from umbilical cord blood based on immunoaffinity aqueous two-phase partitioning, Biotechnol. Lett. 33 (2011) 2373–2377. doi:https://doi.org/10.1007/s10529-011-0727-0.

[44] E. Atefi, R. Joshi, J.A. Mann, H. Tavana, Interfacial Tension Effect on Cell Partition in Aqueous Two-Phase Systems, ACS Appl. Mater. Interfaces. 7 (2015) 21305–21314. doi:https://doi.org/10.1021/acsami.5b05757.

[45] H. Umakoshi, R. Kuboi, I. Komasawa, Control of partitioning of bacterial cells and characterization of their surface properties in aqueous two-phase systems, J. Ferment. Bioeng. 84 (1997) 572–578. doi:https://doi.org/10.1016/S0922-338X(97)81914-9.

[46] M.J. Jacinto, R.R.G. Soares, A.M. Azevedo, V. Chu, A. Tover, J.P. Conde, M.R. Aires-Barros, Optimization and miniaturization of aqueous two phase systems for the purification of recombinant human immunodeficiency virus-like particles from a CHO cell supernatant, Sep. Purif. Technol. 154 (2015) 27–35. doi:https://doi.org/10.1016/j.seppur.2015.09.006.

[47] C.L. Effio, L. Wenger, O. Ötes, S.A. Oelmeier, R. Kneusel, J. Hubbuch, Downstream processing of virus-like particles: Single-stage and multi-stage aqueous two-phase extraction, J. Chromatogr. A. 1383 (2015) 35–46. doi:https://doi.org/10.1016/j.chroma.2015.01.007.

[48] K.S. Vijayaragavan, A. Zahid, J.W. Young, C.L. Heldt, Separation of porcine parvovirus from bovine serum albumin using PEG-salt aqueous two-phase system, J. Chromatogr. B Anal. Technol. Biomed. Life Sci. 967 (2014) 118–126. doi:https://doi.org/10.1016/j.jchromb.2014.07.025.

[49] E. Espitia-Saloma, P. Vázquez-Villegas, O. Aguilar, M. Rito-Palomares, Continuous aqueous two-phase systems devices for the recovery of biological products, Food Bioprod. Process. 92 (2014) 101–112. doi:https://doi.org/10.1016/j.fbp.2013.05.006.

[50] P. Vázquez-Villegas, E. Espitia-Saloma, M. Rito-Palomares, O. Aguilar, Low-abundant protein extraction from complex protein sample using a novel continuous aqueous two-phase systems device, J. Sep. Sci. 36 (2013) 391–399. doi:10.1002/jssc.201200584.

[51] B. Bertrand, K. Mayolo-Deloisa, M. González-González, R. Tinoco-Valencia, L. Serrano-Carreón, F. Martínez-Morales, M.R. Trejo-Hernández, M. Rito-Palomares, Pleurotus ostreatus laccase recovery from residual compost using aqueous two-phase systems, J. Chem. Technol. Biotechnol. 91 (2016) 2235–2242. doi:https://doi.org/10.1002/jctb.4995.

[52] M.V. Rocha, M. Di Giacomo, S. Beltramino, W. Loh, D. Romanini, B.B. Nerli, A sustainable affinity partitioning process to recover papain from Carica papaya latex using alginate as macro-ligand, Sep. Purif. Technol. 168 (2016) 168–176. doi:https://doi.org/10.1016/j.seppur.2016.05.025.

[53] P.A.J. Rosa, A.M. Azevedo, I.F. Ferreira, J. de Vries, R. Korporaal, H.J. Verhoef, T.J. Visser, M.R. Aires-Barros, Affinity partitioning of human antibodies in aqueous two-phase systems, J. Chromatogr. A. 1162 (2007) 103–113. doi:https://doi.org/10.1016/j.chroma.2007.03.067.

[54] K.V.G. Barros, P.M. Souza, M.M. Freitas, E.X.F. Filho, A.P. Junior, P.O. Magalhães, PEG/NaPA aqueous two-phase systems for the purification of proteases expressed by Penicillium restrictum

from Brazilian Savanna, Process Biochem. 49 (2014) 2305–2312. doi:10.1016/J.PROCBIO.2014.09.022.

[55] A.S. Schmidt, A.M. Ventom, J.A. Asenjo, Partitioning and purification of α-amylase in aqueous two-phase systems, Enzyme Microb. Technol. 16 (1994) 131–142. doi:https://doi.org/10.1016/0141-0229(94)90076-0.

[56] J.A. Asenjo, R.E. Turner, S.L. Mistry, A. Kaul, Separation and purification of recombinant proteins from Escherichia coli with aqueous two-phase systems, J Chromatogr A. 668 (1994) 129–137. doi:https://doi.org/10.1016/0021-9673(94)80101-0.

[57] B.A. Andrews, S. Nielsen, J.A. Asenjo, Partitioning and purification of monoclonal antibodies in aqueous two-phase systems, Bioseparation. 6 (1996) 303–313. http://europepmc.org/abstract/MED/9210350.

[58] F. Luechau, T.C. Ling, A. Lyddiatt, Partition of plasmid DNA in polymer-salt aqueous two-phase systems, Sep. Purif. Technol. 66 (2009) 397–404. doi:https://doi.org/10.1016/j.seppur.2008.12.003.

[59] H. Barbosa, A. V. Hine, S. Brocchini, N.K.H. Slater, J.C. Marcos, Affinity partitioning of plasmid DNA with a zinc finger protein, J. Chromatogr. A. 1206 (2008) 105–112. doi:https://doi.org/10.1016/j.chroma.2008.07.095.

[60] S.P. Duarte, A.G. Fortes, D.M.F. Prazeres, J.C. Marcos, Preparation of plasmid DNA polyplexes from alkaline lysates by a two-step aqueous two-phase extraction process, J. Chromatogr. A. 1164 (2007) 105–112. doi:https://doi.org/10.1016/j.chroma.2007.06.061.

[61] M.G. Freire, C.M.S.S. Neves, I.M. Marrucho, J.N. Canongia Lopes, L.P.N. Rebelo, J.A.P. Coutinho, High-performance extraction of alkaloids using aqueous two-phase systems with ionic liquids, Green Chem. 12 (2010) 1715–1718. doi:https://doi.org/10.1039/C0GC00179A.

[62] W. Hummel, H. Schütte, M.R. Kula, Large scale production of d-lactate dehydrogenase for the stereospecific reduction of pyruvate and phenylpyruvate, Eur. J. Appl. Microbiol. Biotechnol. 18 (1983) 75–85. doi:https://doi.org/10.1007/BF00500828.

[63] K.H. Kroner, H. Schütte, W. Stach, M. Kula, Scale-up of formate dehydrogenase by partition, J. Chem. Technol. Biotechnol. 32 (1982) 130–137.

[64] K.H. Kroner, H. Hustedt, M. -R Kula, Evaluation of crude dextran as phase-forming polymer for the extraction of enzymes in aqueous two-phase systems in large scale, Biotechnol. Bioeng. 24 (1982) 1015–1045. doi:https://doi.org/10.1002/bit.260240502.

[65] T. Minuth, H. Gieren, U. Pape, H.C. Raths, J. Thömmes, M.R. Kula, Pilot scale processing of detergent-based aqueous two-phase systems, Biotechnol. Bioeng. 55 (1997) 339–347. doi:https://doi.org/10.1002/(SICI)1097-0290(19970720)55:2<339::AID-BIT11>3.0.CO;2-C.

[66] C. Kepka, E. Collet, J. Persson, Å. Ståhl, T. Lagerstedt, F. Tjerneld, A. Veide, Pilot-scale extraction of an intracellular recombinant cutinase from E. coli cell homogenate using a thermoseparating aqueous two-phase system, J. Biotechnol. 103 (2003) 165–181. doi:https://doi.org/10.1016/S0168-1656(03)00104-4.

[67] P.A. Pawar, K.R. Jafarabad, S.B. Sawant, J.B. Joshi, Enzyme mass transfer coefficient in aqueous two phase systems: Spray extraction columns, Chem. Eng. Commun. 122 (1993) 151–169. doi:10.1080/00986449308936154.

[68] L. Igarashi, T.G. Kieckbusch, T.T. Franco, Xylanase mass transfer studies in aqueous two-phase systems using spray and sieve plate columns, Bioprocess Biosyst. Eng. 26 (2004) 151–157. doi:https://doi.org/10.1007/s00449-003-0329-x.

[69] A. Veide, T. Lindbäck, S.O. Enfors, Continuous extraction of β-d-galactosidase from Escherichia coli in an aqueous two-phase system: effects of biomass concentration on partitioning and mass transfer, Enzyme Microb. Technol. 6 (1984) 325–330. doi:10.1016/0141-0229(84)90062-0.

[70] L.A. Sarubbo, L.A. Oliveira, A.L.F. Porto, J.L. Lima-Filho, G.M. Campos-takaki, E.B. Tambourgi, Performance of a perforated rotating disc contactor in the continuous extraction of a protein using the PEG-cashew-nut tree gum aqueous two-phase system, Biochem. Eng. J. 16 (2003) 221–227. doi:10.1016/S1369-703X(03)00023-8.

[71] L.A. Oliveira, L.A. Sarubbo, A.L.F. Porto, G.M. Campos-Takaki, E.B. Tambourgi, Partition of trypsin in aqueous two-phase systems of poly(ethylene glycol) and cashew-nut tree gum, Process Biochem. 38 (2002) 693–699. doi:10.1016/S0032-9592(02)00191-7.

[72] M.T.H. Cavalcanti, M.G. Carneiro-da-Cunha, I. V. Brandi, T.S. Porto, A. Converti, J.L. Lima Filho, A.L.F. Porto, A. Pessoa, Continuous extraction of α-toxin from a fermented broth of Clostridium perfringens Type A in perforated rotating disc contactor using aqueous two-phase PEG-phosphate system, Chem. Eng. Process. Process Intensif. 47 (2008) 1771–1776. doi:https://doi.org/10.1016/j.cep.2007.09.018.

[73] A.P.B. Rabelo, E.B. Tambourgi, Performance of a pulsed-cap microcolumn for protein extraction, Brazilian J. Chem. Eng. 20 (2003) 357–362. doi:10.1590/S0104-66322003000400003.

[74] M. Bojczuk, D. Żyżelewicz, P. Hodurek, Centrifugal partition chromatography–A review of recent applications and some classic references, J. Sep. Sci. 40 (2017) 1597–1609.

[75] E. Delannay, A. Toribio, L. Boudesocque, J.-M. Nuzillard, M. Zeches-Hanrot, E. Dardennes, G. Le Dour, J. Sapi, J.-H. Renault, Multiple dual-mode centrifugal partition chromatography, a semi-continuous development mode for routine laboratory-scale purifications, J. Chromatogr. A. 1127 (2006) 45–51.

[76] S.A. Oelmeier, C.L. Effio, J. Hubbuch, High throughput screening based selection of phases for aqueous two-phase system-centrifugal partitioning chromatography of monoclonal antibodies, J. Chromatogr. A. 1252 (2012) 104–114.

[77] S.A. Oelmeier, C. Ladd-Effio, J. Hubbuch, Alternative separation steps for monoclonal antibody purification: Combination of centrifugal partitioning chromatography and precipitation, J. Chromatogr. A. 1319 (2013) 118–126.

[78] Y. Shibusawa, N. Takeuchi, K. Sugawara, A. Yanagida, H. Shindo, Y. Ito, Aqueous–aqueous two-phase systems composed of low molecular weight of polyethylene glycols and dextrans for counter-current chromatographic purification of proteins, J. Chromatogr. B. 844 (2006) 217–222.

[79] P. Ciborowski, J. Silberring, Proteomic profiling and analytical chemistry: the crossroads, Elsevier, 2016.

[80] A.M. Hyde, S.L. Zultanski, J.H. Waldman, Y.-L. Zhong, M. Shevlin, F. Peng, General principles and strategies for salting-out informed by the Hofmeister series, Org. Process Res. Dev. 21 (2017) 1355–1370. doi:https://doi.org/10.1021/acs.oprd.7b00197.

[81] R. Sommer, P. Satzer, A. Tscheliessnig, H. Schulz, B. Helk, A. Jungbauer, Combined polyethylene glycol and CaCl2 precipitation for the capture and purification of recombinant antibodies, Process Biochem. 49 (2014) 2001–2009. doi:https://doi.org/10.1016/j.procbio.2014.07.012.

[82] S. Englard, S. Seifter, [22] Precipitation techniques, in: Methods Enzymol., Elsevier, 1990: pp. 285–300. doi:https://doi.org/10.1016/0076-6879(90)82024-V.

[83] A. Tardieu, F. Bonneté, S. Finet, D. Vivares, Understanding salt or PEG induced attractive interactions to crystallize biological macromolecules, Acta Crystallogr. Sect. D Biol. Crystallogr. 58 (2002) 1549–1553. doi:https://doi.org/10.1107/S0907444902014439.

[84] D.H. Atha, K.C. Ingham, Mechanism of precipitation of proteins by polyethylene glycols. Analysis in terms of excluded volume., J. Biol. Chem. 256 (1981) 12108–12117. doi:https://doi.org/10.1016/S0021-9258(18)43240-1.

[85] D. Marenduzzo, K. Finan, P.R. Cook, The depletion attraction: an underappreciated force driving cellular organization, J. Cell Biol. 175 (2006) 681. doi:https://doi.org/10.1083/jcb.200609066.

[86] N. Singh, A. Arunkumar, S. Chollangi, Z.G. Tan, M. Borys, Z.J. Li, Clarification technologies for monoclonal antibody manufacturing processes: Current state and future perspectives, Biotechnol. Bioeng. 113 (2016) 698–716. doi:https://doi.org/10.1002/bit.25810.

[87] T. Yang, J.L. Cleland, X. Lam, J.D. Meyer, L.S. Jones, T.W. Randolph, M.C. Manning, J.F. Carpenter, Effect of zinc binding and precipitation on structures of recombinant human growth

hormone and nerve growth factor, J. Pharm. Sci. 89 (2000) 1480–1485. doi:https://doi.org/10.1002/1520-6017(200011)89:11<1480::AID-JPS10>3.0.CO;2-M.

[88] C. Polson, P. Sarkar, B. Incledon, V. Raguvaran, R. Grant, Optimization of protein precipitation based upon effectiveness of protein removal and ionization effect in liquid chromatography–tandem mass spectrometry, J. Chromatogr. B. 785 (2003) 263–275. doi:https://doi.org/10.1016/S1570-0232(02)00914-5.

[89] H. V Iyer, T.M. Przybycien, A model for metal affinity protein precipitation, J. Colloid Interface Sci. 177 (1996) 391–400. doi:https://doi.org/10.1006/jcis.1996.0049.

[90] A. Jungbauer, Continuous downstream processing of biopharmaceuticals, Trends Biotechnol. 31 (2013) 479–492. doi:https://doi.org/10.1016/j.tibtech.2013.05.011.

[91] G.L. Foutch, A.H. Johannes, Reactors in process engineering, Encycl. Phys. Sci. Technol. (2003) 652–654. doi:https://doi.org/10.1016/B0-12-227410-5/00654-2.

[92] T. McGlone, N.E.B. Briggs, C.A. Clark, C.J. Brown, J. Sefcik, A.J. Florence, Oscillatory flow reactors (OFRs) for continuous manufacturing and crystallization, Org. Process Res. Dev. 19 (2015) 1186–1202. doi:https://doi.org/10.1021/acs.oprd.5b00225.

[93] M.R. Mackley, P. Stonestreet, Heat transfer and associated energy dissipation for oscillatory flow in baffled tubes, Chem. Eng. Sci. 50 (1995) 2211–2224. doi:https://doi.org/10.1016/0009-2509(95)00088-M.

[94] A. Ferreira, J.A. Teixeira, F. Rocha, O2 mass transfer in an oscillatory flow reactor provided with smooth periodic constrictions. Individual characterization of kL and a, Chem. Eng. J. 262 (2015) 499–508. doi:https://doi.org/10.1016/j.cej.2014.09.125.

[95] X. Ni, M.R. Mackley, A.P. Harvey, P. Stonestreet, M.H.I. Baird, N.V.R. Rao, Mixing through oscillations and pulsations—a guide to achieving process enhancements in the chemical and process industries, Chem. Eng. Res. Des. 81 (2003) 373–383. doi:https://doi.org/10.1205/02638760360596928.

[96] X. Ni, Y. Zhang, I. Mustafa, An investigation of droplet size and size distribution in methylmethacrylate suspensions in a batch oscillatory-baffled reactor, Chem. Eng. Sci. 53 (1998) 2903–2919. doi:https://doi.org/10.1016/S0009-2509(98)00124-9.

[97] X. Ni, Y. Zhang, I. Mustafa, Correlation of polymer particle size with droplet size in suspension polymerisation of methylmethacrylate in a batch oscillatory-baffled reactor, Chem. Eng. Sci. 54 (1999) 841–850. doi:https://doi.org/10.1016/S0009-2509(98)00279-6.

[98] S. Gao, X. Ni, R.H. Cumming, C.A. Greated, P. Norman, Experimental investigation of bentonite flocculation in a batch oscillatory baffled column, (1998). doi:https://doi.org/10.1080/01496399808545720.

[99] F. Castro, A. Ferreira, J.A. Teixeira, F. Rocha, Protein crystallization as a process step in a novel meso oscillatory flow reactor: study of lysozyme phase behavior, Cryst. Growth Des. 16 (2016) 3748–3755. doi:https://doi.org/10.1021/acs.cgd.6b00262.

[100] F. Castro, A. Ferreira, J.A. Teixeira, F. Rocha, Influence of mixing intensity on lysozyme crystallization in a meso oscillatory flow reactor, Cryst. Growth Des. 18 (2018) 5940–5946. doi:https://doi.org/10.1021/acs.cgd.8b00721.

[101] A.M. Lopes, D.P. Silva, A.A. Vicente, A. Pessoa-Jr, J.A. Teixeira, Aqueous two-phase micellar systems in an oscillatory flow micro-reactor: study of perspectives and experimental performance, J. Chem. Technol. Biotechnol. 86 (2011) 1159–1165. doi:https://doi.org/10.1002/jctb.2642.

[102] F. Castro, A. Ferreira, F. Rocha, A. Vicente, J.A. Teixeira, Precipitation of hydroxyapatite at 37° C in a meso oscillatory flow reactor operated in batch at constant power density, AIChE J. 59 (2013) 4483–4493. doi:https://doi.org/10.1002/aic.14193.

[103] F. Castro, A. Ferreira, F. Rocha, A. Vicente, J.A. Teixeira, Continuous-flow precipitation of hydroxyapatite at 37 C in a meso oscillatory flow reactor, Ind. Eng. Chem. Res. 52 (2013) 9816–9821. doi:https://doi.org/10.1021/ie400710b.

[104] A.C.A. Roque, A.S. Pina, A.M. Azevedo, R. Aires-Barros, A. Jungbauer, G. Di Profio, J.Y.Y. Heng, J. Haigh, M. Ottens, Anything but conventional chromatography approaches in bioseparation, Biotechnol. J. 15 (2020) 1900274. doi:https://doi.org/10.1002/biot.201900274.

[105] A.T. Hanke, M. Ottens, Purifying biopharmaceuticals: knowledge-based chromatographic process development, Trends Biotechnol. 32 (2014) 210–220. doi:https://doi.org/10.1016/j.tibtech.2014.02.001.

[106] G. Guiochon, L.A. Beaver, Separation science is the key to successful biopharmaceuticals, J. Chromatogr. A. 1218 (2011) 8836–8858. doi:https://doi.org/10.1016/j.chroma.2011.09.008.

[107] R.K. Swanson, R. Xu, D. Nettleton, C.E. Glatz, Proteomics-based, multivariate random forest method for prediction of protein separation behavior during cation-exchange chromatography, J. Chromatogr. A. 1249 (2012) 103–114. doi:https://doi.org/10.1016/j.chroma.2012.06.009.

[108] A. Seidel-Morgenstern, Experimental determination of single solute and competitive adsorption isotherms, J. Chromatogr. A. 1037 (2004) 255–272.

Chapter 2 – Continuous Aqueous Two-Phase Extraction of fungal amylase using Oscillatory Flow Reactor: a proof of concept

Abstract

The usage of aqueous two-phase extraction (ATPE) has been proven as an efficient operation for the clarification and purification of biological products, despite the limited use of this technique at large. ATPE has the potential of being implemented in continuous, but most studies are predominantly done in batchwise mode. An oscillatory flow reactor (OFR) is a type of tubular continuous reactor that has been used in distinct processes from polymerization, flocculation and crystallization to liquid-liquid reactions. One of the most important features of this type of reactor is the uniform mixing that is provided by the combination of the periodically spaced restrictions and the oscillatory motion of the fluid. The continuous mode and the particular characteristics of OFR could therefore be the answer for a more cost-competitive ATPE. In this work, the partition of an industrial commercial enzyme – α-amylase – preparation in PEG-phosphate systems was initially studied in batch and the systems presenting the highest yield of partition to the top phase were transferred to the continuous mode using the OFR, where different conditions for frequency and amplitude of oscillation, and total mass flow rate were evaluated, using a design of experiments (DoE) approach. With a system composed of 20%(w/w) PEG1500 and 9%(w/w) potassium phosphate at pH 7.4, the yield in the batch system was 85%, while in continuous ATPE in the OFR was between 77% and 96% for three different frequencies (1, 3 and 5 Hz), amplitudes (1, 2 and 3 mm) and total mass flow rates (4, 32, 60 g/min). It was also proven that: i) a fully continuous ATPE process (with continuous separation) can be obtained without loss of performance; ii) continuous ATPE of the α-amylase from a *Saccharomyces cerevisiae* broth is feasible and shows with improved results when compared with the commercial enzyme preparation. These results show that OFR can be successfully used for continuous ATPE, opening the door to their widespread use by the biotechnological industry.

2.1. Introduction

Aqueous two-phase extraction (ATPE) has been used for the separation and concentration of different biological products – cell constituents, like plasma membranes [1–3] and extracellular vesicles [4,5], different types of cells, as erythrocytes [6–9], leucocytes [10] and stem cells [11–13], microorganisms [14], viral particles [15–17], bacteriophages [18], proteins [19–26], nucleic acids [27–29] and low molecular weight compounds [30]. Aqueous two-phase systems (ATPS) are formed when two hydrophilic solutes are mixed above a critical concentration. There are five main types of ATPS: i) polymer-polymer (e.g., polyethylene glycol (PEG) – dextran); ii) polymer-salt (e.g., PEG – phosphate); alcohol-salt (e.g., 1-propanol – phosphate), micellar ATPS (e.g., Triton X-114 – phosphate [31]) and ionic liquid (IL) based ATPS [32]. The wide application of ATPE has been possible due to some advantages: i) low cost; ii) reduced time to reach the equilibrium of the system; iii) high biocompatibility because of the high content of water; iv) possible re-use of the phases; v) ease to scale up; vi) propensity to process integration [32]. Despite all the strengths presented above, large-scale ATPE has been reported in the literature a few times [33–36] and industrial applications are very rare [32].

Currently, the biotech industry is dominated by batchwise mode operations, however, the increasing demand for biological products, namely biopharmaceuticals, has been the moving force for a gradual change from batch to continuous bioprocessing [37]. The advantages of continuous over batch manufacturing are well known from other industries: i) high volumetric productivity; ii) low cycle times; iii) reduced plant footprint and capital cost; iv) steady state operation; v) streamlined process flow [32,37]. Considering all the advantages aforementioned, ATPE can be an important tool in the biotech industry of the future, given its high possibility of being successfully adapted to continuous mode [32].

Most of the work done regarding ATPE has been developed in batchwise mode and at bench scale. The batch ATPE comprehends 5 main stages: i) preparation of the stocks; ii) mixing of the solutions to obtain the phase; iii) phases settling; iv) recovery of the phase containing the product of interest, v) back or multi extraction [32]. For continuous ATPE, all these stages must occur in the same equipment and this device should have multiple inlets and outlets be able to mix the

solutions, allowing phases to settle and have several outputs for the separation of the phases [32]. The characteristics of the device needed are not very specific, hence the most used equipment for continuous ATPE are mixer settlers [38] and different types of column extractors, e.g., spray columns, perforated rotating disk contactors and pulsed columns [32,39].

All the devices stated before present some relevant drawbacks: i) difficulty in obtaining a full hydrodynamic characterization of the process [40]; ii) back-mixing (formation of a liquid jet instead of the formation of droplets, when the flow rate is too high) [41,42]; iii) flooding (recovery of the raffinate phase together with the product of interest in the extract phase, due to too high flow rates) [43]; iv) emulsification (formation of very small droplets that increase the time needed for the coalescence and, thus, contaminating the phase of interest) [44] and v) separation efficiency [43].

Oscillatory flow reactor (OFR) is a type of tubular/channel reactor provided with periodic constrictions (baffles) operating under oscillatory flow mixing [45]. The liquid or multiphase fluid is typically oscillated in the axial direction using diaphragms, bellows, or pistons, at one end or both ends of the tube, developing an efficient mixing mechanism where fluid moves from the walls to the center of the tube with an intensity controlled by the oscillation frequency (f) and amplitude (x_0) [45]. OFR has been used in multiple processes and it has been proven to be efficient in heat [46] and mass transfer [47], liquid-liquid reaction [48], polymerization [49,50], flocculation [51], crystallization [52,53] and precipitation [54,55]. This type of equipment has not been often used for continuous ATPE, but there is one example in the literature where this reactor was used for the extraction of glucose-6-phosphate dehydrogenase, using an micellar system [56], highlighting the suitable characteristics of this equipment for ATPE.

OFR used here for the continuous ATPE has two distinct regions: one of them with restrictions and the other with a straight tube. The former is the zone where the mixing of the solutions occurs, because of a combination of the oscillation and the net flow; the latter is the settling region. This type of equipment presents advantages compared with the devices described in the literature: mixing and settling processes occur in two different regions which prevents flooding and emulsification, problems observed in columns; the possibility of multiple inlets and outlets

contributes to the versatility of the reactor, contrasting with mixer-settlers and columns; the plug flow conditions are well-established and the hydrodynamic characterization of the system is well-known; the oscillatory flow allows lower net flow velocity and, hence, lower working volumes and less time to reach steady state.

In 2020, the industrial enzymes market had a total value of $7.5 billion with a contribution of 25-35% of α-amylase [57]. α-amylase is a hydrolyzing enzyme that cleaves α-(1,4)-D-glucosidic linkage of starch and other polysaccharides to produce low molecular weight sugars such as glucose, maltose and dextrin [57]. This type of enzyme has been used extensively in detergent, paper, pharmaceutical and textile industries, and also in starch processing [57]. The extensive usage of α-amylase makes this enzyme a good model protein to use in this study.

This work presents the development of a proof of concept of a process of continuous ATPE using an OFR. For that purpose, the partition of a commercial enzyme – α-amylase from *Aspergillus oryzae* – preparation in different PEG/phosphate systems was studied in batch. The compositions presenting the highest yield of partition to the top phase were transferred to the oscillatory flow plate reactor with 2D smooth periodic constrictions [58], and the continuous ATPE was further optimized regarding the operating conditions of the reactor (flow rate, oscillation frequency and amplitude). In the end, a fully continuous ATPE process (with continuous separation of the phases) of the pure enzyme was evaluated, as well as a process of extraction of the α-amylase from a *S. cerevisiae* cellular broth.

2.2. Materials and methods

2.2.1. Chemicals and Biologicals

PEG with molecular weights of 400, 1000, 3350 and 6000 Da, 3,5-Dinitrosalicylic acid (DNS) and Starch were purchased from Sigma-Aldrich (St Louis, Missouri, USA) PEG 1500 came from Acros Organics (New Jersey, USA). Potassium hydrogen phosphate (K_2HPO4), potassium dihydrogen phosphate (KH_2PO_4) and sodium dihydrogen phosphate (NaH_2PO_4) were acquired from Panreac (Darmstadt Germany). 10X Phosphate-Buffered Saline (PBS) was purchased from Fisher

Bioreagents (New Jersey, USA). Sodium chloride (NaCl) came from Fisher Scientific (Hampton, New Hampshire, USA). Maltose monohydrate came from Merck (Rahway, New Jersey, USA).

A commercial preparation of α-amylase from *Aspergillus oryzae* was obtained from Sigma-Aldrich (St Louis, Missouri, USA).

2.2.2. Batch Aqueous Two-Phase Extraction

Batch aqueous two-phase systems of 1.5 g were prepared by weighing out the appropriate amounts of 50% (w/w) PEG, 40% (w/w) potassium phosphate pH 7.4, protein solution and water to achieve the required final composition. The 40% (w/w) potassium phosphate pH 7.4 was prepared by using a mass ratio of potassium hydrogen phosphate (K_2HPO4) to potassium dihydrogen phosphate (KH_2PO_4) of 1.83.

After the weighting, the phase components were mixed for 10 seconds on a Vortex agitator, from VWR International (Radnor, Pennsylvania, USA), and left on the bench for 15 minutes to ensure the total separation of the two phases and their volumes were measured. Samples from the upper and bottom phases were taken for the determination of enzymatic activity and protein concentration. The yield of the partition to the top phase, Y_{top}, was defined as the ratio of the enzyme activity in the upper phase to the sum of activities in both phases. The partition coefficient, Kp, was defined as the quotient of the enzyme activity in the upper phase to that in the lower phase. Phase compositions were established using phase diagrams from [59].

2.2.3. Continuous aqueous two-phase extraction

Continuous ATPE was performed in a modular OFR (OFRTech, Portugal) [57], presented in Figure 2.1. The apparatus consists of a 460 cm long tube with a working volume of 113 mL: 42 mL with 2D smooth periodic constrictions (the region where the mixing of the solutions takes place), having an internal diameter of 4 mm in the straight section and 1.65 mm in the constrictions; 71 mL without the restrictions (the zone where the separation of the phases occurs). The 50% (w/w)

PEG 1500, 40% (w/w) potassium phosphate pH 7.4 and protein solutions were fed into the reactor by peristaltic pumps (Watson Marlow 205S pumps) and the mixture inside the reactor was oscillated using a syringe piston moved by a linear motor that controlled the oscillation frequency (f) and amplitude (x_0).

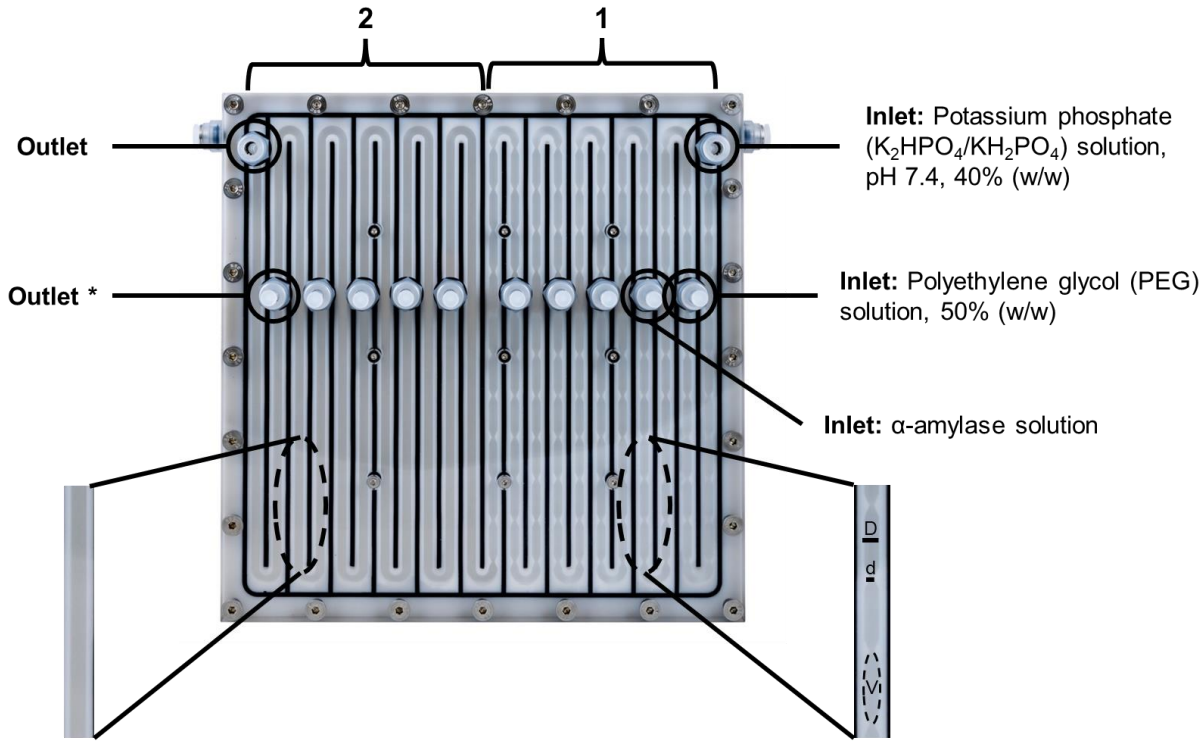

Figure 2.1. Schematic representation of the experimental set-up for continuous aqueous two-phase (ATPE) experiments. Potassium phosphate, polyethylene glycol (PEG) and α-amylase are fed by peristatic pumps into the oscillatory flow reactor (OFR) plate, where mixing occurs through an oscillatory unit controlled by a control unit (not presented in the image). The reactor is divided in two regions: 1 – Region with restrictions where the mixing of the components occurs, where the diameter of the tube (D), diameter of the constriction (d) and the volume between constrictions (V) is 4.00 mm, 1.65 mm and 0.344 mL, respectively; 2 – Region with smooth-walls tube where for the separation of the phases.

*Outlet used for the fully continuous ATPE (section 3.2.2).

Three Central Composite designs (CCD) of 13-run experiments were implemented in Minitab® Statistical Software to maximize the yield of partition to the top phase of pure α-amylase from *Aspergillus oryzae*. The tested variables were evaluated at 3 different levels, selected based on the available literature and to ensure the full mixing of the solutions, and included the total mass flow rate, F_m (4, 32 and 60 mL/min), the maximum oscillatory velocity (*OV*, Equation 2.1.), and the frequency of oscillation, *f* (1, 3 and 5 Hz). The Strouhal number (*St*, Equation 2.2.) was kept constant at $\frac{1}{\pi}$, $\frac{1}{2\pi}$, $\frac{1}{3\pi}$, respectively, in each CCD and, consequently, so was the amplitude of oscillation, x_0 (1, 2, 3, respectively).

$$OV = 2\pi x_0 f \quad (2.1.)$$

$$St = \frac{D}{4\pi x_0} \quad (2.2.)$$

In equation 2.2., *D* is the internal diameter of the tube in the straight section.

Before each experiment, the reactor was filled with 40% potassium phosphate buffer, at pH 7.4, to avoid the formation of bubbles that could influence the process. Continuous ATPE was performed by pumping the 50% (w/w) PEG solution into the OFR 34 cm downstream of the inlet, where it was combined the phosphate solution continuously added. Simultaneously, the protein solution (with or without cells) was continuously injected 74 cm downstream of the first inlet. After waiting three residence times – time required for 3 renovations of the reactor volume (computed by the ratio between 3 times OFR volume (113 mL) and the flow rate) – to ensure steady-state conditions, 120 g were collected at the reactor end. Fifteen minutes after the process finished, the upper and bottom phases were separated (in the fully continuous ATPE, this separation occurred in the end of the reactor), and their volumes were measured. Once the enzyme activities in both phases were determined by 3,5–dinitrosalicylic (DNS) acid method, a second-order polynomial model was fitted to the response data (yield) obtained from the design and analysis of variance (ANOVA) was carried out using Minitab® software.

2.2.4. Enzyme Activity Assay

The enzyme activity of α-amylase was analysed using the 3,5–dinitrosalicylic (DNS) acid method in 96 wells microplate (U96 MicroWell® plate, NUNC™, USA), that was adapted from [60], 980 µL of 10 mg/mL starch in 20 mM monosodium phosphate (NaH_2PO_4), 6.7 mM sodium chloride (NaCl) pH 6.0 and 20 µL of the sample were added to each well. For the blanks, the sample solution was replaced by water. A standard curve with maltose in a suitable concentration range – 2 to 20 mM – was used for the determination of total reducing sugars. The microplate was incubated at 25ºC in a rotary shaker. After this, 20 µL of each one of wells were transferred to a new microplate and together with 80 µL of MilliQ water and 100 µL of DNS reagent. This microplate was covered and placed in a water bath – at 100ºC – for 5 minutes. After cooling to room temperature, 500 µL of MilliQ water were added to each well and the plate was put in a wave shaker for 2 minutes. Finally, 250 µL of the content of each well was transferred to another 96 round wells microplate. The reducing sugar (maltose) obtained after the hydrolysis of starch, catalyzed by α-amylase, was quantified by reading the absorbance of the samples inside the wells at 540 nm. One enzyme activity unit (U) was defined as the quantity of enzyme needed to produce 1 µmol of maltose per min.

2.2.5. Size Exclusion Chromatography

Size exclusion chromatography (SEC) was used to analyze the concentration of the α-amylase of the upper and lower phases of the ATPS. Samples were firstly diluted in phosphate buffer saline (PBS) and then run at isocratic mode, with 1.5 column volumes (CV) of the same buffer at 1 mL/min, using either TSKgel® Super G3000PWXL, from Tosoh Bioscience (Tokyo, Japan), or BioSep-SEC-s3000 from Phenomenex (Torrence, California, USA). A standard curve with pure α-amylase in a suitable concentration range – 0.05 to 5 g/L – was used for the determination of the enzyme concentration.

2.2.6. Isoelectric Point Determination

The zeta potential (surface charge) of the α-amylase was determined using Zetasizer Nano ZS (Malvern Instruments Ltd., UK) over a pH range from 3 to 7 at fixed ionic strength (buffer molarity of 10 mM). All measurements were made using a protein solution with a concentration of 0.1 g/L and replicated six times.

2.2.7. Viscosity Determination

The measurements of the viscosity of the top and bottom phases of the batch ATPS were performed in the temperature range between 293.15 K and 353.15 K, at atmospheric pressure, using a SVM 3000 Anton Paar rotation Stabinger viscosimeter-densimeter (Graz, Austria), where the standard uncertainty for the temperature is 0.02 K. Triplicates of each sample were performed to ensure accuracy and the reports results are the average values.

2.2.8. Protein Gel Electrophoresis

Sodium dodecyl sulfate-polyacrylamide gel electrophoresis (SDS-PAGE) was performed to evaluate the purity of the feedstocks and the resolubilized precipitates. Samples were diluted in a loading buffer containing 62.5 mM Tris-HCl, pH 6.2, 2% SDS, 0.01% bromophenol blue and 10% glycerol and denatured in reducing conditions (0.1 M DTT) in a water bath at 100 ºC for 10 min. Samples were applied to a 12% acrylamide gel, prepared from a 40% acrylamide/bis-acrylamide stock solution (29:1), and ran at 100 V using a running buffer composed of 25 mM Tris-HCl, 192 mM glycine and 0.1% (w/v) SDS at pH 8.3. The molecular marker used was Precision Plus ProteinTM Dual Color Standards (Bio-Rad). Gels were stained overnight with 0.1% Coomassie Brilliant Blue R-250 in 30% ethanol and 10% acetic acid and destained by successively washing with a 30% (v/v) ethanol and 10% (v/v) acetic acid solution.

2.3. Results and discussion

2.3.1. Batch Aqueous Two–Phase Extraction

The four main steps to build a primary recovery process using ATPS are the following: i) physicochemical characterization of the product of interest and the impurities; ii) choice of the type of ATPS; iii) selection of the system parameters; and iv) evaluation of the influence of such parameters on the recovery yield [61]. In the case of this work, the feed sample initially used to set up the ATPE system was a purified commercial preparation and afterwards an unclarified fermentation broth was used to validate the conditions found.

Firstly, the isoelectric point (pI) – 3.3 – and the molecular weight – 54 kDa – of the α-amylase from *A. oryzae* were determined (data not shown). Hereinafter, the polymer-salt (namely, PEG-salt) was the type of ATPS chosen. This choice is mainly due to the low cost compared with the other main types [39].

In the PEG-salt system, pI of the product of interest is important to know beforehand because the pH of the system should be higher than this value to create an electrostatic affinity between the negatively charged molecule and the polymer, which possesses a positive dipolar momentum because of the terminal hydroxyl groups [61,62]. Besides, the partition is highly dependent on the molecular weight of the product of interest, for example, for hydrophilic high molecular weight compounds (> 10 kDa), such as proteins, the partition to the top phase is typically favored in systems with lower molecular weights (< 4000 Da) and lower tie-line length (TLL) (between 10 and 40% [61], equation 2.3.).

$$TLL = \sqrt{\left(x_{lower} - x_{upper}\right)^2 + \left(y_{lower} - y_{upper}\right)^2} \quad (2.3.)$$

In equation 3, x_{upper} and y_{upper} are phosphate and PEG composition in the upper phase and x_{lower} and y_{lower} are phosphate and PEG composition in the lower phase, respectively.

The feasibility of using PEG/phosphate systems for the partition of the α-amylase from *A. oryzae* was initially assessed using a commercial enzyme preparation with a concentration of 800 mg/L. The partition of the α-amylase was studied in ATPS using an univariate analysis where each

parameter is studied one at the time [63,64]. In the case of this work, the parameters evaluated were: i) PEG molecular weight (MW); ii) % (w/w) NaCl; iii) volume ratio (V_R), i.e., the ratio between the volumes of the upper and lower phase. One disadvantage of this approach is the possibility of not finding the absolute optimal point [64], however, in this case, that fact is not problematic since, as the ultimate goal of this work is to compare the performance of two modes of operation – batch *vs.* continuous in an OFR.

Table 2.1. Composition of the systems used to study the partition of the α-amylase.

System	PEG MW (Da)	% PEG (w/w)	% Potassium Phosphate (w/w)	% NaCl (w/w)
1	400	17	20	–
2	1000	15	14	–
3	1500	13	13	–
4	3350	12	11	–
5	6000	15	12.5	–
6	1500	13	13	2
7	1500	13	13	4
8	1500	13	13	7
9	3350	12	11	6
10	3350	12	11	9
11	1500	18	11	–
12	1500	20	9	–

The compositions of the different systems used are presented in Table 2.1.

2.3.1.1. The influence of PEG molecular weight

The first parameter evaluated was the PEG molecular weight. The results are presented in Figure 2.2.

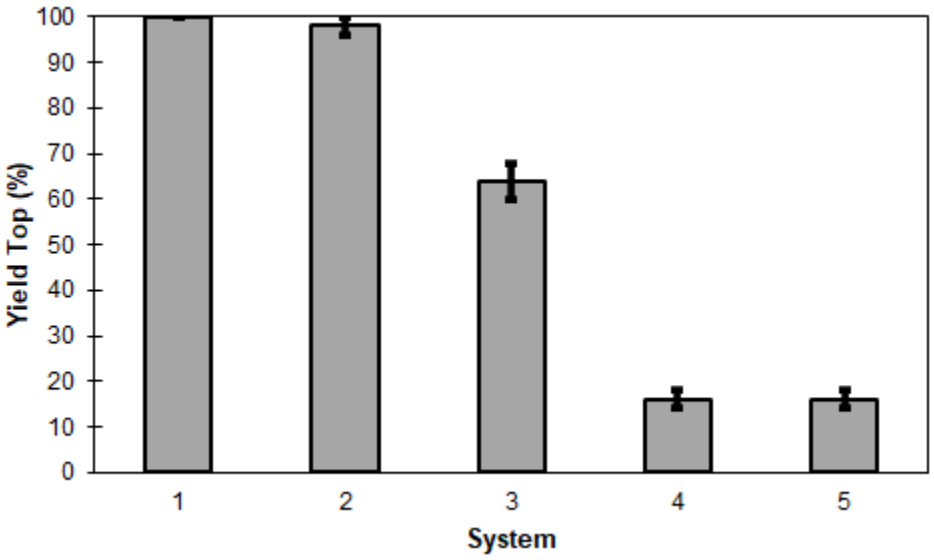

Figure 2.2. The yield of the partition to the top phase of systems where different PEG molecular weights were used. The composition of the systems is described in Table 2.1. All values shown are mean values of triple determinations.

As already mentioned, the recovery of proteins in the upper phase is usually higher when the PEG molecular weight is lower than 4000 Da [61]. In this case, the recovery to the top phase is favored due to the pH of the system – 7.4. At this pH value, α-amylase has a negative overall charge: on the one hand, there is the creation of an electrochemical affinity between the protein and the PEG already described above [61,62]; on the other hand, the repulsive electrostatic interaction between the negatively charged α-amylase and phosphate ions excludes the protein from the

lower phase to the PEG-rich phase [65]. In Figure 2.2., for PEG with a molecular weight lower than 3350 Da, the recovery of the α-amylase in the top phase is between 64 and 100%. However, for the cases of PEG3350 and PEG6000, that yield decreases to 16% in both cases, which is explained by the availability of free volume in the upper phase [61,66].

The partition studies proceeded with the optimization of system **3** [13%(w/w) PEG 1500; 13%(w/w) K_2HPO_4/KH_2PO_4] and **4** [12%(w/w) PEG 3350,11%(w/w) K_2HPO_4/KH_2PO_4] and not with the systems **1** or **2**, since these already exhibited a recovery of almost 100%. In addition, the high molecular weight of the PEG used in systems **3** and **4**, may lead to a higher purity. Indeed, low molecular weight polymers allow for increased the partition coefficient of the product, but also of protein impurities present [67].

2.3.1.2. The influence of NaCl

The addition of sodium chloride (NaCl) sought the improvement of the recovery presented by systems 3 and 4. Neutral salts, such as NaCl, have a well-documented effect: the ions added have different hydrophobicity, and the hydrophobic ones push the partition of their counter ions to the phase with higher hydrophobicity and vice versa [67,68]. Adding another salt to the system, can induce a more pronounce salting-out effect that drives the biomolecules to move from the salt-rich to the PEG-rich phase [67,68]. However, in the case of the α-amylase from A. oryzae, the addition of NaCl did not enhance the partition to the top phase, on the contrary it led to a decrease in the recovery yield of the α-amylase (Figure 2.3.).

The yield of extraction decreases with the increase of the %(w/w) NaCl in the systems with both PEG 1500 and 3350. It is documented in the literature that the concentration of NaCl enhances the migration towards the polymer-rich phase of compounds with a molecular weight lower than 50 kDa [61]. Schmidt and colleagues studied the partition of the α-amylase from *Bacillus subtilis* in different PEG-polymer and PEG-salt systems and, for the systems PEG 4000 10%(w/w) – phosphate 12.5%(w/w), pH 7.0, the increment in the NaCl concentration led to a higher partition coefficient [24]. The protein used in that work was not the same as in this one, however, the

molecular weight and the isoelectric point of the α-amylase from *Bacillus subtilis* are 48 kDa and 5, respectively [24], not so different from the enzyme from *A. oryzae*. The lower yield could be explained by a reversible or irreversible denaturation of the enzyme due to the high concentration of salt and resulting in a lower value of enzyme activity [61].

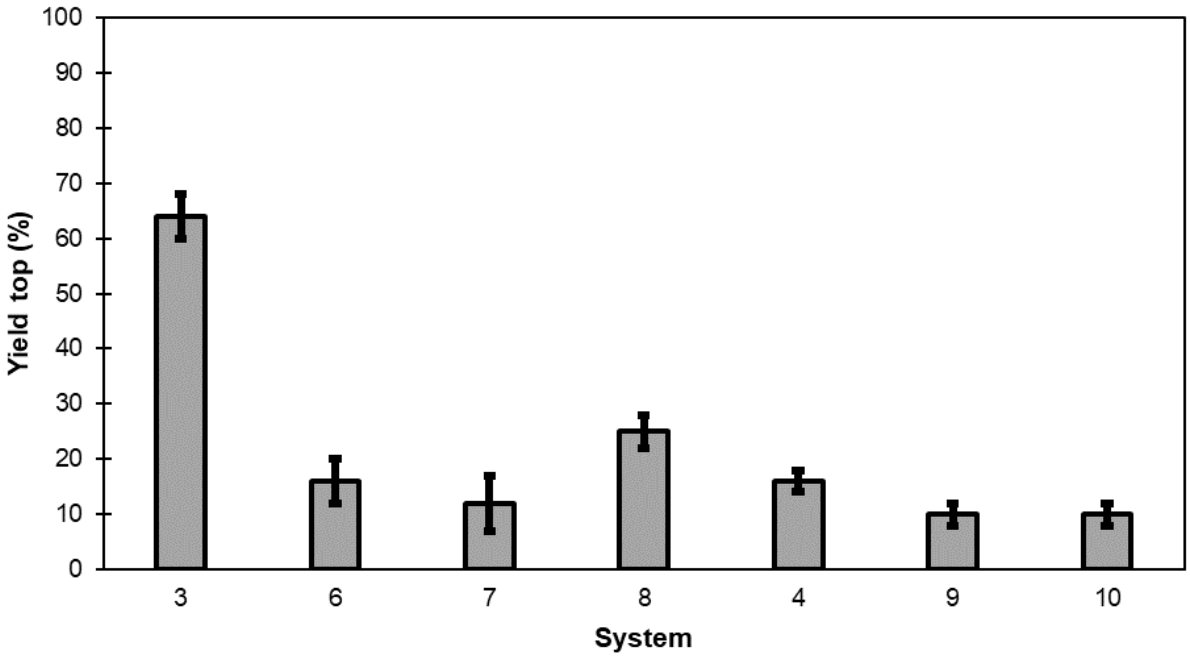

Figure 2.3. The yield of the partition to the top phase of systems where different NaCl concentrations were used. The composition of the systems is described in Table 2.1. All values shown are mean values of triple determinations.

2.3.1.3. The influence of Volume Ratio

As the addition of NaCl did not improve the yield of extraction, changing the volume ratio (V_R) was the next stage. So far, all systems have V_R near to 1, in order to prevent any concentration effects. An increase of the V_R is usually associated with an enhancement of the recovery for the product of interest because of the higher free volume present in the top phase [39,61], and this was observed for α-amylase (Figure 2.4.). It is noteworthy to mention that this comparison is possible, because the three system compositions 4 were in the same tie-line of the phase diagram

[58], which implies that all the upper and lower phases have the same concentration. The optimization was stopped at a V_R of 3.33 because the yield improvement was small compared with the system with V_R of 1.67 and, at some point, the increasing of the volume ratio will not be favourable – the free volume of the bottom phase decreases, the biomolecules have no space and the partition of possible impurities to the top phase is facilitated. Furthermore, a higher V_R can lead to a dilution of the target product.

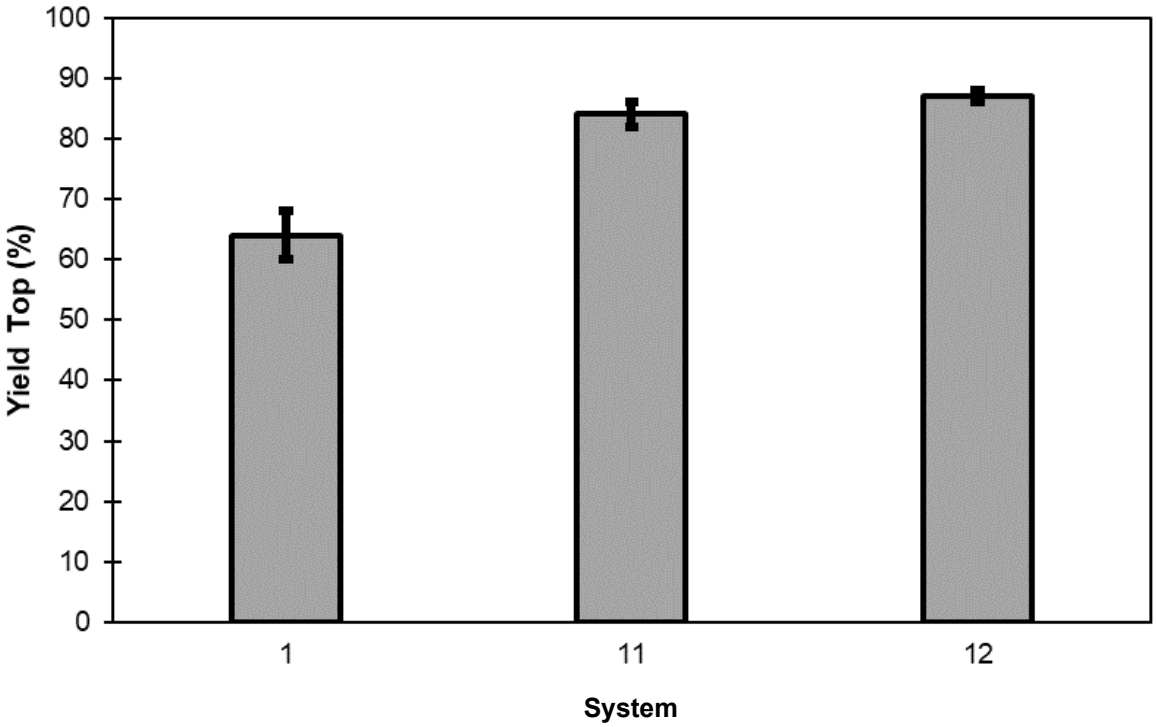

Figure 2.4. The yield of the partition to the top phase of systems where different V_R were used: 1.00, 1.67 and 3.33 for systems 1, 12 and 13, respectively. The composition of the systems is described in Table 2.1. All values shown are mean values of triple determinations.

2.3.1.4. The influence of sample concentration and loading

The sample concentration and loading have an impact on the partition of the protein of interest to the upper phase. In the literature, it is documented that, for PEG-salt systems, a sample load

of 40% w/w of the total system with a concentration lower than 2 mg/mL does not present a risk of saturation of the recovery phase [39,61]. So far, the sample loading and concentration were 10% w/w and 0.80 mg/mL, respectively, both were increased to 37.5% (w/w) and 1.20 mg/mL, respectively. The former could not be increased any further because that value was the remaining percentage of the system.

This increment in the mass of protein loaded did not negatively influence the performance of the ATPS: from a yield of (87 ± 1) %, a partition coefficient of 2.0 ± 0.3 and a volume ratio of 3.3 ± 0.0, to (85 ± 1) %, 1.6 ± 0.2 and 3.4 ± 0.3, respectively.

2.3.2. Continuous aqueous two-phase extraction (ATPE)

2.3.2.1. Optimization of the conditions using central composite design (CCD)

In this study, the transition from batch to continuous ATPE was carried out with an OFR (Figure 2.1.), under the conditions established in batch mode – 20% (w/w) PEG1500, 9% (w/w) potassium phosphate pH 7.4, 37.5 % (w/w) 1.20 mg/mL α-amylase. Potassium phosphate was first mixed with the PEG solution, and then with the feed. The sample to be analyzed was only collected after three residence times to guarantee that steady-state conditions had been achieved.

Primarily, the assessment and the statistical optimization through CCD were done using as input variables, the total mass flow rate (F_m), oscillation frequency (f) and oscillation amplitude (x_0), and using as output variables, the yield in the top phase (Y_{top}), the partition coefficient (K_P) and the volume ratio (V_R). Unfortunately, the resulting models were not statistically significant (p-value>0.05), probably due to the non-trivial contribution of x_0. For the ATPE to be successfully performed, mixing is crucial, and the increase of oscillation amplitude has two effects: i) rise of the maximum oscillatory velocity (*OV*) (Equation 2.1.), increasing the mixing intensity (for the same F_m) [45]; ii) decline of the Strouhal number (Equation 2) that implies a higher effectivity of the vortices propagation and, hence, higher efficiency at transferring mass, however this effect is not linear [45,69,70]. For this reason, another statistical optimization process was chosen with 3 different CCD being implemented, each with a constant *Str* and as input variables, the *OV* (only

dependent on *f*) and F_m. In summary, for each different CCD, the value of *Str* was $\frac{1}{\pi}$, $\frac{1}{2\pi}$ or $\frac{1}{3\pi}$ (hence, x_0 was 1, 2 or 3 mm), and for each experiment, the value of *f* was 1, 3 or 5, and F_m was 4, 32 or 60 g/min. The contour plots obtained for the models with Y_{top} as output are presented in Figure 2.5.

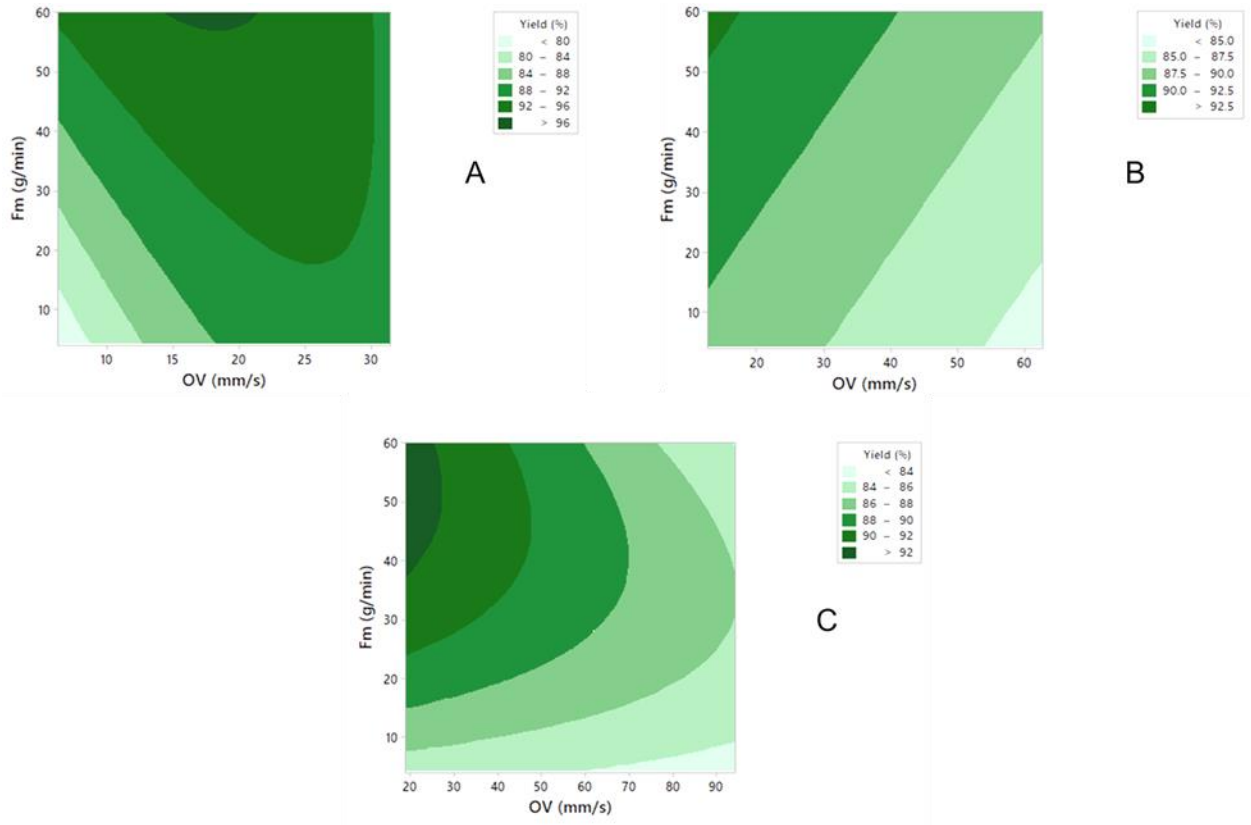

Figure 2.5. Two-dimensional contour plots showing the interaction effects of total mass flow (F_m) and oscillatory velocity (*OV*) on the yield of the partition to the top phase (Y_{top}). The three graphs are for different values of Strouhal number: A) $\frac{1}{\pi}$; B) $\frac{1}{2\pi}$; C) $\frac{1}{3\pi}$.

The three models obtained are all statistically significant, however, it is noteworthy that, for Str = $\frac{1}{2\pi}$, a full quadratic model presented a p-value>0.05, because the square and 2-way interaction

coefficients were not statistically meaningful (data not shown), reason why the linear model was chosen in this case.

For the higher value of Strouhal number (Figure 2.5.A), the Y_{top} is optimal when F_m is in the maximum value used, the same does not happen with *OV*; for lower values of Strouhal number (Figure 2.5. B and C), the Y_{top} is favored by high F_m and low OV. To analyze the possible reasons for these effects, equations 3, 4 and 5 are presented below.

$$Re_n = \frac{\rho u D}{\mu} \text{ (2.4.)}$$

$$Re_o = \frac{2\pi x_0 f \rho D}{\mu} = \frac{OV\rho D}{\mu} \text{ (2.5.)}$$

$$\psi = \frac{Re_0}{Re_n} = \frac{OV}{u} \text{ (2.6.)}$$

In equations 2.4., 2.5. and 2.6., Re_n is the net flow Reynolds number, Re_o is the oscillatory Reynolds number, Ψ is the velocity ratio, ρ is the fluid density, μ is the dynamic viscosity, u is the net flow velocity, and D is the tube diameter. The viscosity of the aqueous two-phase system (μ_s) can be calculated by the following equation [71]:

$$\mu_S = \frac{\mu_{top} V_R + \mu_{bot}}{V_R + 1} \text{ (2.7.)}$$

Where μ_{top} and μ_{bot} are the dynamic viscosity of the top and bottom phases, respectively, and V_R is the volume ratio of the system. The viscosity was not measured experimentally for the continuous ATPE assays, but it was obtained for the batch ones – μ_{top} = (7.68 ± 0.03) cP and μ_{bot} = (1.82 ± 0.05) cP. For analytical purposes, it will be assumed that these values do not change significantly between all the continuous ATPE experiments,

In the literature, it is described that, for liquids: i) the transition to turbulent flow occurs at Re_o higher than 50, and, that for values between 100 and 300, plug-flow characteristics are exhibited, and vortices are axi-symmetrical generated within each constriction cavity (known as soft mixing regime); ii) at Re_n higher than 250, the effects of net flow become relevant, and the advantage of using oscillatory flow decreases significantly; iii) Ψ must be higher than one – oscillatory velocity

higher than linear velocity – and, for plug-flow operation, values between 2 and 10 have been recommended [45,70].

For $St = \frac{1}{\pi}$ (Figure 2.5.A), the values of Re_o, Re_n and Ψ range between 4.46 and 23.95, 3.50 and 51.24, and 0.09 and 6.56, respectively. For $St = \frac{1}{2\pi}$ (Figure 2.5.B), between 8.6 and 45.26, 3.45 and 49.89, and 0.17 and 13.06, respectively. For $St = \frac{1}{3\pi}$ (Figure 2.5.C), between 12.76 and 67.27, 3.31 and 51.24, and 0.26 ad 19.61, respectively.

When $St = \frac{1}{\pi}$, the effectivity of the vortices propagation was higher, Re_o and Re_n values were very low, which can cause inadequate degree of mixing, exactly what happened when the F_m and *OV* were on the lowest values used, when Y_{top} decreased to around 80%. For example, when *OV* = 2π mm/s (f = 1 Hz) and F_m = 4 g/min, Re_o, Re_n and Ψ are 4.68, 3.56 and 1.31, respectively and V_R is lower compared with the batch results (2.42 vs 3.33, respectively). The low values of Re_o, Re_n and ψ are the probable reason for a low degree of mixing and, hence, a low volume ratio that affects negatively affected the yield of the partition to the top phase, due to the excess free volume available in the bottom phase [72].

As aforementioned, it was expected that the optimum result would be obtained for the highest values of Re_o and Ψ. However, when *OV* = 10π mm/s (f = 5 Hz) and F_m = 4 g/min, Re_o, Re_n and Ψ are 23.95, 3.65 and 6.56, respectively, the Y_{top} obtained was higher compared with the batch result – 91% vs 85% – but the V_R was significantly lower – 2.19 vs 3.33. For this value of *Str*, when the F_m = 4 g/min (lowest value), the V_R was always lower than 3.00, demonstrating that, when the amplitude was low, a high F_m (hence, high Re_n) was the driving force of a proper degree of mixing (V_R similar comparing with the batch result) and better partition of the protein to the top phase (higher K_p and Y_{top} vs batch), and not the Re_o and Ψ – the last is lower than 1 for the best results obtained.

When *St* is equal to $\frac{1}{2\pi}$ and $\frac{1}{3\pi}$ (Figure 2.5.B and 2.5.C, respectively), the high F_m (hence, high Re_o) is also the driving force of a proper degree of mixing (V_R similar compared with the batch result) and better partition of the protein to the top phase (higher K_p and Y_{top} vs batch) being the

optimum values obtained when *OV* is minimum and F_m = 60 g/min. When the F_m is at the lowest value (4 g/min) the V_R was almost always lower than 3.00, independently of the values of Re_0 and Ψ. It is also noteworthy that, for both values of *St*, when F_m = 60 g/min was used, the Y_{top} and K_p were always higher than in the batch assays, and V_R was similar, pointing out once more for the importance of the net flow inside the OFR in this type of multiphase system.

For each model, it was predicted the values of *OV* (and the consequent f) and F_m that lead to the optimal Y_{top} for each Str (Table 2.2.).

Table 2.2. Predicted conditions by the three different models (each with one value of *St*) – *OV*, *f* and F_m – and the optimal Y_{top} forecasted for those conditions.

St	**Predicted Conditions**			**Optimal Y_{top} (%)**
	***OV* (mm/s)**	***f* (Hz)**	**F_m (g/min)**	
$\frac{1}{\pi}$	17.7	2.82	60	96
$\frac{1}{2\pi}$	12.6	1.00	60	93
$\frac{1}{3\pi}$	18.9	1.00	54	93

The highest result was obtained for *St* = $\frac{1}{\pi}$ (x_0 = 1 mm), *OV* = 17.7 mm/s (f = 2.82 Hz) and F_m = 60 g/min. These conditions were reproduced experimentally and the Y_{top} obtained was (94.2 ± 0.9) %, K_p = 4.7 ± 0.7, and V_R = 3.48 ± 0.08. These results indicate that: i) predicted and observed Y_{top}

are very similar, showing the high predictability degree of the model; ii) the continuous ATPE using OFR increased the yield performance comparing with batch (Y_{top} = (85 ± 1) %); iii) this increased performance is due to higher protein partition to the top phase because the increment of the K_p, given that the V_R is very similar to the value observed in batch.

2.3.2.2. Full continuous aqueous two-phase extraction

The optimization described previously was done using a continuous ATPE setup but not continuous separation of the two phases, since all the outlet was collected in a vessel where phases were allowed to settle. The next step of this work was to try to achieve the fully continuous extraction and phase separation, applying the optimum conditions achieved previously (i.e., x_0 = 1 mm, f = 2.89 Hz, F_m = 60 g/min). For that, many configurations were analyzed, but the one that produced the best results was described in section 2.3 and in Figure 2.1.

With the setup used, a good separation of both phases was achieved. Indeed, the percentage of the total mass and total volume of the top phase obtained in the first outlet was (98.14 ± 0.06)% and (98.27 ± 0.07)%, respectively. Knowing that the separation of the phases is one of the challenges in the continuous ATPE, this result represents an improvement compared with the devices previously used: i) in the case of different types of column extractors, this separation was poorly and often not calculated [41–43]; ii) in the case of mixer settlers, the separation was not done *per se*, since the performance of the separation is enhanced by using a multistage extraction, which increases the complexity of the overall process [38].

In these assays, the extraction yield, i.e., the percentage of α-amylase obtained in the first exit (first outlet presented in Figure 2.1., where the majority of the top phase was collected) was (97.3 ± 0.1)% and, if taken into account the second exit (last outlet of the OFR), the percentage of total protein obtained in the top phase, that value goes to (98.94 ± 0.03)%. These values are significantly larger than the Y_{top} obtained in section 3.2.1. The V_R obtained was 3.7 ± 0.4, a value in the range of the one obtained in the previous section (3.48 ± 0.08), implying that the highest yield is due to the rise of the K_p to 24.0 ± 0.4 (compared with the 4.7 ± 0.7 in the one outlet

situation). This large increment can be explained by a destabilization of the chemical equilibrium of overall ATPS, creating a new one inside the rest of the reactor and going out in the second exit, since this formation was not apparent in the decanter right after the assays. One way to check if this is the case would be to use a pump in the first outlet instead of just a valve that does not allow the control of the flowrate.

2.3.2.3. Continuous aqueous two-phase extraction (ATPE) from a cellular broth

The optimization of the continuous ATPE was done using commercial α-amylase preparation for a matter of simplicity, since using impure samples increase the complexity of all optimization process, but the goal of an extraction is to isolate the product of interest from the other molecules. For that purpose, a mock broth of *Saccharomyces cerevisiae* and α-amylase from *A. oryzae* were used. The original organism was not used because, due to its fungal hyphal mode of growth, it is normally grown using solid-state fermentation (SSF) [73]. The case of *S. cerevisiae* is the opposite, since it is a yeast that is widely used in liquid fermentation, namely for the production of ethanol [74], and it is one of the most used hosts in biotechnology due to the ease of transformation with exogenous DNA together with efficient homologous recombination capabilities [75]. This mock broth also represents an eventual real case, since α-amylase from *A. oryzae* is an extracellular enzyme [76].

For all the assays performed with the mock broth, it was used an 18-hours culture of *S. cerevisiae*, because this time of growth allowed the maximum number of cells possible combined with the small influence in the enzyme activity, since it was seen the decrease in this activity when the α-amylase was mixed with cultures with higher number of hours, probably due to the ethanol produced by this yeast.

Firstly, the extraction of α-amylase from the broth was done in batchwise mode to investigate if the presence of cells could potentially affect the performance of the extraction. The results obtained were Y_{top} = (84.2 ± 0.9) %, K_p = 1.6 ± 0.1 and V_R = 3.27 ± 0.08, indicating that the presence of cells did not disturb the partition of α-amylase. On the other hand, the results of the partition

of the cells were not very consistent, possibly pointing that the high concentration of polymer and/or salt is responsible for the plasmolysis of the *S. cerevisiae* cells, theory that is supported by the appearance of a large and broad chromatographic peak, in SEC analysis, after the peak corresponding to the α-amylase, pointing to the existence of other (intracellular) proteins in both top and bottom phases (data not shown).

Then, the continuous ATPE was performed with the optimal conditions presented in the section 3.2.1 (i.e., x_0 = 1 mm, f = 2.89 Hz, F_m = 60 g/min), and with just one outlet, to enable the comparison between the case with and without cells. The results obtained were Y_{top} = (96.6 ± 0.6) %, K_P = 9 ± 2 and V_R = 3.41 ± 0.09. The V_R is similar to the one obtained without cells, indicating that the presence of cells does not disturb the chemical equilibrium of the system, but the Y_{top} and K_p increased significantly. Once again, as stated in the section 2.3.2.1, Y_{top} and K_p of the continuous ATPE were higher comparing with the batch process, pointing that the flow regime inside the OFR increases the performance of this type of extraction, because of an improvement of the partition to the top phase, consequence of a possible better mass transfer.

2.4. Conclusion

The utilization of ATPE for the clarification and purification of biological products has a long history, but only in bench and lab scales and mostly in batchwise mode, being the large scale and the continuous mode relegated until now, because no equipment was able to perform it efficiently. The work herein presented tackles this issue, demonstrating that continuous ATPE using OFR is a viable technique for the initial purification of biologic products, exemplified by the partition the of commercial α-amylase with a recovery of more than 94% and a partition coefficient higher than 4.7, improving the results obtained from the optimization in batchwise mode (85% and 1.6, respectively), suggesting that the flow regime inside the OFR increases the performance of the ATPE.

This work also pointed out that a full continuous ATPE (extraction and separation of the phases) can be performed in this type of reactor, as well as the clarification of the α-amylase from a cell

broth of *S. cerevisiae*. The former case was performed using a valve that seemed to have disturbed the equilibrium between the two phases, leading to a higher partition of the protein to the top phase, when compared to phase separation outside the reactor. The latter showed that, firstly, the partition of the enzyme was not significantly affected by the presence of the cells and, lastly, that the flow regime inside the OFR was able to increase the performance of the ATPE once again.

To conclude, this work sets foundations that can contribute to the implementation of continuous ATPE in the downstream processing of, for example, food enzyme from a cell broth as capture step using an oscillatory flow reactor, although further research is still needed, particularly building a continuous downstream bioprocessing, beginning right after the cell broth containing the product of interest and using continuous operations after the OFR, like membrane processes.

2.5. References

[1] P. Navas, D. David Nowack, D. James Morré, Isolation of purified plasma membranes from cultured cells and hepatomas by two-phase partition and preparative free-flow electrophoresis, Cancer Res. 49 (1989) 2147–2156.

[2] D.M. Morré, D.J. Morre, Aqueous two-phase partition applied to the isolation of plasma membranes and Golgi apparatus from cultured mammalian cells, J. Chromatogr. B Biomed. Sci. Appl. 743 (2000) 377–387. doi:https://doi.org/10.1016/S0378-4347(00)00058-X.

[3] H. Everberg, R. Peterson, S. Rak, P. Tjerneld, C. Emanuelsson, Aqueous two-phase partitioning for proteomic monitoring of cell surface biomarkers in human peripheral blood mononuclear cells, J. Proteome Res. 5 (2006) 1168–1175. doi:https://doi.org/10.1021/pr050469z.

[4] J. Kim, H. Shin, J. Kim, J. Kim, J. Park, Isolation of high-purity extracellular vesicles by extracting proteins using aqueous two-phase system, PLoS One. 10 (2015). doi:https://doi.org/10.1371/journal.pone.0129760.

[5] H. Shin, C. Han, J.M. Labuz, J. Kim, J. Kim, S. Cho, Y.S. Gho, S. Takayama, J. Park, High-yield isolation of extracellular vesicles using aqueous two-phase system, Sci. Rep. 5 (2015). doi:https://doi.org/10.1038/srep13103.

[6] J.M. Van Alstine, D.E. Brooks, Cell membrane abnormality detected in erythrocytes from patients with multiple sclerosis by partition in two-polymer aqueous-phase systems., Clin. Chem. 30 (1984) 441–443. doi:https://doi.org/10.1093/clinchem/30.3.441.

[7] K.A. Sharp, M. Yalpani, S.J. Howard, D.E. Brooks, Synthesis and application of a poly(ethylene glycol)-antibody affinity ligand for cell separations in aqueous polymer two-phase systems, Anal. Biochem. 154 (1986) 110–117. doi:https://doi.org/10.1016/0003-2697(86)90503-8.

[8] P. Jimeno, A.I. Garcia-Perez, J. Luque, M. Pinilla, Changes in glycolytic enzyme activities in aging erythrocytes fractionated by counter-current distribution in aqueous polymer two-phase systems, Biochem. J. 279 (1991) 237–243. doi:https://doi.org/10.1042/bj2790237.

[9] M. Tsukamoto, S. Taira, S. Yamamura, Y. Morita, N. Nagatani, Y. Takamura, E. Tamiya, Cell separation by an aqueous two-phase system in a microfluidic device, Analyst. 134 (2009) 1994–1998. doi:https://doi.org/10.1039/B909597G.

[10] J.R. SooHoo, G.M. Walker, Microfluidic aqueous two phase system for leukocyte concentration from whole blood, Biomed. Microdevices. 11 (2009) 323–329. doi:https://doi.org/10.1007/s10544-008-9238-8.

[11] M. González-González, M. Rito-Palomares, Application of affinity aqueous two-phase systems for the fractionation of CD133+ stem cells from human umbilical cord blood, J. Mol. Recognit. 28 (2015) 142–147. doi:https://doi.org/10.1002/jmr.2374.

[12] A.F. Sousa, P.Z. Andrade, R.M. Pirzgalska, T.M. Galhoz, A.M. Azevedo, C.L. da Silva, M. Raquel Aires-Barros, J.M.S. Cabral, A novel method for human hematopoietic stem/progenitor cell isolation from umbilical cord blood based on immunoaffinity aqueous two-phase partitioning, Biotechnol. Lett. 33 (2011) 2373–2377. doi:https://doi.org/10.1007/s10529-011-0727-0.

[13] E. Atefi, R. Joshi, J.A. Mann, H. Tavana, Interfacial Tension Effect on Cell Partition in Aqueous Two-Phase Systems, ACS Appl. Mater. Interfaces. 7 (2015) 21305–21314. doi:https://doi.org/10.1021/acsami.5b05757.

[14] H. Umakoshi, R. Kuboi, I. Komasawa, Control of partitioning of bacterial cells and characterization of their surface properties in aqueous two-phase systems, J. Ferment. Bioeng. 84 (1997) 572–578. doi:https://doi.org/10.1016/S0922-338X(97)81914-9.

[15] M.J. Jacinto, R.R.G. Soares, A.M. Azevedo, V. Chu, A. Tover, J.P. Conde, M.R. Aires-Barros, Optimization and miniaturization of aqueous two phase systems for the purification of recombinant human immunodeficiency virus-like particles from a CHO cell supernatant, Sep. Purif. Technol. 154 (2015) 27–35. doi:https://doi.org/10.1016/j.seppur.2015.09.006.

[16] C.L. Effio, L. Wenger, O. Ötes, S.A. Oelmeier, R. Kneusel, J. Hubbuch, Downstream processing of virus-like particles: Single-stage and multi-stage aqueous two-phase extraction, J. Chromatogr. A. 1383 (2015) 35–46. doi:https://doi.org/10.1016/j.chroma.2015.01.007.

[17] K.S. Vijayaragavan, A. Zahid, J.W. Young, C.L. Heldt, Separation of porcine parvovirus from bovine serum albumin using PEG-salt aqueous two-phase system, J. Chromatogr. B Anal. Technol. Biomed. Life Sci. 967 (2014) 118–126. doi:https://doi.org/10.1016/j.jchromb.2014.07.025.

[18] E. Espitia-Saloma, P. Vázquez-Villegas, O. Aguilar, M. Rito-Palomares, Continuous aqueous two-phase systems devices for the recovery of biological products, Food Bioprod. Process. 92 (2014) 101–112. doi:https://doi.org/10.1016/j.fbp.2013.05.006.

[19] P. Vázquez-Villegas, E. Espitia-Saloma, M. Rito-Palomares, O. Aguilar, Low-abundant protein extraction from complex protein sample using a novel continuous aqueous two-phase systems device, J. Sep. Sci. 36 (2013) 391–399. doi:https://doi.org/10.1002/jssc.201200584.

[20] B. Bertrand, K. Mayolo-Deloisa, M. González-González, R. Tinoco-Valencia, L. Serrano-Carreón, F. Martínez-Morales, M.R. Trejo-Hernández, M. Rito-Palomares, Pleurotus ostreatus laccase recovery from residual compost using aqueous two-phase systems, J. Chem. Technol. Biotechnol. 91 (2016) 2235–2242. doi:https://doi.org/10.1002/jctb.4995.

[21] M.V. Rocha, M. Di Giacomo, S. Beltramino, W. Loh, D. Romanini, B.B. Nerli, A sustainable affinity partitioning process to recover papain from Carica papaya latex using alginate as macro-

ligand, Sep. Purif. Technol. 168 (2016) 168–176. doi:https://doi.org/10.1016/j.seppur.2016.05.025.

[22] P.A.J. Rosa, A.M. Azevedo, I.F. Ferreira, J. de Vries, R. Korporaal, H.J. Verhoef, T.J. Visser, M.R. Aires-Barros, Affinity partitioning of human antibodies in aqueous two-phase systems, J. Chromatogr. A. 1162 (2007) 103–113. doi:https://doi.org/10.1016/j.chroma.2007.03.067.

[23] K.V.G. Barros, P.M. Souza, M.M. Freitas, E.X. Ferreira Filho, A.P. Junior, P.O. Magalhães, PEG/NaPA aqueous two-phase systems for the purification of proteases expressed by Penicillium restrictum from Brazilian Savanna, Process Biochem. 49 (2014) 2305–2312. doi:https://doi.org/10.1016/j.procbio.2014.09.022.

[24] A.S. Schmidt, A.M. Ventom, J.A. Asenjo, Partitioning and purification of α-amylase in aqueous two-phase systems, Enzyme Microb. Technol. 16 (1994) 131–142. doi:https://doi.org/10.1016/0141-0229(94)90076-0.

[25] J.A. Asenjo, R.E. Turner, S.L. Mistry, A. Kaul, Separation and purification of recombinant proteins from Escherichia coli with aqueous two-phase systems, J Chromatogr A. 668 (1994) 129–137. doi:https://doi.org/10.1016/0021-9673(94)80101-0.

[26] B.A. Andrews, S. Nielsen, J.A. Asenjo, Partitioning and purification of monoclonal antibodies in aqueous two-phase systems, Bioseparation. 6 (1996) 303–313. http://europepmc.org/abstract/MED/9210350.

[27] F. Luechau, T.C. Ling, A. Lyddiatt, Partition of plasmid DNA in polymer-salt aqueous two-phase systems, Sep. Purif. Technol. 66 (2009) 397–404. doi:https://doi.org/10.1016/j.seppur.2008.12.003.

[28] H. Barbosa, A. V. Hine, S. Brocchini, N.K.H. Slater, J.C. Marcos, Affinity partitioning of plasmid DNA with a zinc finger protein, J. Chromatogr. A. 1206 (2008) 105–112. doi:https://doi.org/10.1016/j.chroma.2008.07.095.

[29] S.P. Duarte, A.G. Fortes, D.M.F. Prazeres, J.C. Marcos, Preparation of plasmid DNA polyplexes from alkaline lysates by a two-step aqueous two-phase extraction process, J. Chromatogr. A. 1164 (2007) 105–112. doi:https://doi.org/10.1016/j.chroma.2007.06.061.

[30] M.G. Freire, C.M.S.S. Neves, I.M. Marrucho, J.N. Canongia Lopes, L.P.N. Rebelo, J.A.P. Coutinho, High-performance extraction of alkaloids using aqueous two-phase systems with ionic liquids, Green Chem. 12 (2010) 1715–1718. doi:https://doi.org/10.1039/C0GC00179A.

[31] F. Mashayekhi, A.S. Meyer, S.A. Shiigi, V. Nguyen, D.T. Kamei, Concentration of mammalian genomic DNA using two-phase aqueous micellar systems, Biotechnol. Bioeng. 102 (2009) 1613–1623. doi:https://doi.org/10.1002/bit.22188.

[32] D. Ferreira-Faria, M.R. Aires-Barros, A.M. Azevedo, Continuous aqueous two-phase extraction: from microfluidics to integrated biomanufacturing, Fluid Phase Equilib. 508 (2020) 112438. doi:https://doi.org/10.1016/j.fluid.2019.112438.

[33] W. Hummel, H. Schütte, M.R. Kula, Large scale production of d-lactate dehydrogenase for the stereospecific reduction of pyruvate and phenylpyruvate, Eur. J. Appl. Microbiol. Biotechnol. 18 (1983) 75–85. doi:https://doi.org/10.1007/BF00500828.

[34] K.H. Kroner, H. Hustedt, M. -R Kula, Evaluation of crude dextran as phase-forming polymer for the extraction of enzymes in aqueous two-phase systems in large scale, Biotechnol. Bioeng. 24 (1982) 1015–1045. doi:https://doi.org/10.1002/bit.260240502.

[35] T. Minuth, H. Gieren, U. Pape, H.C. Raths, J. Thömmes, M.R. Kula, Pilot scale processing of detergent-based aqueous two-phase systems, Biotechnol. Bioeng. 55 (1997) 339–347. doi:https://doi.org/10.1002/(SICI)1097-0290(19970720)55:2<339::AID-BIT11>3.0.CO;2-C.

[36] C. Kepka, E. Collet, J. Persson, Å. Ståhl, T. Lagerstedt, F. Tjerneld, A. Veide, Pilot-scale extraction of an intracellular recombinant cutinase from E. coli cell homogenate using a thermoseparating aqueous two-phase system, J. Biotechnol. 103 (2003) 165–181. doi:https://doi.org/10.1016/S0168-1656(03)00104-4.

[37] K.B. Konstantinov, C.L. Cooney, White paper on continuous bioprocessing May 20–21 2014 continuous manufacturing symposium, J. Pharm. Sci. 104 (2015) 813–820. doi:https://doi.org/10.1002/jps.24268.

[38] P.A.J. Rosa, A.M. Azevedo, S. Sommerfeld, M. Mutter, W. Bäcker, M.R. Aires-Barros, Continuous purification of antibodies from cell culture supernatant with aqueous two-phase systems: From concept to process, Biotechnol. J. 8 (2013) 352–362. doi:10.1002/biot.201200031.

[39] M. Rito-Palomares, J. Benavides, Aqueous Two-Phase Systems for Bioprocess Development for the Recovery of Biological Products, Springer, 2017.

[40] S.L. Mistry, A. Kaul, J.C. Merchuk, J.A. Asenjo, Mathematical modelling and computer simulation of aqueous two-phase continuous protein extraction, J. Chromatogr. A. 741 (1996) 151–163. doi:https://doi.org/10.1016/0021-9673(96)00179-3.

[41] A. Venâncio, J.A. Teixeira, Protein mass transfer studies on a spray column using the PEG-Reppal PES 100 aqueous two-phase system, Bioprocess Eng. 13 (1995) 251–255. doi:https://doi.org/10.1007/BF00417636.

[42] L. Igarashi, T.G. Kieckbusch, T.T. Franco, Xylanase mass transfer studies in aqueous two-phase systems using spray and sieve plate columns, Bioprocess Biosyst. Eng. 26 (2004) 151–157. doi:https://doi.org/10.1007/s00449-003-0329-x.

[43] M.T.H. Cavalcanti, M.G. Carneiro-da-Cunha, I. V. Brandi, T.S. Porto, A. Converti, J.L. Lima Filho, A.L.F. Porto, A. Pessoa, Continuous extraction of α-toxin from a fermented broth of Clostridium perfringens Type A in perforated rotating disc contactor using aqueous two-phase PEG-phosphate system, Chem. Eng. Process. Process Intensif. 47 (2008) 1771–1776. doi:https://doi.org/10.1016/j.cep.2007.09.018.

[44] J.S.R. Coimbra, F. Mojola, A.J.A. Meirelles, Dispersed phase hold-up in a perforated rotating disc contactor (PRDC) using aqueous two-phase systems, J. Chem. Eng. Japan. 31 (1998) 277–280. doi:https://doi.org/10.1252/jcej.31.277.

[45] T. McGlone, N.E.B. Briggs, C.A. Clark, C.J. Brown, J. Sefcik, A.J. Florence, Oscillatory flow reactors (OFRs) for continuous manufacturing and crystallization, Org. Process Res. Dev. 19 (2015) 1186–1202. doi:https://doi.org/10.1021/acs.oprd.5b00225.

[46] M.R. Mackley, P. Stonestreet, Heat transfer and associated energy dissipation for oscillatory flow in baffled tubes, Chem. Eng. Sci. 50 (1995) 2211–2224. doi:https://doi.org/10.1016/0009-2509(95)00088-M.

[47] A. Ferreira, J.A. Teixeira, F. Rocha, O2 mass transfer in an oscillatory flow reactor provided with smooth periodic constrictions. Individual characterization of kL and a, Chem. Eng. J. 262 (2015) 499–508. doi:https://doi.org/10.1016/j.cej.2014.09.125.

[48] X. Ni, M.R. Mackley, A.P. Harvey, P. Stonestreet, M.H.I. Baird, N.V.R. Rao, Mixing through oscillations and pulsations—a guide to achieving process enhancements in the chemical and process industries, Chem. Eng. Res. Des. 81 (2003) 373–383. doi:https://doi.org/10.1205/02638760360596928.

[49] X. Ni, Y. Zhang, I. Mustafa, An investigation of droplet size and size distribution in methylmethacrylate suspensions in a batch oscillatory-baffled reactor, Chem. Eng. Sci. 53 (1998) 2903–2919. doi:https://doi.org/10.1016/S0009-2509(98)00124-9.

[50] X. Ni, Y. Zhang, I. Mustafa, Correlation of polymer particle size with droplet size in suspension polymerisation of methylmethacrylate in a batch oscillatory-baffled reactor, Chem. Eng. Sci. 54 (1999) 841–850. doi:https://doi.org/10.1016/S0009-2509(98)00279-6.

[51] S. Gao, X. Ni, R.H. Cumming, C.A. Greated, P. Norman, Experimental investigation of bentonite flocculation in a batch oscillatory baffled column, (1998). doi:https://doi.org/10.1080/01496399808545720.

[52] F. Castro, A. Ferreira, J.A. Teixeira, F. Rocha, Protein crystallization as a process step in a novel meso oscillatory flow reactor: study of lysozyme phase behavior, Cryst. Growth Des. 16 (2016) 3748–3755. doi:https://doi.org/10.1021/acs.cgd.6b00262.

[53] F. Castro, A. Ferreira, J.A. Teixeira, F. Rocha, Influence of mixing intensity on lysozyme crystallization in a meso oscillatory flow reactor, Cryst. Growth Des. 18 (2018) 5940–5946. doi:https://doi.org/10.1021/acs.cgd.8b00721.

[54] F. Castro, A. Ferreira, F. Rocha, A. Vicente, J.A. Teixeira, Precipitation of hydroxyapatite at 37° C in a meso oscillatory flow reactor operated in batch at constant power density, AIChE J. 59 (2013) 4483–4493. doi:https://doi.org/10.1002/aic.14193.

[55] F. Castro, A. Ferreira, F. Rocha, A. Vicente, J.A. Teixeira, Continuous-flow precipitation of hydroxyapatite at 37 C in a meso oscillatory flow reactor, Ind. Eng. Chem. Res. 52 (2013) 9816–9821. doi:https://doi.org/10.1021/ie400710b.

[56] A.M. Lopes, D.P. Silva, A.A. Vicente, A. Pessoa-Jr, J.A. Teixeira, Aqueous two-phase micellar systems in an oscillatory flow micro-reactor: study of perspectives and experimental performance, J. Chem. Technol. Biotechnol. 86 (2011) 1159–1165. doi:https://doi.org/10.1002/jctb.2642.

[57] J.S. Paul, N. Gupta, E. Beliya, S. Tiwari, S.K. Jadhav, Aspects and recent trends in microbial α-amylase: a review, Appl. Biochem. Biotechnol. 193 (2021) 2649–2698. doi:https://doi.org/10.1007/s12010-021-03546-4.

[58] A.M.A. Ferreira, F.A.N. Da Rocha, J.A. Couto-Teixeira, A.A.M. de O. Soares, Apparatus for mixing based on oscillatory flow reactors provided with smooth periodic constrictions, (2016).

[59] B.Y. Zaslavsky, Aqueous two-phase partitioning: physical chemistry and bioanalytical applications, CRC press, 1994. doi:https://doi.org/10.1016/0014-5793(95)90055-1.

[60] G.L. Miller, Use of dinitrosalicylic acid reagent for determination of reducing sugar, Anal. Chem. 31 (1959) 426–428. doi:https://doi.org/10.1021/ac60147a030.

[61] J. Benavides, M. Rito-Palomares, Practical experiences from the development of aqueous two-phase processes for the recovery of high value biological products, J. Chem. Technol. Biotechnol. Int. Res. Process. Environ. Clean Technol. 83 (2008) 133–142. doi:https://doi.org/10.1002/jctb.1844.

[62] B.B. Nerli, M. Espariz, G.A. Picó, Thermodynamic study of forces involved in bovine serum albumin and ovalbumin partitioning in aqueous two-phase systems, Biotechnol. Bioeng. 72 (2001) 468–474. doi:https://doi.org/10.1002/1097-0290(20000220)72:4<468::AID-BIT1008>3.0.CO;2-L.

[63] K. Selber, F. Nellen, B. Steffen, J. Thömmes, M.-R. Kula, Investigation of mathematical methods for efficient optimisation of aqueous two-phase extraction, J. Chromatogr. B Biomed. Sci. Appl. 743 (2000) 21–30. doi:https://doi.org/10.1016/S0378-4347(00)00045-1.

[64] M.A. Torres-Acosta, K. Mayolo-Deloisa, J. González-Valdez, M. Rito-Palomares, Aqueous Two-Phase Systems at Large Scale: Challenges and Opportunities, Biotechnol. J. 14 (2019) 1800117. doi:https://doi.org/10.1002/biot.201800117.

[65] A.M. Azevedo, P.A.J. Rosa, I.F. Ferreira, M.R. Aires-Barros, Optimisation of aqueous two-phase extraction of human antibodies, J. Biotechnol. 132 (2007) 209–217. doi:https://doi.org/10.1016/j.jbiotec.2007.04.002.

[66] H. Cabezas Jr, Theory of phase formation in aqueous two-phase systems, J. Chromatogr. B Biomed. Sci. Appl. 680 (1996) 3–30. doi:https://doi.org/10.1016/0378-4347(96)00042-4.

[67] M. Iqbal, Y. Tao, S. Xie, Y. Zhu, D. Chen, X. Wang, L. Huang, D. Peng, A. Sattar, M.A.B. Shabbir, Aqueous two-phase system (ATPS): an overview and advances in its applications, Biol. Proced. Online. 18 (2016) 18. doi:https://doi.org/10.1186/s12575-016-0048-8.

[68] S. Raja, V.R. Murty, V. Thivaharan, V. Rajasekar, V. Ramesh, Aqueous two phase systems for the recovery of biomolecules–a review, Sci. Technol. 1 (2011) 7–16. doi:https://doi.org/10.5923/j.scit.20110101.02.

[69] P.C. Cruz, C.R. Silva, F.A. Rocha, A.M. Ferreira, Mixing Performance of Planar Oscillatory Flow Reactors with Liquid Solutions and Solid Suspensions, Ind. Eng. Chem. Res. 60 (2021) 2663–2676. doi:https://doi.org/10.1021/acs.iecr.0c04991.

[70] M.S.R. Abbott, A.P. Harvey, G.V. Perez, M.K. Theodorou, Biological processing in oscillatory baffled reactors: operation, advantages and potential, Interface Focus. 3 (2013) 20120036. doi:https://doi.org/10.1098/rsfs.2012.0036.

[71] S. Papavinasam, The main environmental factors influencing corrosion, in: Corros. Control Oil Gas Ind., Gulf Professional Publishing Houston, 2014: pp. 179–247.

[72] V.H. Nagaraja, R. Iyyaswami, Aqueous two phase partitioning of fish proteins: partitioning studies and ATPS evaluation, J. Food Sci. Technol. 52 (2015) 3539–3548. doi:https://doi.org/10.1007/s13197-014-1425-4.

[73] G.M. Daba, F.A. Mostafa, W.A. Elkhateeb, The ancient koji mold (Aspergillus oryzae) as a modern biotechnological tool, Bioresour. Bioprocess. 8 (2021) 52.

[74] M.J. Viktor, S.H. Rose, W.H. Van Zyl, M. Viljoen-Bloom, Raw starch conversion by Saccharomyces cerevisiae expressing Aspergillus tubingensis amylases, Biotechnol. Biofuels. 6 (2013) 1–11.

[75] A. Tippelt, M. Nett, Saccharomyces cerevisiae as host for the recombinant production of polyketides and nonribosomal peptides, Microb. Cell Fact. 20 (2021) 1–24.

[76] K. Oda, D. Kakizono, O. Yamada, H. Iefuji, O. Akita, K. Iwashita, Proteomic analysis of extracellular proteins from Aspergillus oryzae grown under submerged and solid-state culture conditions, Appl. Environ. Microbiol. 72 (2006) 3448–3457.

Chapter 3 – Continuous precipitation of antibodies using oscillatory flow reactor: a proof of concept

*This chapter has been published as: Ferreira-Faria, D., Domingos-Moreira, F., Aires-Barros, M. R., Ferreira, A., & Azevedo, A. M. (2023). Continuous precipitation of antibodies using oscillatory flow reactor: A proof of concept. *Separation and Purification Technology*, *317*, 123924.

Abstract

Antibodies are among the most important drugs in the pharmaceutical industry. Their increasing demand has pressured the industry to increase upstream antibody titers, making downstream processing the new manufacturing bottleneck. Precipitation is an attractive alternative to current purification platforms by reducing costs, increasing yields, and decreasing the scale-up process complexity. In the present work, continuous precipitation of antibodies using an oscillatory flow reactor (OFR) was explored. The combination of cross-linking (zinc chloride, $ZnCl_2$) and volume exclusion (polyethylene glycol, PEG) agents was examined for precipitation of antibodies from an artificial IgG and FBS mixture, mimicking the supernatant of antibody-producing cells. The PEG/$ZnCl_2$ ratio was first optimized in batch and further implemented in the OFR under continuous operation, where the influence of mixing intensity (frequency, amplitude and flow rate) was investigated. Continuous precipitation carried out in the OFR with 14% PEG6000 and 4 mM $ZnCl_2$ enabled the recovery of over 99% of antibodies with 90% purity, demonstrating the implementation viability of this operation for the initial capture of antibodies. It must be also highlighted that precipitation did not affect the secondary structure of the antibody according to circular dichroism measurements.

3.1. Introduction

Over the past five years, rapid advances in genetic engineering and the development of personalized therapy have placed antibodies at the forefront of medicine, being the best-selling

drugs in the biopharmaceuticals market with global sales reaching $130.9 billion in 2020 and expected to achieve $300 billion by 2025 [1]. Therapeutic monoclonal antibodies (mAbs) dominate the biopharma market, with the number of approved mAbs now exceeding 100 in the US, with over 200 under development due to the competition with biosimilars and the approval of new drugs for the treatment of several diseases including cancer, autoimmune and infectious diseases [1,2].

To fulfil market demands, improvements in cell line productivity were made with antibody titers achieving nowadays up to 25 g/L [3]. However, these rapid advances in production have left downstream processing as a manufacturing bottleneck, accounting for almost 80% of total costs [4,5]. Currently, mAb purification is based on a common sequence of unit operations, including three chromatographic steps, ultrafiltration and virus inactivation [6]. Protein A (ProA) affinity chromatography used almost exclusively for the initial capture of antibodies is the most limiting step, representing up to 50% of total downstream costs. Although highly selective for antibodies, it has been challenged by the high production titers achieved, leading to high resin costs and low throughput [7].

The increasing pressure to reduce costs along with the competition of biosimilars and the achievement of high production titers have led to an increased demand to improve the efficiency of downstream processing [8]. Thus, in an attempt to eliminate the limitations posed by ProA affinity chromatography, there has been a growing interest in several non-chromatographic alternatives such as precipitation, aqueous two-phase extraction and crystallization [9–14].

In addition, shifting from batch to continuous processing is regarded as a promising approach to increase productivity while reducing operational costs and facility footprint. Several studies have reported both semi-continuous and integrated continuous processing in antibody manufacturing with promising results, including continuous precipitation [8,12].

Precipitation is one of the earliest developed methods for large-scale purification of biological products. More recently, it has shown great potential as a capture step of mAbs, either by being implemented before a chromatography process to reduce the impurity load (host cell proteins and DNA) and maximize the use of the resin or even by replacing ProA affinity chromatography

as purification method [8,15–17]. Precipitation is a low-cost and robust technique, operated both in batch and continuous mode, that combines high yields with an easy scale-up. In chromatography, to process a higher titer supernatant, it is required to use either a larger column or an increased number of cycles of a given column, due to the stoichiometric reaction between antibodies and Protein A. Conversely, precipitation scales with the supernatant volume and titer, requiring less volume of precipitant for higher product titers since in this case, the solubility decreases [17]. Besides, it tends to become more selective as product titer increases, achieving higher yields and purities which makes it especially suitable for high titer supernatants [18].

Previous studies have reported the use of calcium chloride ($CaCl_2$) and cold ethanol [19], $CaCl_2$ and polyethylene glycol (PEG) [20], zinc chloride ($ZnCl_2$) and PEG [11,21], and $ZnCl_2$ alone [16] for antibody precipitation. Among these combinations, the addition of the polymer and metal ion stands out because not only they are low cost and effective at low dosage but also do not denature the antibody during precipitation and form precipitates that are easy to resolubilize [22]. PEG acts by volume exclusion, lowering the solubility of antibodies in a semi-logarithmic behaviour with respect to its concentration [23]. Although considered an attractive precipitant, it lacks selectivity. Thus, it is usually combined with other precipitating agents, such as $ZnCl_2$ [21,22], to be able to compete with chromatography. Divalent zinc cations form relatively stable complexes with antibodies by binding to histidine and cysteine residues on their surface, supposedly through exposed imidazole and thiol groups, respectively, cross-linking protein molecules and thus leading to precipitation [24]. The addition of $ZnCl_2$ has been shown to decrease the amount of PEG required for precipitation, which is considered advantageous since PEG tends to increase the viscosity of the solution [21,25]. More recently, Burgstaller *et al.,* recovered mAbs with a 95% yield and a purity of 97% by continuous precipitation with 2 mM ZnCl2 and 7% PEG6000 in a tubular reactor with continuous recovery of the precipitate using a tangential flow filtration module [21].

Research carried out so far has been focused on the study of protein precipitation in continuous stirred tank reactors (CSTRs) and continuous tubular reactors (CTRs) [22]. However, at the industrial scale, CSTRs are often associated with problems regarding shear forces and low mixing

efficiency [26]. Even though tubular reactors enable to overcome most of these limitations, they require a high superficial velocity to obtain good mixing [27].

Oscillatory flow reactor (OFR) is a potential alternative since they provide efficient mixing without increasing the solution flow and can, therefore, be operated at lower flow rates. OFR consists of a column containing periodic constrictions (baffles) where the fluid is typically oscillated in the axial direction, at one or both ends, developing a uniform mixing (oscillatory flow mixing) created by the formation and cessation of eddies when the flow interacts with the constrictions [28]. Over the last years, OFR has been used for several processes including crystallization, flocculation and precipitation of different products from lysozyme to paracetamol, hinting at their potential for antibody precipitation [29–31].

OFR has some general advantages when compared with a CTR. In the latter, the mixing relies on high net velocity in order to achieve a high enough Reynolds number, resulting in excessive tube lengths, because of the long residence times [27,32]. In the OFR, the periodical oscillation makes the fluid interact with the restrictions, creating strong vortices and allowing lower net flow velocity, shorter tube lengths and, hence, lower working volumes [32]. Additionally, it is possible to operate under plug-flow conditions, which means that the residence time is the same in all the fluid inside the reactor [32,33]. Other advantages of this type of reactor are enhanced heat and mass transfer capabilities, linear scalability, minimal concentration gradients and easy implementation of process analytical technology (PAT) [32].

This work presents the development of a process for the continuous precipitation of proteins with an OFR using human serum antibodies as model protein. To do so, the effect of different precipitants was studied in batch, namely PEG and $ZnCl_2$, which have already been reported in antibody precipitation, and NaCl which has been described to precipitate proteins by salting-out [34,35]. Using the optimal condition determined in batch, continuous precipitation was implemented in the oscillatory flow plate reactor with 2D smooth periodic constrictions [36] and further optimized regarding the operating conditions of the reactor (flow rate, oscillation frequency and amplitude).

3.2. Materials and methods

3.2.1. Chemicals and biologicals

PEG with molecular weight of 3350 and 6000 Da were purchased from Acros Organics (New Jersey, USA). Sodium chloride (NaCl), $ZnCl_2$, Tris-Base and acetic acid (CH_3COOH) 100% were obtained from Thermo Fisher Scientific (Rockford, IL, USA). Potassium hydrogen phosphate (K_2HPO_4) and potassium dihydrogen phosphate (KH_2PO_4) came from Panreac (Darmstadt Germany). Citric acid ($C_6H_8O_7$), monosodium dihydrogen citrate (C_6H_7NaO7), sodium acetate (CH_3COONa), DL-dithiothreitol (DTT) solution 1M in water, ammonium persulfate and N,N,N',N'tetramethylethylenediamine (TEMED) were purchased from Merk (Darmstadt, Germany). Acrylamide/bisacrylamide 40% solution and Coomassie Brilliant Blue R-250 were acquired from Bio-Rad (Hercules, CA, USA). BCA™ Protein Assay Kit was bought from Thermo Fisher Scientific.

Human serum IgG was used as a model protein in the form of human γ-globulins, from Merck Life Science (Darmstadt, Germany). Fetal bovine serum (FBS), also provided by Merck, was used to represent impurities.

3.2.2. Precipitation optimization

Small-scale batch precipitation studies were performed with different feeds – pure IgG solution, FBS and artificial IgG and FBS mixture. Precipitation experiments, in a final volume of 1 mL, were prepared by mixing 500 µL of feed with the appropriate volumes of precipitants solutions, and water to achieve the final volume, giving a final concentration of either 2 g/L pure IgG, 5% (v/v) FBS or 2 g/L IgG combined in 5%(v/v) FBS (artificial mixture). Aqueous stock solutions of 54% (w/v) PEG and 100 mM $ZnCl_2$ were used. All feeds were prepared in the buffer with the pH under study at double the concentration to compensate for the two-fold dilution.

Preliminary studies were performed to evaluate how the precipitation of pure IgG was affected by the pH (7, 8.5, 10), PEG concentration (0. 7.5 and 10% (w/v)) and salt concentration (0, 10 and

20 mM NaCl or $ZnCl_2$). Further optimization was performed by studying the precipitation of pure IgG in the presence of two molecular weight PEG molecules, namely 3350 Da (PEG3350) and 6000 Da (PEG6000), at concentrations from 2 to 18% (w/v), combined with $ZnCl_2$ at concentrations from 1 to 10 mM, in 50 mM phosphate buffer at pH 7. Afterwards, FBS precipitation was analyzed over the same range of PEG concentrations combined with 6 or 10 mM of $ZnCl_2$, in 50 mM phosphate buffer at pH 7. Finally, precipitation of IgG from an artificial IgG:FBS mixture was analyzed over a range of PEG and $ZnCl_2$ concentrations selected based on previous experiments with pure IgG and FBS solutions. For all experiments, samples were incubated for 20 min at room temperature on the disk rotator (JP Selecta, Barcelona, Spain), centrifuged at 4,000 *g* for 10 min (Hermle Z233 M-2 Microliter Centrifuge, Hermle, Germany) and the withdrawn supernatant was analyzed by Protein G affinity chromatography and the BCA assay. Precipitation yield was defined as the percentage of mass of antibody or proteins that did not remain in the feed solution after precipitation and was calculated by subtracting of the mass of antibody/proteins in the supernatant obtained after centrifugation to the respective initial mass and then dividing the result by the initial mass of antibody/protein. This yield does not consider the resolubilization step.

3.2.3. Continuous precipitation

Continuous IgG precipitation was performed in a modular OFR (OFRTech, Portugal) [36], depicted in Figure 3.1. The device consists of a 460 cm long tube provided with 2D smooth periodic constrictions (2D-SPCs) with an internal diameter of 4 mm in the straight section and 1.65 mm in the constrictions, with a working volume of 42 mL and a total volume of 51 mL. The precipitants and artificial mixture were fed into the reactor by peristaltic pumps (Watson Marlow 205S pumps) and the fluid inside the reactor was oscillated using a syringe piston moved by a linear motor. The OFR was operated under oscillatory flow mixing controlled by the oscillation frequency (f) and amplitude (x_0).

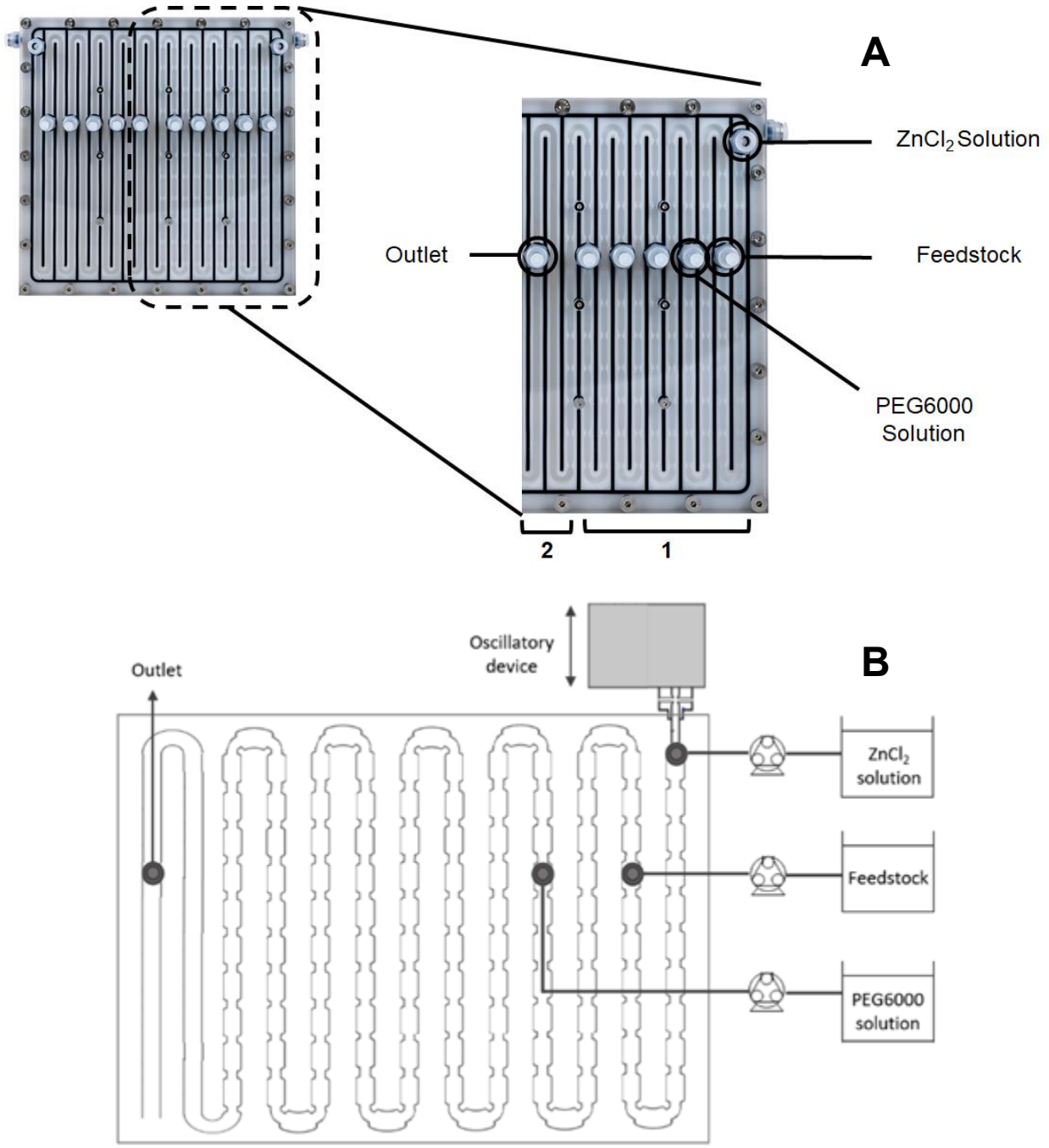

Figure 3.1. Experimental set-up for continuous antibody precipitation experiments. A) Real set up of the OFR plate: zone 1 – reagents mixing and precipitation (with restrictions); zone 2 – without restrictions. B) Schematic representation of OFR set up. Precipitants and artificial IgG and FBS solution (feedstock) are fed by peristatic pumps into the OFR plate, where mixing occurs through

an oscillatory unit controlled by a control unit; the precipitation solution is then collected in the outlet. Dark circles represent the inlets or outlet of the reactor.

A Box-Behnken design (BBD) of 15-run experiments was implemented in Minitab® Statistical Software to maximize the yield and purity of antibody precipitation from the artificial IgG and FBS mixture. The tested variables were evaluated at 3 different levels, selected based on the available literature and to ensure the full suspension of solids, and included the net flow rate, Q (4, 22 and 40 mL/min), the oscillation frequency, f (1, 3 and 5 Hz) and oscillation amplitude, x_0 (1, 2 and 3 mm). Before each experiment, the reactor was filled with 16.7 mM $ZnCl_2$ solution to avoid the formation of bubbles that could influence the precipitation. Continuous precipitation was performed by pumping the feed (mimetic solution) into the OFR 34 cm downstream of the inlet, where it was combined with 16.7 mM $ZnCl_2$ solution continuously added. Simultaneously, a 54% (w/v) PEG6000 solution was continuously injected 74 cm downstream of the first inlet. The flow rates of each solution were selected to achieve a volume ratio of 0.5:0.26:0.24 of feed, PEG6000 and $ZnCl_2$ solution, respectively. This resulted in a final concentration of 2 g/L of IgG and 5%(v/v) of FBS in 50 mM phosphate buffer (pH 7), 14% (w/v) of PEG6000 and 4 mM of $ZnCl_2$. After waiting four residence times to ensure steady-state conditions, samples were collected at the reactor end during one residence time, centrifuged at 4,000 *g* for 10 min and the supernatant was withdrawn and the precipitate resolubilized. The residence time was defined as the ratio between the working volume of the reactor (42 mL) and the sum of the three flow rates, in each assay. Once the yield and purity were determined by Protein G affinity chromatography, a second-order polynomial model was fitted to the response (yield and purity) data obtained from the design and analysis of variance (ANOVA) was carried out using Minitab® software.

3.2.4. Resolubilization

After precipitation and centrifugation, the supernatant was withdrawn, and the precipitate pellet dried overnight at 37 ºC. The dried precipitate was then dissolved in 850 µL – for batch

precipitation – or 34 mL – for continuous precipitation – of 50 mM citrate buffer (pH 3) for 45 min on a disk rotator at 12 rpm. After adjusting the pH of the resolubilized precipitate to pH 8 by adding 1 M Tris-Base to a final volume of 1 mL and 40 mL, respectively, the samples were analyzed with Protein G affinity chromatography and BCA assay. Resolubilization yield was defined as the amount of precipitated mass that was resolubilized. An overall precipitation yield was defined considering the individual yields of both steps: precipitation and resolubilization.

3.2.5. Isoelectric point determination

Zeta potential (surface charge) of the antibodies (γ-globulins) and FBS was determined using Zetasizer Nano ZS (Malvern Instruments Ltd., UK) over a pH range from 3 to 9 at fixed ionic strength (buffer molarity of 10 mM). All measurements were made using a protein solution with a concentration of 0.1 g/L and replicated twice.

3.2.6. Protein G affinity chromatography

Antibody concentration used to estimate the yield and purity was determined by affinity chromatography in ÄKTA^{TM} 10 Purifier system (Cytiva, Uppsala, Sweden) using an analytical POROS Protein G affinity column (2.1 x 30 mm, 0.1 mL; Applied Biosystems, Foster City, CA, USA). Mobile phase A was 10 mM sodium phosphate, 150 mM NaCl, pH 8.5. Mobile phase B was 12 mM HCl, 150 mM NaCl, pH 2-3. Samples were diluted 4 or 10 times with mobile phase A. The system was run at a flow rate of 1 mL/min. The column was equilibrated with 15 column volumes (CV) of mobile phase A before injecting 0.5 mL of sample, eluted with 25 CV of mobile phase B and re-equilibrated with 33 CV of mobile phase A. The absorbance was measured at 280 nm. γ-globulins were used as calibration standards in concentrations ranging from 6 to 500 µg/mL. The IgG purity was calculated as the ratio of the antibody peak area to the sum of all peak areas (peak areas of antibody (retention time 2.9 min) and FBS proteins' (retention time 0.4 min)). For accurate purity determination, a calibration curve correlating the area ratio (IgG area/ total area)

and the percentage of antibody was further used. More information regarding this calibration curve can be found in the supplementary material provided.

3.2.7. Total protein quantification

Total protein concentration was determined using Pierce™ BCA Protein Assay Kit. The assays were performed in transparent 96-well plates (Costar) according to manufacturer instructions for the standard protocol and the absorbance was read at 562 nm in a Spectramax 384 Plus microplate reader (Molecular Devices, Sunnyvale, CA, USA). Samples were diluted in PBS buffer when necessary. Bovine gamma globulin (BGG) and bovine serum albumin (BSA) were used as standards in the precipitate and feed samples, respectively. To avoid possible interference from PEG and $ZnCl_2$, blanks of the supernatants and precipitates were also measured. From the total protein concentration and the antibody concentration determined by Protein G chromatography, the concentration of FBS proteins in feed and precipitate samples were estimated.

3.2.8. Circular dichroism spectroscopy

Far-UV CD analysis was performed on a PiStra-180 Chirascan CD spectropolarimeter from Applied Photophysics (Leatherhead, UK). Before CD measurements, precipitate samples were purified by affinity chromatography using a HiTrap™ Protein G HP affinity column (1 mL; Cytiva, Sweden) and buffer-exchanged into Milli-Q water using HiTrap™ Desalting column (5 mL; Cytiva, Sweden). Briefly, the desalting column was preequilibrated with 10 CV of Milli-Q water, at a flow rate of 5 mL/min, before loading 1.5 mL of sample and running in isocratic mode. CD spectra were recorded over the wavelength range 200-250 nm in a 1 mm quartz cuvette at a sample concentration of 0.5 mg/mL, using a bandwidth of 5 nm and a time constant of 1 s. Background corrections were done by subtracting the CD spectra of the empty cuvette. The mean residue ellipticity (MRE) ($deg.cm^2.dmol^{-1}$) was calculated considering a mean residue weight (MRW) of 114 Da for the antibody as per the following equation:

$$MRE = \frac{MRW \times \theta}{10 \times d_l \times c}$$

where θ is the measured ellipticity (millidegrees), d_l is the path length (cm) and c is the concentration (g/L).

3.3. Results and discussion

3.3.1. Precipitation optimization

Optimization of antibody precipitation was first carried out with pure IgG solution and later with an artificial IgG and FBS solution and was based on the yield and purity. The precipitation yield was calculated based on the antibody remaining in the supernatant; yield obtained through antibody concentration in the precipitate was only used to estimate the yield of resolubilization.

Prior to precipitation assays, the isoelectric points (pI) of the IgG solution and and isoionic point FBS were determined (6.5 and 4.3, respectively), as they could have a great influence on precipitation.

3.3.1.1. Precipitation of pure IgG solution

PEG and $ZnCl_2$ have been reported to successfully precipitate antibodies [11,21], while the addition of NaCl in high concentrations has been described to precipitate proteins by salting-out [35]. Therefore, precipitation with PEG/$ZnCl_2$ was analysed over a pH range from 7 to 10. This range was selected in order to be closer as possible to the pI of the antibody and as far as possible from the pI of the impurities. Unlike PEG and $ZnCl_2$, NaCl had no influence on precipitation despite the pH (data not shown) and was considered not suitable for IgG precipitation. Precipitation of the antibodies was shown to be positively influenced by the increase in the concentration of PEG and $ZnCl_2$ and in pH, reaching almost 100% yield when performed at pH 8.5 and pH 10, with either 10 or 20 mM $ZnCl_2$. However, Dutra *et al.,* [16] have reported a pH drop from 7.2 to 6 when 12 mM $ZnCl_2$ was added. In fact, pH measurements later performed confirmed that the addition of

10 mM $ZnCl_2$ decreased the pH of the solution by one value. Hence, the yields obtained at pH 8.5 and 10 correspond in fact to lower pH values. To ensure a constant pH throughout precipitation, further experiments were carried out using a buffer with a higher buffering capacity (buffer concentration was increased to 50 mM). Given that cell culture supernatants and animal serum are typically at neutral pH, performing precipitation at pH 7 is advantageous as it does not require prior conditioning. Since precipitation with 10 or 20 mM $ZnCl_2$ resulted in similar yields, a lower concentration range (0 to 10 mM) was screened over a range of PEG concentrations between 0 and 18% (w/v) (Figure 3.2. A and B). Based on the literature, PEG3350 and PEG6000 were used to study the influence of the molecular weight of this polymer on precipitation efficiency.

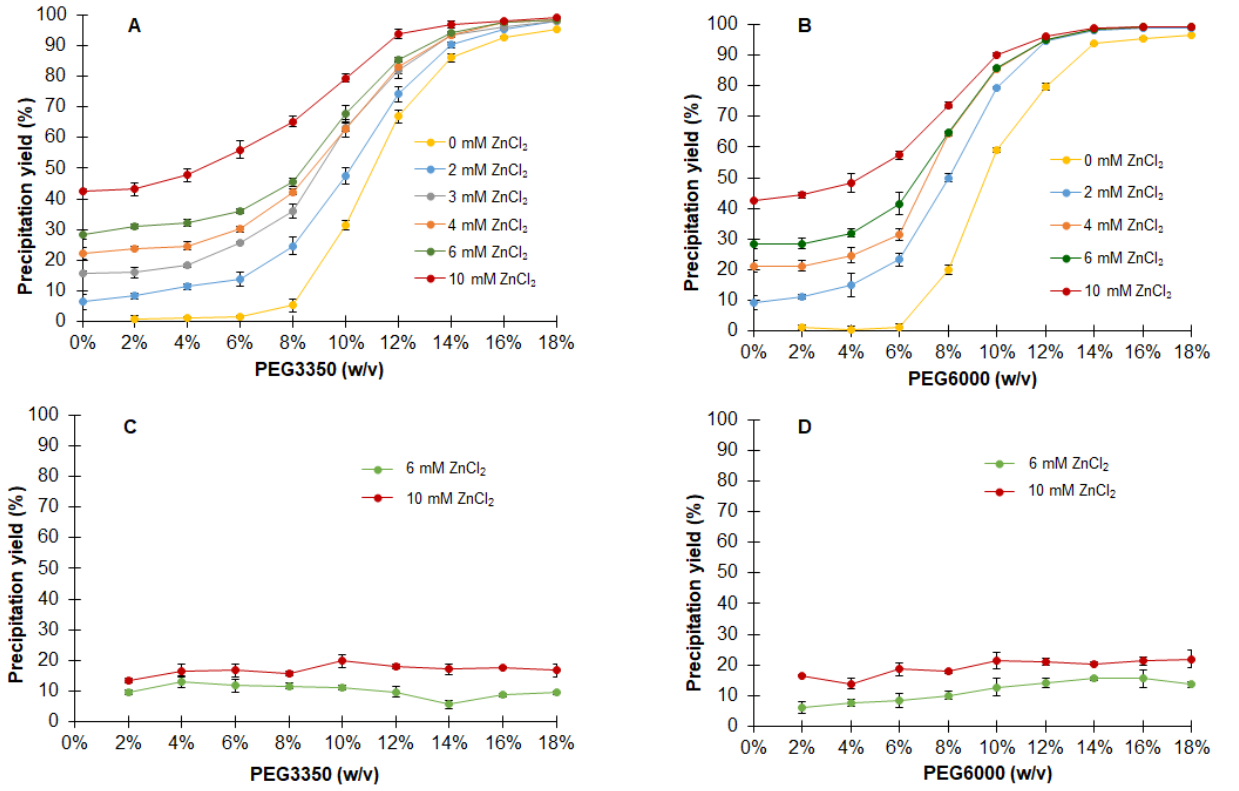

Figure 3.2. – Precipitation yield of 2 g/L IgG (A and B) and 5% (v/v) FBS at increasing concentrations of $ZnCl_2$ and PEG3350 (A and C) or PEG6000 (B and D). Experiments were performed at pH 7, in 50 mM phosphate buffer. Yield was determined based on the quantification of the remaining soluble proteins. All values shown are mean values of triple determinations.

According to Figure 3.2., precipitation of antibodies increases with increasing PEG and $ZnCl_2$ concentrations, as expected due to their volume exclusion and cross-linking properties, respectively. However, when PEG concentrations are high – 16% (w/v) for PEG3350 and 12% (w/v) for PEG6000 – using high concentrations of zinc bring little added benefit regarding the precipitation efficiency. When compared side-by-side, PEG6000 is slightly more efficient, enabling high yields (>97%) to be obtained for concentrations of 14% and above compared to PEG3350 where concentrations of at least 18% are needed to obtain similar yields, regardless of the $ZnCl_2$ concentration used.

The key to a successful precipitation capture step is an efficient harvest and resolubilization of the precipitate. Based on the mechanism of $ZnCl_2$ precipitation described, resolubilization was achieved by lowering the pH to 3. At this pH value, Zn^{2+} cations are no longer able to crosslink with specific protein amino acids residues (particularly histidine and cysteine residues), due to their protonation [16,37]. This resolubilization approach proved to be efficient, as the yields obtained through the soluble antibody remaining in the supernatant (Figure 3.2.) and the resolubilized precipitated antibody (data not shown) were very similar.

3.3.1.2. Precipitation of artificial IgG and FBS mixture

To assess the potential selectivity of PEG and $ZnCl_2$ for the precipitation of antibodies, the precipitation of key proteins was performed over the same range of PEG concentrations with the most promising $ZnCl_2$ concentrations previously established – 6 and 10 mM, at pH 7. FBS was chosen to represent impurities since culture media of mammalian cells are occasionally supplemented with 5-10%(v/v) serum, and additionally, it also simulates plasma protein fractionation [38]. According to Figure 3.2. C and D, neither the concentration nor the molecular weight of PEG appears to influence the precipitation of serum proteins, unlike the $ZnCl_2$ concentration which appears to promote FBS proteins precipitation at higher concentrations. Even so, for the highest zinc concentration tested in pure IgG solution experiments (10 mM), only less than 20% of FBS precipitated (Figure 3.2. C and D).

After establishing that the PEG/$ZnCl_2$ system successfully precipitates antibodies but not FBS proteins, precipitation of antibodies from an artificial mixture composed of 2 g/L IgG and 5% (w/v) FBS was subsequently evaluated, envisaging process integration into a purification platform of IgG from antibody-producing cell culture fluids or from animal serum.

Given that PEG concentration did not seem to influence FBS precipitation, further precipitation of the artificial mixture was carried out with the minimal concentrations of PEG necessary to precipitate pure IgG with the highest yields, over the same $ZnCl_2$ concentrations (2-10 mM). According to Figure 3.2. and as seen in pure IgG precipitation experiments, antibody yield increases with increasing PEG and $ZnCl_2$ concentrations and PEG molecular weight, but in general the differences are minimal; yields between 92-98% were obtained with 14-16% (w/v) PEG3350, while 14% (w/v) PEG6000 enabled to precipitate over 99% of antibodies. After precipitation, the precipitate was dissolved and measured with Protein G affinity chromatography for purity. Antibody purity increased from an initial 50% to 85-90%, which is comparable to the 90% purity presented by Burgstaller *et al.,* [21] and Li *et al.,* [11] (Figure 3.3.). Although the purity values obtained are very similar, a decrease in purity is observed for increasing PEG and $ZnCl_2$ concentrations and PEG molecular weight, unlike what was observed for the yield. The decrease in purity with the addition of higher $ZnCl_2$ concentrations is not unexpected since Zn^{2+} is known to form complexes with BSA, the major component of the serum, by binding to the protein site-I and site-II, thus favoring its precipitation [39]. Besides, it is possible that this cation binds to other proteins of the serum such as transferrin. SDS-PAGE analyses of precipitate samples (see supplementary material) confirmed the high purities obtained, with most impurities (FBS) remaining in the supernatant. Based on total protein and antibody concentration, it was determined that 85-90% of impurities were removed.

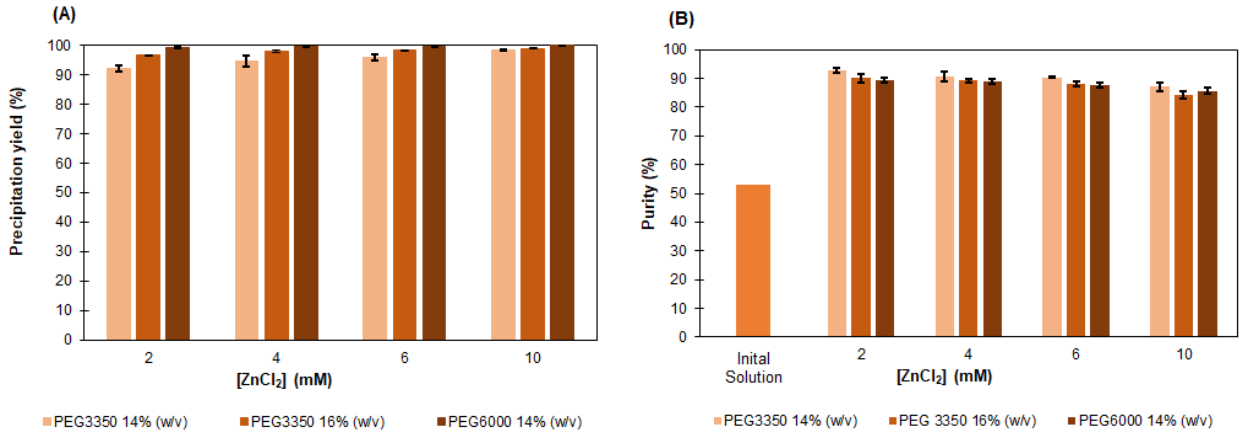

Figure 3.3. Precipitation yield (A) and purity (B) of IgG from artificial IgG and FBS mixture with increasing PEG and $ZnCl_2$ concentrations. Experiments were performed at pH 7. Affinity chromatography and BCA assay were used to determine the mass of IgG and total protein, respectively. All values shown are mean values of triple determinations.

The best precipitation condition should aim at a higher yield than purity since precipitation is usually used as an initial recovery step and it is preferable to recover as much IgG as possible in the first unit operations of a purification process. Thus, for further continuous precipitation in the reactor, 14% (w/v) PEG6000 combined with 4 mM $ZnCl_2$ were selected, which allowed the overall recovery of over 99% of IgG with 88% purity and a removal of 89% of impurities.

3.3.2. Continuous precipitation

In this study, the transition from batch to continuous precipitation of antibodies was carried out with an OFR (Figure 3.1.), under the optimal conditions established – 14% (w/v) PEG6000 and 4 mM $ZnCl_2$. The feed (artificial IgG and FBS mixture) was first mixed with $ZnCl_2$ solution to initiate precipitate nucleation and only after PEG was added as volume exclusion agent to facilitate the growth of the precipitates, since simultaneous addition of these precipitants appears to be less efficient [11]. Samples were collected at the reactor outlet, after four residence times, to guarantee that the steady-state conditions had been achieved, and during one residence time. In

the literature, for precipitation processes, two to three residence times are usually used as a criterion to start sample collecting [31]. To investigate the effect of the number of residence times (ratio between process time t and residence time τ – t/τ) on the steady state, the concentration of proteins at the OFR outlet was measured at different times, confirming that steady state has been achieved at the time set for sample collection, i.e., four residence times (Figure 3.4.). Sample collection could be performed earlier, *e.g.*, after three residence times. After two residence times, there is still some variability between assays, which is no longer observed at 3 or 4 residence times.

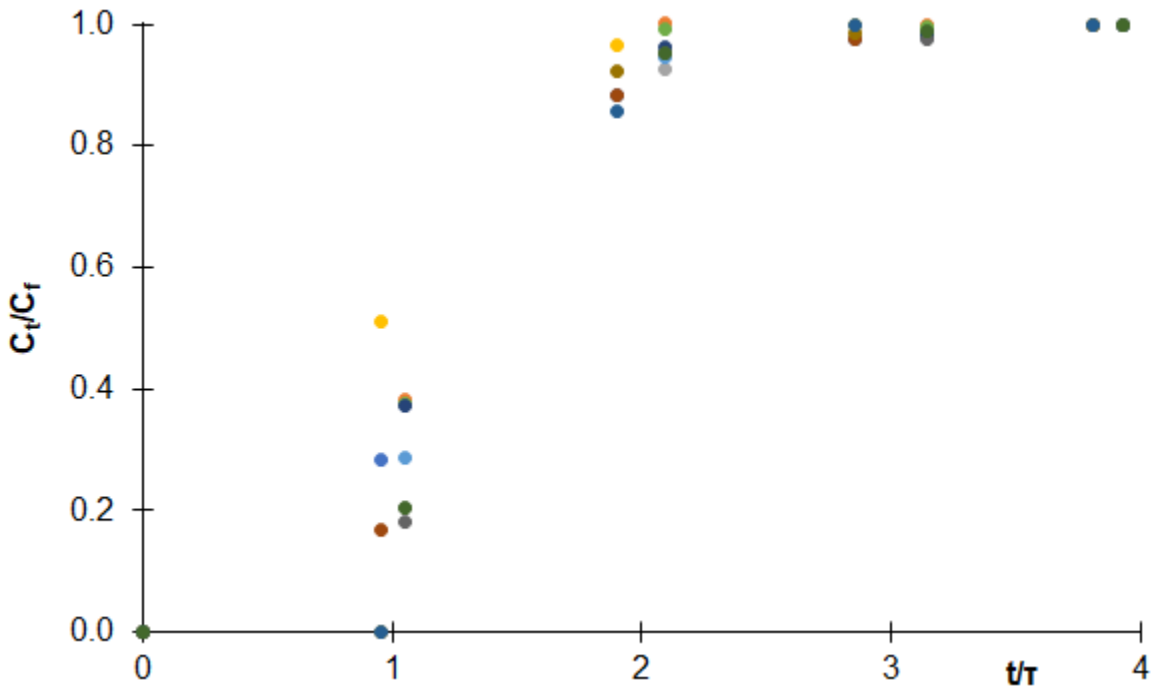

Figure 3.4. Evolution of the ratio between relative total protein concentration (C_t/C_f) over the number of residence times (ratio between process time and residence times – t/τ). Different colours represent distinct conditions of amplitude, frequency and total flow rate: 2 mm, 5 Hz, 4 mL/min; 1 mm, 5 Hz, 22 mL/min; 3 mm, 1 Hz, 22 mL/min; 2 mm, 5 Hz, 40 mL/min; 2 mm, 3 Hz, 22 mL/min (three times); 1 mm, 1 Hz, 22 mL/min; 1 mm, 3 Hz, 40 mL/min; 2 mm, 3 Hz, 22 mL/min; 2 mm, 1 Hz, 4 mL/min; 3 mm, 3 Hz, 4 mL/min; 3 mm, 3 Hz, 4 mL/min; 3 mm, 5 Hz, 22 mL/min. All values shown are from a unique determination.

The impact of the operating variables of the reactor, namely the total net flow rate (Q), oscillation frequency (f) and oscillation amplitude (x_0), on the yield and purity of IgG was assessed and statistically optimized through BBD. The ranges employed were selected based on the literature and preliminary studies, regarding frequency and flow rate, respectively, while the amplitude values, which correspond to the center-to-peak amplitude measured in the straight section of the tube, were selected to ensure that the highest amplitude tested would not enable the movement of the total fluid of more than one constriction (0.344 mL). The yields obtained (Figure 3.5.) were all very similar (97-99%), but nonetheless some conclusions can be drawn. Figure 3.5. shows that the yield generally increases as the flow rate increases, regardless of the oscillation frequency and amplitude, since the increase of kinetic energy at higher flow rates leads to faster collision of particles, thus enhancing precipitation [40]. In addition, increasing the frequency of oscillations from 1 to 5 Hz, in general, improved the yield for the three studied flow rates. The increase in the frequency enables to reach greater oscillatory velocities, which should be higher than the net flow velocity to ensure the full flow reversal necessary for an efficient mixing. Interestingly, the amplitude does not seem to influence much the yield, which was unexpected since previous studies had demonstrated that amplitude has a predominant role in fluid mixing by controlling the axial dispersion (length of the eddy), whereas frequency affects radial mixing [41]. Since higher amplitudes lead to the formation and faster destruction of eddies, which are crucial for efficient mixing, low/medium amplitudes are usually desired to achieve the highest yields [40].

Unlike batch experiments where the precipitation yields and overall yields were very similar, the analysis of the collected precipitate from the continuous precipitation runs originates yields of only 86-90%, implying that 10% of IgG was not recovered. Indeed, after centrifugation a detachment of the precipitate was visible when removing the supernatant, suggesting that centrifugation should be performed at higher centrifugal force/time or replaced with another harvest operation to avoid precipitate loss (*e.g.*, TFF). In addition, Hammerschmidt *et al.,* have reported that yield was enhanced when using TFF compared with centrifugation [17].

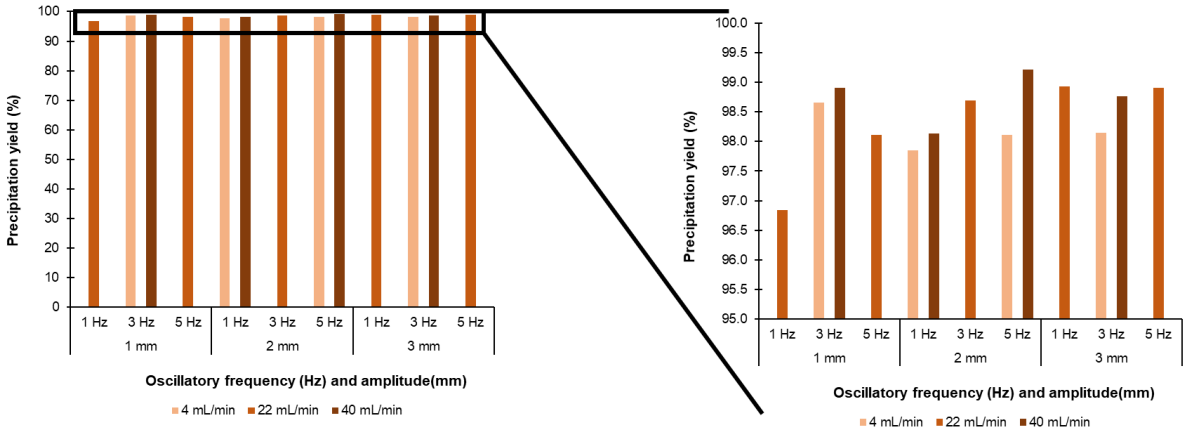

Figure 3.5. Antibody yield from continuous precipitation of artificial IgG and FBS mixture in the OFR, under different operating conditions. Precipitation was performed with 14% PEG6000 and 4 mM ZnCl2 at pH 7. The yield was determined based on the quantification of the remaining soluble antibody, by affinity chromatography. Darker colours represent higher flow rates.

Purity values above 87% were obtained for all studied operating conditions and further SDS-PAGE analyses confirmed that in fact most impurities (FBS) did not remain in the precipitate (data not shown). Although the purity of IgG was considered dependent on three independent variables, only two factors – the flow rate and oscillation frequency – were found to significantly affect it (p-value < 0.05) (data not shown). According to the contour plots (Figure 3.6.), frequency and amplitude appear to have opposite effects on the response, with greater purities being achieved with the decrease in frequency. When analyzing the interaction between these two parameters, purity improves at the intervals' boundaries, especially when working at the highest amplitude (3 mm) and lowest frequency (1 Hz). Unlike yield, greater purities are obtained at lower flow rates. At high velocities (or high flow rates), molecules move faster due to the increase of kinetic energy, resulting in increased collision rates. This may lead to a partial loss of the selectivity of precipitation towards IgG, resulting in the precipitation/inclusion of impurities in crystal lattice and, consequently, in lower purities.

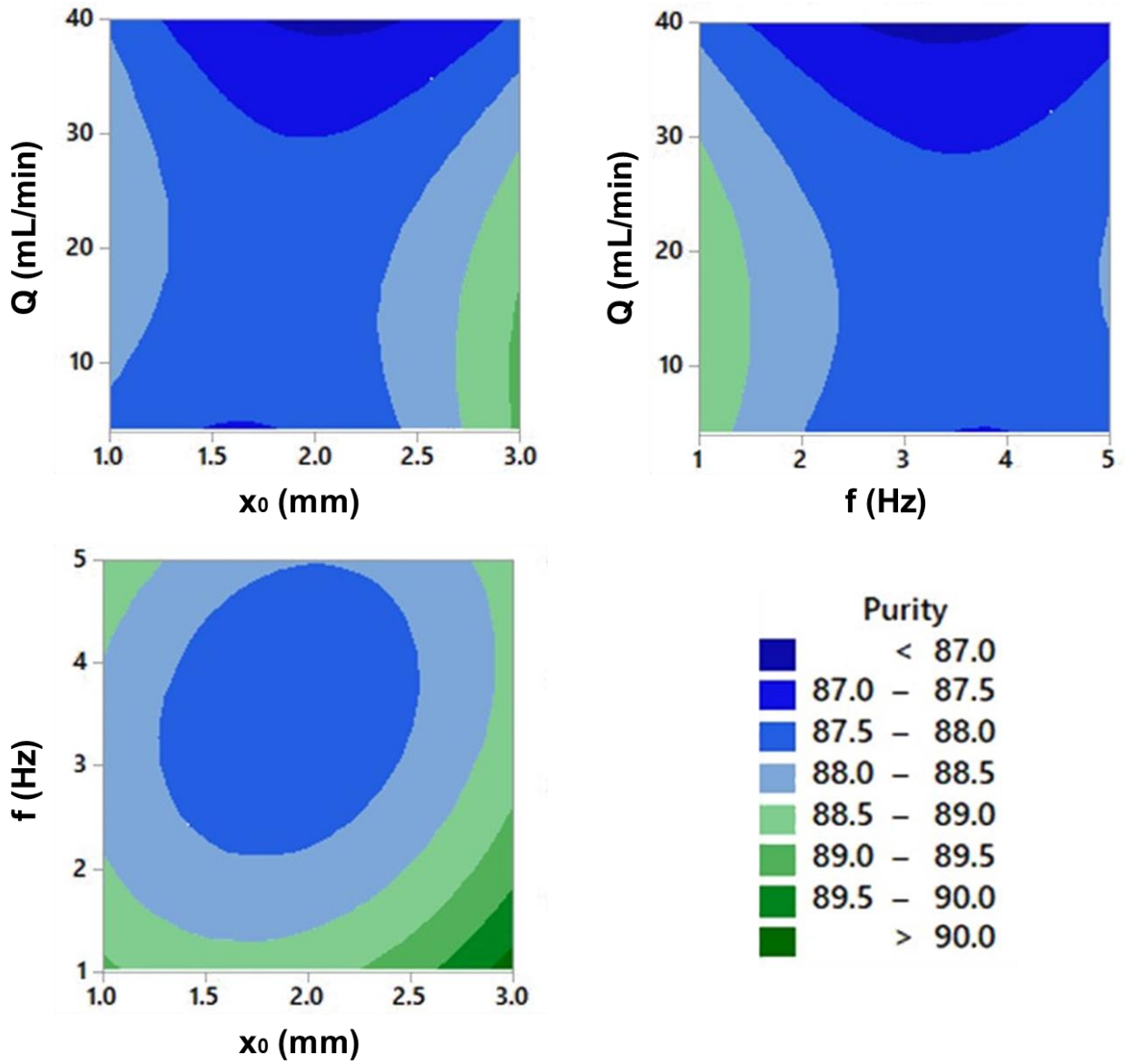

Figure 3.6. Two-dimensional contour plots showing the interaction effects of flow rate (*Q*), amplitude (x_0) and frequency (*f*) on antibody purity. The greener the graphic, the higher the purity under those conditions would be. Thus, the optimal response is found to be at the maximum amplitude (3 mm), minimum frequency (1 Hz) and low flow rate (6 mL/min).

The designed model is able to explain 93.97% of the variations observed and predicts that an optimal purity of 90.6% could be achieved when operating at 6 mL/min with an amplitude of 3

mm and frequency of 1 Hz. The total residence time in the OFR under these conditions is 7 min, which is between the 2.5 min and the 22.5 min used by Burgstaller *et al.,* [21] for antibody precipitation in a tubular reactor. In their case, the precipitation yield and the antibody purity were both around 80%, respectively, for all residence times used. In this work, the continuous precipitation of antibodies was performed under the optimal operating conditions, using 14% (w/v) PEG6000 and 4 mM $ZnCl_2$, and enabled to recover 99.1 ± 0.2% of antibodies with a purity of 90.0 ± 0.7%, while removing 89.4 ± 0.5% of impurities (Table 3.1.).

Table 3.1. Summary of optimized IgG precipitation from the artificial mixture using 14% (w/v) PEG6000 and 4 mM $ZnCl_2$ in batch mode and continuous mode in the OFR (3 mm, 1 Hz and 6 mL/min). Yield supernatant and yield precipitate refer to IgG yield based on supernatant and precipitate protein measurements, respectively. Values are shown as the mean ± standard deviation.

	Batch	**Continuous**
Residence time (min)	20	7
Yield supernatant (%)	99.7 ± 0.2	99.1 ± 0.2
Yield precipitate (%)	98 ± 1	87 ± 1
Initial purity (%)	53.1±0.0	55 ± 1
Final purity (%)	88.9 ± 0.9	90.0 ± 0.7
Impurity removal (%)	88.7 ± 0.4	89.4 ± 0.5

Burgstaller and co-workers have used a total flow rate of 8 mL/min, modifying the residence time by increasing the reactor volume, between 21.7 and 195 mL, values that are not so different from

the ones used in the present work, namely 6 mL/min and 42 mL of working volume (51 mL of total volume), respectively [21].

3.3.3. Antibody structure stability

Precipitation takes advantage of the aggregation and clustering of proteins. Since aggregation usually leads to activity losses and can even induce adverse immune responses [42], it is important to assess potential changes in the secondary structure of IgG due to phase change during precipitation, the recovery method or the low pH used in resolubilization.

CD spectroscopy was selected as the detection method, as it has been extensively used for determination of protein structure and for monitoring conformational changes. Samples purified by precipitation and resolubilized did not reveal any changes in the secondary structure when compared to IgG that did not undergo precipitation (spectra were strikingly similar) (Figure 3.7.).

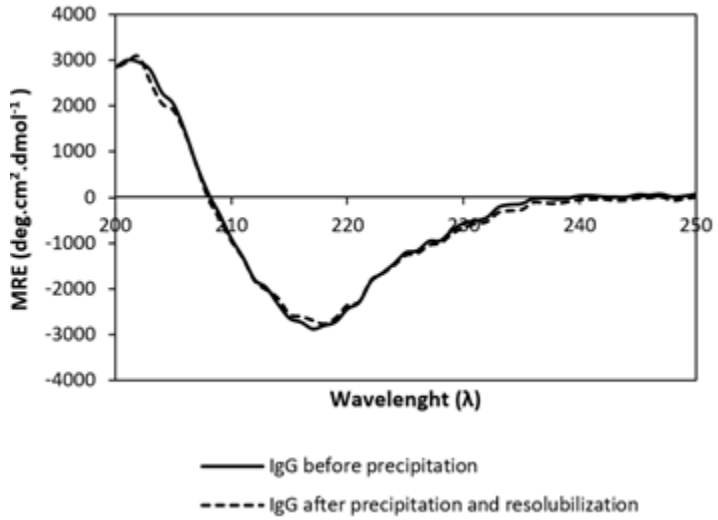

Figure 3.7. Comparison of far-UV CD spectra of IgG before and after precipitation and resolubilization. Before CD spectroscopy, the resolubilized precipitate was purified by Protein G affinity chromatography and buffer-exchanged into milli-Q water using a desalting column to avoid buffer interferences.

3.4. Conclusion

Advances in genetic engineering have turned antibodies into the best-selling drugs in the biopharmaceutical market. To keep up with the increasing demand and advances in production, alternative purification methods, that are both efficient and cost-effective, need to be adopted. The work herein presented demonstrated that continuous precipitation using an OFR is a viable technique for the initial purification of human antibodies, exemplified by the purification of IgG from an artificial IgG and FBS mixture, enabling to recover over 99% of antibodies with 90% purity.

The combination of different precipitants, namely PEG/NaCl and PEG/$ZnCl_2$, was successfully evaluated in batch under different pH, with precipitation proven to be the most efficient when performed with 14% (w/v) PEG6000 and 4 mM $ZnCl_2$ at pH 7. Transferring precipitation to continuous operation mode was demonstrated in an OFR with the sequential addition of $ZnCl_2$ and PEG. The influence of the operating variables of the reactor, namely the total flow rate, the frequency and the amplitude of oscillations were studied and optimized through DoE construction with regards to yield and purity. Higher yields were obtained under high turbulence (high flow rate, high frequency and medium amplitude), contrarily to purity, suggesting that high turbulence may lead to a partial loss of selectivity.

CD spectroscopy did not reveal any changes in the secondary structure of antibodies after precipitation, centrifugation and resolubilization. Unlike resolubilization of the precipitate using a low-pH buffer which proved to be an efficient approach, recovery of the precipitate by centrifugation after continuous precipitation caused a partial loss of IgG due to the visible detachment of the precipitate when removing the supernatant.

The process herein described showed results comparable to the continuous precipitation studies in the literature using tubular reactors, with the advantage of the OFR operation allowing higher yields. Besides, additional units can be added in series to increase its volume capacity, making OFR promising to integrate precipitation into a large-scale purification sequence.

To conclude, this work sets foundations that can contribute to the implementation of continuous precipitation in downstream processing of therapeutic antibodies as a single capture step, using

an oscillatory flow reactor, although further research and optimization are still needed, particularly using other complex feedstocks, namely cell culture supernatants and animal serum, since real feedstocks have a lower initial IgG purity (typically around 30%) than the artificial feed tested (50% purity).

3.5. References

[1] R.-M. Lu, Y.-C. Hwang, I.-J. Liu, C.-C. Lee, H.-Z. Tsai, H.-J. Li, H.-C. Wu, Development of therapeutic antibodies for the treatment of diseases, J. Biomed. Sci. 27 (2020) 1–30. doi:https://doi.org/10.1186/s12929-019-0592-z.

[2] D.S. Chahar, S. Ravindran, S.S. Pisal, Monoclonal antibody purification and its progression to commercial scale, Biologicals. 63 (2020) 1–13. doi:https://doi.org/10.1016/j.biologicals.2019.09.007.

[3] M. Kuczewski, E. Schirmer, B. Lain, G. Zarbis-Papastoitsis, A single-use purification process for the production of a monoclonal antibody produced in a PER. C6 human cell line, Biotechnol. J. 6 (2011) 56–65. doi:https://doi.org/10.1002/biot.201000292.

[4] B. Somasundaram, K. Pleitt, E. Shave, K. Baker, L.H.L. Lua, Progression of continuous downstream processing of monoclonal antibodies: Current trends and challenges, Biotechnol. Bioeng. 115 (2018) 2893–2907. doi:https://doi.org/10.1002/bit.26812.

[5] A.M. Azevedo, P.A.J. Rosa, I.F. Ferreira, A. Pisco, J. De Vries, R. Korporaal, T.J. Visser, M.R. Aires-Barros, Affinity-enhanced purification of human antibodies by aqueous two-phase extraction, Sep. Purif. Technol. 65 (2009) 31–39. doi:https://doi.org/10.1016/j.seppur.2008.03.006.

[6] H.F. Liu, J. Ma, C. Winter, R. Bayer, Recovery and purification process development for monoclonal antibody production, MAbs. 2 (2010) 480–499. doi:https://doi.org/10.4161/mabs.2.5.12645.

[7] B. Kelley, Very large scale monoclonal antibody purification: the case for conventional unit operations, Biotechnol. Prog. 23 (2007) 995–1008. doi:https://doi.org/10.1021/bp070117s.

[8] S. Großhans, G. Wang, C. Fischer, J. Hubbuch, An integrated precipitation and ion-exchange chromatography process for antibody manufacturing: process development strategy and continuous chromatography exploration, J. Chromatogr. A. 1533 (2018) 66–76. doi:https://doi.org/10.1016/j.chroma.2017.12.013.

[9] A.M. Azevedo, P.A.J. Rosa, I.F. Ferreira, M.R. Aires-Barros, Chromatography-free recovery of biopharmaceuticals through aqueous two-phase processing, Trends Biotechnol. 27 (2009) 240–247. doi:https://doi.org/10.1016/j.tibtech.2009.01.004.

[10] J. Thömmes, M. Etzel, Alternatives to chromatographic separations, Biotechnol. Prog. 23 (2007) 42–45. doi:https://doi.org/10.1021/bp0603661.

[11] Z. Li, Q. Gu, J.L. Coffman, T. Przybycien, A.L. Zydney, Continuous precipitation for monoclonal antibody capture using countercurrent washing by microfiltration, Biotechnol. Prog. 35 (2019) e2886. doi:https://doi.org/10.1002/btpr.2886.

[12] O. Yang, S. Prabhu, M. Ierapetritou, Comparison between batch and continuous monoclonal antibody production and economic analysis, Ind. Eng. Chem. Res. 58 (2019) 5851–5863.

[13] A.M. Azevedo, A.G. Gomes, P.A.J. Rosa, I.F. Ferreira, A.M.M.O. Pisco, M.R. Aires-Barros, Partitioning of human antibodies in polyethylene glycol–sodium citrate aqueous two-phase systems, Sep. Purif. Technol. 65 (2009) 14–21. doi:https://doi.org/10.1016/j.seppur.2007.12.010.

[14] W. Chen, X. Li, M. Guo, F.J. Link, S.S. Ramli, J. Ouyang, I. Rosbottom, J.Y.Y. Heng, Biopurification of monoclonal antibody (mAb) through crystallisation, Sep. Purif. Technol. 263 (2021) 118358. doi:https://doi.org/10.1016/j.seppur.2021.118358.

[15] W. Liu, X. Fan, X. Wang, Z. Bao, Y. Sun, K. Rai, A. Shaliutina-Kolešová, J. Su, M. Xian, R. Nian, Salt-enhanced permeabilization for monoclonal antibody precipitation and purification in a tubular reactor with a depth filtration membrane with advanced chromatin extraction, Biochem. Eng. J. 151 (2019) 107332. doi:https://doi.org/10.1016/j.bej.2019.107332.

[16] G. Dutra, D. Komuczki, A. Jungbauer, P. Satzer, Continuous capture of recombinant antibodies by ZnCl2 precipitation without polyethylene glycol, Eng. Life Sci. 20 (2020) 265–274. doi:https://doi.org/10.1002/elsc.201900160.

[17] N. Hammerschmidt, B. Hintersteiner, N. Lingg, A. Jungbauer, Continuous precipitation of IgG from CHO cell culture supernatant in a tubular reactor, Biotechnol. J. 10 (2015) 1196–1205. doi:https://doi.org/10.1002/biot.201400608.

[18] B. Kelley, Industrialization of mAb production technology: the bioprocessing industry at a crossroads, in: MAbs, Taylor & Francis, 2009: pp. 443–452. doi:https://doi.org/10.4161/mabs.1.5.9448.

[19] A. Tscheliessnig, P. Satzer, N. Hammerschmidt, H. Schulz, B. Helk, A. Jungbauer, Ethanol precipitation for purification of recombinant antibodies, J. Biotechnol. 188 (2014) 17–28. doi:https://doi.org/10.1016/j.jbiotec.2014.07.436.

[20] R. Sommer, P. Satzer, A. Tscheliessnig, H. Schulz, B. Helk, A. Jungbauer, Combined polyethylene glycol and CaCl2 precipitation for the capture and purification of recombinant antibodies, Process Biochem. 49 (2014) 2001–2009. doi:https://doi.org/10.1016/j.procbio.2014.07.012.

[21] D. Burgstaller, A. Jungbauer, P. Satzer, Continuous integrated antibody precipitation with two-stage tangential flow microfiltration enables constant mass flow, Biotechnol. Bioeng. 116 (2019) 1053–1065. doi:https://doi.org/10.1002/bit.26922.

[22] Q. Gu, Z. Li, J.L. Coffman, T.M. Przybycien, A.L. Zydney, High throughput solubility and redissolution screening for antibody purification via combined PEG and zinc chloride precipitation, Biotechnol. Prog. 36 (2020) e3041. doi:https://doi.org/10.1002/btpr.3041.

[23] S.-L. Sim, T. He, A. Tscheliessnig, M. Mueller, R.B.H. Tan, A. Jungbauer, Protein precipitation by polyethylene glycol: a generalized model based on hydrodynamic radius, J. Biotechnol. 157 (2012) 315–319. doi:https://doi.org/10.1016/j.jbiotec.2011.09.028.

[24] T. Yang, J.L. Cleland, X. Lam, J.D. Meyer, L.S. Jones, T.W. Randolph, M.C. Manning, J.F. Carpenter, Effect of zinc binding and precipitation on structures of recombinant human growth hormone and nerve growth factor, J. Pharm. Sci. 89 (2000) 1480–1485. doi:https://doi.org/10.1002/1520-6017(200011)89:11<1480::AID-JPS10>3.0.CO;2-M.

[25] D.H. Atha, K.C. Ingham, Mechanism of precipitation of proteins by polyethylene glycols. Analysis in terms of excluded volume., J. Biol. Chem. 256 (1981) 12108–12117. doi:https://doi.org/10.1016/S0021-9258(18)43240-1.

[26] G.L. Foutch, A.H. Johannes, Reactors in process engineering, Encycl. Phys. Sci. Technol. (2003) 652–654. doi:https://doi.org/10.1016/B0-12-227410-5/00654-2.

[27] P. Stonestreet, A.P. Harvey, A mixing-based design methodology for continuous oscillatory flow reactors, Chem. Eng. Res. Des. 80 (2002) 31–44. doi:https://doi.org/10.1205/026387602753393204.

[28] M.S.R. Abbott, A.P. Harvey, G.V. Perez, M.K. Theodorou, Biological processing in oscillatory baffled reactors: operation, advantages and potential, Interface Focus. 3 (2013) 20120036. doi:https://doi.org/10.1098/rsfs.2012.0036.

[29] F. Castro, A. Ferreira, J.A. Teixeira, F. Rocha, Protein crystallization as a process step in a novel meso oscillatory flow reactor: study of lysozyme phase behavior, Cryst. Growth Des. 16 (2016) 3748–3755. doi:https://doi.org/10.1021/acs.cgd.6b00262.

[30] P. Cruz, F. Rocha, A. Ferreira, Effect of operating conditions on batch and continuous paracetamol crystallization in an oscillatory flow mesoreactor, CrystEngComm. 18 (2016) 9113–9121. doi:https://doi.org/10.1039/C6CE01648K.

[31] F. Castro, A. Ferreira, F. Rocha, A. Vicente, J.A. Teixeira, Continuous-flow precipitation of hydroxyapatite at 37 C in a meso oscillatory flow reactor, Ind. Eng. Chem. Res. 52 (2013) 9816–9821. doi:https://doi.org/10.1021/ie400710b.

[32] T. McGlone, N.E.B. Briggs, C.A. Clark, C.J. Brown, J. Sefcik, A.J. Florence, Oscillatory flow reactors (OFRs) for continuous manufacturing and crystallization, Org. Process Res. Dev. 19 (2015) 1186–1202. doi:https://doi.org/10.1021/acs.oprd.5b00225.

[33] P.C. Cruz, C.R. Silva, F.A. Rocha, A.M. Ferreira, Mixing Performance of Planar Oscillatory Flow Reactors with Liquid Solutions and Solid Suspensions, Ind. Eng. Chem. Res. 60 (2021) 2663–2676. doi:https://doi.org/10.1021/acs.iecr.0c04991.

[34] Y. Shih, J.M. Prausnitz, H.W. Blanch, Some characteristics of protein precipitation by salts, Biotechnol. Bioeng. 40 (1992) 1155–1164. doi:https://doi.org/10.1002/bit.260401004.

[35] E.D. Strange, D.L. Van Hekken, V.H. Holsinger, Effect of sodium chloride on the solubility of caseins, J. Dairy Sci. 77 (1994) 1216–1222. doi:https://doi.org/10.3168/jds.S0022-0302(94)77060-0.

[36] A. Ferreira, F. Rocha, J.A. Teixeira, F. Castro, M.S.V.P. Ferreira, Modular oscillatory flow plate reactor, 2017.

[37] H. V Iyer, T.M. Przybycien, A model for metal affinity protein precipitation, J. Colloid Interface Sci. 177 (1996) 391–400. doi:https://doi.org/10.1006/jcis.1996.0049.

[38] M. Arora, Cell culture media: a review, Mater Methods. 3 (2013) 24. doi:https://doi.org/10.13070/mm.en.3.175.

[39] S. Ostojić, V. Dragutinović, M. Kićanović, B.R. Simonović, A DSC study of zinc binding to bovine serum albumin (BSA), J. Serbian Chem. Soc. 72 (2007) 331–337. doi:https://doi.org/10.2298/JSC0704331O.

[40] F. Castro, A. Ferreira, J.A. Teixeira, F. Rocha, Influence of mixing intensity on lysozyme crystallization in a meso oscillatory flow reactor, Cryst. Growth Des. 18 (2018) 5940–5946. doi:https://doi.org/10.1021/acs.cgd.8b00721.

[41] N. Reis, A.A. Vicente, J.A. Teixeira, M.R. Mackley, Residence times and mixing of a novel continuous oscillatory flow screening reactor, Chem. Eng. Sci. 59 (2004) 4967–4974. doi:https://doi.org/10.1016/j.ces.2004.09.013.

[42] S. Hermeling, D.J.A. Crommelin, H. Schellekens, W. Jiskoot, Structure-immunogenicity relationships of therapeutic proteins, Pharm. Res. 21 (2004) 897–903. doi:10.1023/b:pham.0000029275.41323.a6.

3.S. Supplementary Material

3.S.1. Purity determination by Protein G chromatography

The samples prepared according to Table 3.S.1 were loaded into the Protein G chromatography column (POROS Protein G affinity column; 2.1 x 30 mm; 0.1 mL; Applied Biosystems, Foster City, CA, USA) and a regression was built between IgG purity (%) and the ratio between Area IgG to Total Area. The Protein G chromatograms exhibited two peaks: i) a flow-through peak representative of the proteins (impurities) that do not bind to Protein G (the area of which can be called Area Impurities); and ii) an elution peak containing the IgG that is effectively adsorbed by the column (the area of which can be called Area IgG). The Total Area is the sum of these two peaks areas.

Table 3.S.1. Preparation of the samples used to construct a calibration curve to measure the purity.

IgG Purity (%)	IgG (g/L)	FBS (% v/v)
0	0.00	10.0
10	0.44	10.0
20	1.00	10.0
30	1.71	10.0
40	2.67	10.0
50	4.00	10.0
60	4.00	6.67
70	4.00	4.29
80	4.00	2.50
90	4.00	1.11
100	4.00	0.00

It should be noted that this approach is only possible because we are working with an artificial mixture of proteins that do not contain other small molecules that would absorb also at 280 nm. In the case of a real cell culture supernatant, this approach would not be valid.

3.S.2. Protein gel electrophoresis

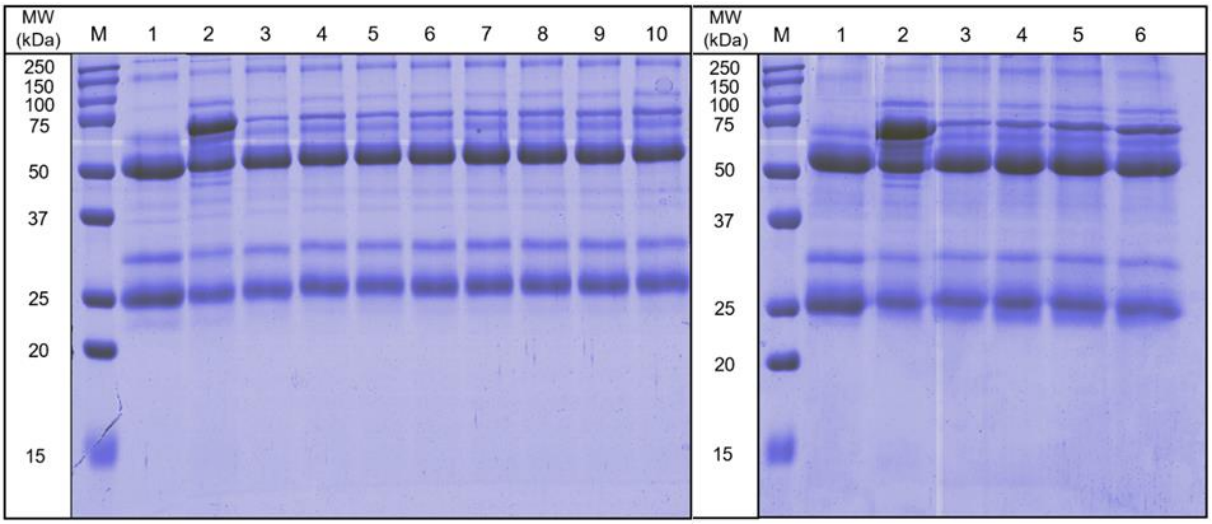

Figure 3.S.2. Qualitative purity analysis of resolubilized precipitates of artificial IgG and FBS mixture by SDS-PAGE electrophoresis. Left: M – Molecular weight marker; Lane 1 – pure IgG feedstock; Lane 2 – Artificial IgG and FBS mixture; Lanes 3-10 – Precipitates obtained from precipitation under the following conditions: Lane 3 – 2 mM $ZnCl_2$ and 14% (w/v) PEG3350; Lane 4 – 2 mM $ZnCl_2$ and 16% (w/v) PEG3350; Lane 5 – 4 mM ZnCl2 and 14% PEG3350; Lane 6 – 4 mM $ZnCl_2$ and 16% (w/v) PEG3350; Lane 7 – 6 mM $ZnCl_2$ and 14% (w/v) PEG3350; Lane 8 – 6 mM $ZnCl_2$ and 16% (w/v) PEG3350; Lane 9 – 10 mM $ZnCl_2$ and 14% (w/v) PEG3550; Lane 10 – 10 mM $ZnCl_2$ and 16% PEG3350. Right: M – Molecular weight marker; Lane 1 – pure IgG feedstock; Lane 2 – Artificial IgG and FBS mixture; Lanes 3-6 – Precipitates obtained from precipitation under the following conditions: Lane 3 – 2 mM $ZnCl_2$ and 14% (w/v) PEG6000; Lane 4 – 4 mM $ZnCl_2$ and 14% (w/v) PEG6000; Lane 5 – 6 mM $ZnCl_2$ and 14% (w/v) PEG6000; Lane 6 – 10 mM $ZnCl_2$ and 14% (w/v) PEG6000. All samples were loaded in the gel with the same mass.

Sodium dodecyl sulfate-polyacrylamide gel electrophoresis (SDS-PAGE) was performed to qualitatively evaluate the purity of the feedstocks and the resolubilized precipitates. Samples were diluted in a loading buffer containing 62.5 mM Tris-HCl pH 6.2, 2% SDS, 0.01% bromophenol blue and 10% glycerol and denatured in reducing conditions (0.1 M DTT) in a water bath at 100

ºC for 10 min. Samples were applied to a 12% acrylamide gel, prepared from a 40% acrylamide/bis-acrylamide stock solution (29:1), and ran at 100 V using a running buffer composed of 25 mM Tris-HCl, 192 mM glycine and 0.1% (w/v) SDS at pH 8.3. The molecular marker used was Precision Plus Protein™ Dual Color Standards (Bio-Rad). Gels were stained overnight with 0.1% Coomassie Brilliant Blue R-250 in 30% ethanol and 10% acetic acid and destained by successively washing with a 30% (v/v) ethanol and 10% (v/v) acetic acid solution.

The SDS-PAGE profile of the human γ-globulins used as model human IgG presents multiple bands under reducing conditions. In addition to the 50 kDa heavy chain band (H) and the 25 kDa light chain (L) other bands appeared, that could correspond to H2L2, H2L, HL, vL, vH, cL, cH, etc.

Chapter 4 – Immuno-affinity chromatography of secretory immunoglobulin A

*This chapter has been published as Ferreira-Faria, D., Scheich, D., Tombak, E. M., Virumäe, K., Männik, A., Jungbauer, A., & Lingg, N. (2024). Capture of fully assembled secretory immunoglobulin A by affinity chromatography with nanobodies as ligands. *Separation and Purification Technology*, *343*, 127009.

Abstract

Secretory immunoglobulin A (sIgA) has a big potential for passive immunization and other therapeutic applications. This complex molecule with a molecular mass of 410 kDa consists of two IgA monomers linked by a connecting chain (JC) and a secretory component (SC). Fully assembled sIgA was overexpressed in CHO cells. In order to exploit the therapeutic potential of recombinant sIgA expressed in CHO cells, a platform process for capture of the antibody, directly from the clarified culture supernatant using available affinity chromatography material, was investigated. The hydrodynamic radius was 10.2 ± 0.9 nm determined by dynamic light scattering and the isoelectric point 5.5 by electrophoretic mobility using the Malvern Zeta sizer. Capture Select IgA and Capture Select IgA-CH1 chromatography media with camelid-derived single-domain antibody fragments comprising the 3 complementary-determining regions (CDRs) domain antibody fragment with a 13 kDa or 14 kDa as ligand have been used to purify the antibody. sIgA was directly captured from the clarified culture supernatant and a highly purified, full-length, correctly assembled sIgA was obtained. The residence time must be in the range of 5-10 min to achieve a high binding capacity. The effective diffusivity of sIgA was in the range of 10^{-9} cm^2 s^{-1} and the equilibrium capacity was in the range of 10 mg/ml packed bed. We conclude that the current version of the resin has a pore size that is too small for this type of molecule to achieve substantial resin utilization and productivity, although affinity ligand-based purification led to high degree of purity suited for an industrial capture process.

4.1. Introduction

Secretory immunoglobulin A (sIgA) has big potential for passive immunization and other therapeutic applications [1-3], and it is the second most abundant type of antibody in the human body, playing a prominent role in host-pathogen defense [4, 5]. sIgA is a large complex molecule consisting of five different polypeptide chains that must be correctly assembled. Monomeric IgA (mIgA) is formed by linking the heavy chain (HC) and light chain (LC) through disulfide bridges. Dimeric IgA (dIgA) is formed linkage of two mIgA to a J chain. Through association with a secretory component (SC) sIgA is formed [6]. In order to exploit the therapeutic potential of recombinant sIgA expressed in CHO cells, a platform process for capture of the antibody directly from the clarified culture supernatant would be desirable. Immunoaffinity chromatography with a single domain antibody ligand is currently the only option for a capture step directly from the culture supernatant. Capture Select IgA binds to the Fc domain of IgA, while Capture Select IgA-CH1 binds to the CH1 domain. Both ligands are immobilized to a typical agarose-based chromatography material. Severe pore diffusion limitation using this agarose-based chromatography material is expected due to the high molecular mass of sIgA. Non-affinity based chromatographic methods have been applied in the purification of sIgA from caprine whey. A combination of flow-through chromatography, followed by a bind and elute step on a macroporous resin have been shown to be effective, but these methods do not meet the criteria of a direct capture of sIgA from culture supernatant [7]. A complex method is to bind dIgA on a protein L column and reconstitute the sIgA by passing the secretory component over the saturated protein L column. This method works only for kappa light chain containing antibodies and the procedure must be modified for lambda light chain containing antibodies [8].

It is obvious that the loading of the sIgA to the affinity chromatography will be severely mass transport/pore diffusion controlled. To understand and model the loading of sIgA on these chromatography materials the molecular size or hydrodynamic radius, isoelectric point and pore size of the affinity chromatography medium are the minimum requirement. The molecular size of a protein can be determined by dynamic light scattering. Modern equipment for measurement

of hydrodynamic radius (Zeta sizer) will also provide information on the electrophoretic mobility at different pH-values and therefore the isoelectric point. The migration of the protein is measured in an electric field yielding into zeta potential [9].

To understand the extend of the expected pore diffusion limitation the pore size, particle size and particle porosity of the chromatography beads must be known inverse size exclusion chromatography (iSEC) is the method of choice to determine the pore size and distribution of compressible chromatography media. A range of non-adsorbing probes such as dextrans with known hydrodynamic radius are injected and from the retention time, the distribution coefficient is determined. The simplest model assumes that the particle contains only cylindrical pores with uniform size and the distribution coefficient can be correlated with radius of the pores. The advantage of the method is that it can be employed at buffer conditions used in the separation process [10-14].

Since severe pore diffusion limitation in the adsorption process is expected, the well know pore diffusion model can be employed to predict the breakthrough curve. It requires effective diffusivity, particle size, and residence time as parameters. The dynamic binding capacity will heavily depend on residence time.

The CHO cell culture supernatant may also contain a greater variety of product-related impurities. Free peptide chains of HC, LC, JC and SC may be present, as well as the formation of dimeric peptides such as LC dimers. More importantly, free mIgA, dIgA or multimers may be formed during production.

The secretory component (SC) bound to the dIgA is a remaining polypeptide of the polymeric immunoglobin receptor, protecting sIgA from degradation [15]. Figure 4.1. shows mIgA as the subclass IgA1, dIgA and sIgA. Differences in the mIgA subclasses have been observed in the constant heavy chains, and the hinge region of IgA1 is extended, providing additional sites for O- and N-glycosylation. 7 N-glycosylation sites are located on the SC and one on the J-chain, adding to the wide range of possible glycosylation profiles [16]. The complex molecule sIgA can be expressed in CHO cells and it is secreted into the culture supernatant. The cells can be removed

by solid-liquid separation such as microfiltration or centrifugation and the clarified supernatant can be subjected to a chromatographic capture step.

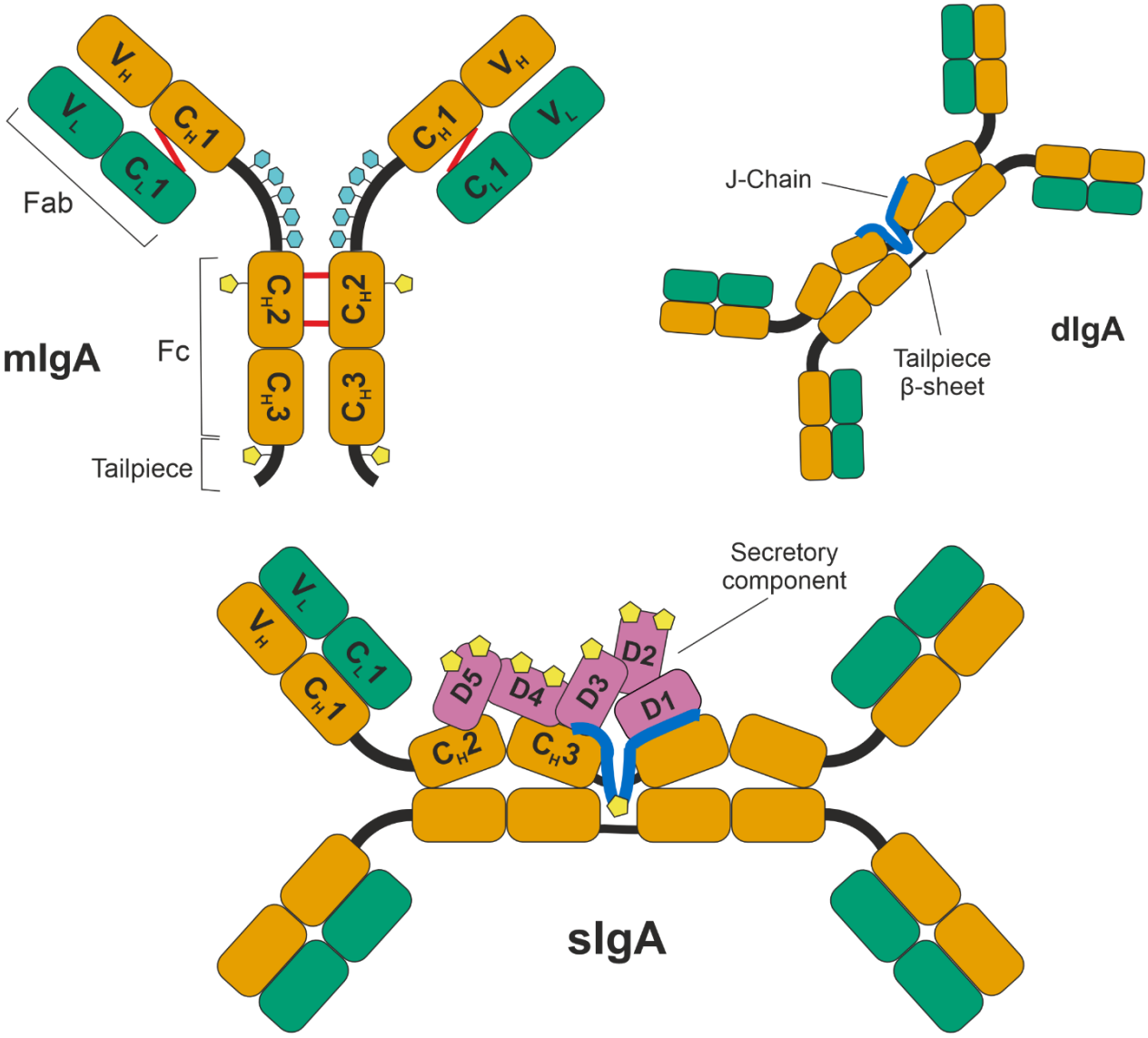

Figure 4.1. Schematic representation of the structure of monomeric IgA (top left), dimeric IgA (top right) connected via the Joining Chain (J-Chain) and secretory IgA (bottom), including the secretory component (SC). Heavy chains (HC) of the IgA molecules are shown in orange, light chains (LC) in green. mIgA is shown as the IgA1 subtype, which has a longer hinge region with up to 5 O-glycosylation (light blue) sites per chain. N-glycosylation sites are shown in yellow and found on the HC, J-Chain and SC. The J-Chain connects with two of the tailpieces of HC, while the

remaining two form a β-sheet. The SC consists of 5 subunits, which reside on one side of the sIgA molecule.

Here, we evaluated the performance of two CaptureSelect resins as a capture step for sIgA. The breakthrough during loading was fitted with a model to characterize diffusional behavior. The hydrodynamic size and pI of purified sIgA was determined, as well as the pore size of the used resins. An economic feasibility analysis was carried out and compared to a protein A purification process for IgG [17-19]. Lastly, a macroporous resin structure is proposed and simulated to show the potential improvement in productivity.

4.2. Materials and Methods

4.2.1. Experimental setup

The CHO cell culture supernatant containing the fully assembled sIgA was kindly provided by Icosagen Cell Factory OÜ. Empty Tricorn 10/50 and 10/100 columns (Cytiva, Sweden) were packed with the affinity resins CaptureSelect IgA and IgA-CH1 (ThermoFisher Scientific, USA). The resulting column volumes were 4.24 mL for CaptureSelect IgA and 4.63 mL for CaptureSelect IgA-CH1. CHO cell culture supernatant was sterile filtered through a 0.22 µm membrane before loading onto the column. An initial equilibration with 2 CV of PBS was followed by the feed loading phase and a 5 CV washing step with PBS once loading was concluded. Elution was carried out with 5 CV of 0.1M Glycine buffer, pH 3.0. An additional washing step of 5 CV PBS was used before stripping the column with 5 CV of 0.5M acetic acid. Experiments were conducted on an ÄKTA Avant 25 chromatography workstation (Cytiva, Sweden) using a UV detector set to 280nm to detect the protein. The chosen residence times were 1.6 (CaptureSelect IgA-CH1) and 1.8 minutes (CaptureSelect IgA) as well as 5 and 10 minutes for both columns. Flowthrough of the loading phase was collected in fractions of 6 mL for offline analytics. The software used was Unicorn 7.6 (Cytiva, Sweden).

4.2.2. sIgA ELISA

A 96-well NUNC MaxiSorp plate (Invitrogen, USA) is coated overnight at 4 °C with of the capture protein SpsA in PBS (5 µg/mL). This pneumococcal surface protein binds specifically to the SC of the sIgA [20, 21]. Afterwards, the plate is washed (PBS-Tween 20) before blocking unoccupied binding spots with 2% w/v BSA in PBS-Tween 20 for one hour at room temperature. Each sample is diluted to an approximate concentration of 200 ng/mL sIgA in PBS-Tween 20 containing 1% w/v BSA. sIgA standard is diluted to 250 ng/mL and a dilution series is carried out for the standard and samples in a separate 96-well plate. The MaxiSorp plate is washed and 100 µL sample are transferred from each well of the dilution plate and incubated under shaking at room temperature for 1 hour. The secondary antibody "anti-hIgA-HRP antibody conjugate" (Invitrogen, USA) is diluted to 100 ng/mL. After washing the plate, 100 µL of the diluted secondary antibody conjugate are applied to each well and incubated shaking at 37 °C for one hour. The plate is washed before staining with TMB Peroxidase EIA Substrate Kit (Bio-Rad, USA). After 5 minutes the reaction is stopped by denaturation of the enzyme with 0.5M sulfuric acid (H_2SO_4) and measured at 405 nm. The intensity of the staining can be correlated to the amount of bound sIgA molecules.

4.2.3. Determination of hydrodynamic radius and isoelectric point

Hydrodynamic radius (R_h) and isoelectric point (pI) of the sIgA were determined using Zetasizer Nano ZSP (Malvern Instruments Ltd., UK). For the determination of the R_h, the eluates of both columns were diluted 10x with MiliQ water and a size distribution was obtained, where the value with the maximum intensity is the R_h of sIgA, since the samples have a high degree of purity. For the determination of the pI, the eluates were diluted 10x in low concentration buffers (10 mM) of different pH values – 3, 4, 5, 6, 7, 8, 9 –, and the zeta potential of the diluted samples was measured. Since the zeta potential is an indication of the surface charge, the pH where this value goes to zero is the pI.

4.2.4. SDS-PAGE

Each sample (5 µL) was mixed with 4× LDS sample buffer (10 µL) (Invitrogen, USA) and water (5 µL). This mixture was heated for 10 min at 95 °C. The prepared samples (15 µL) were loaded onto an SDS-polyacrylamide NuPAGE™ 3-8% Tris-Acetate Protein Gel, 1.0 mm (Invitrogen, USA). To determine molecular weights, 10 µL of HiMark™ Pre-stained Protein Standard (Thermo Fisher Scientific, USA) was used. The electrophoretic separations were run for 90 min at a voltage of 150 V and a current of 400 mA in Tris-Glycine running buffer. Then the gels were incubated in fixing solution for 20 min and afterwards stained for 30 min (0.11% m/V Coomassie R250, 0.02% m/V Bismarck Brown R, 40% ethanol and 10% acetic acid). After treatment with a destaining solution (25% ethanol, 8% acetic acid), the bands were clearly visible. The gel was incubated in RO-H2O for 15 min prior to scanning. During all incubation steps, the gels were gently agitated using an orbital shaker.

4.2.5. Inverse size exclusion

The measurement was carried out using an Agilent 1290 Infinity UPLC system (Agilent, USA) equipped with DAD and refractive index (RI) detector. Capture Select IgA/IgA-CH1 columns were analyzed with pulse injections of 2% v/v acetone solution, pDNA and differently sized dextran standards (Merck, Germany). PBS was used as running buffer for the analysis, preparing the dextran standards (5, 25, 80, 270 and 670 kDa) at a concentration of 10 µg/mL and 5 µg/mL for the 670 kDa standard. The columns were operated at a residence time of 5 minutes. pDNA and acetone signals were measured at 260 and 280nm respectively using the diode array detector. Dextran signals were monitored using the RI detector, all response peaks were analyzed using the software PeakFit. Results were corrected for extra-column volume and column housing. An empty Tricorn 10/50 column was prepared, turning the top adapted down until the two filters are in contact. All pulses were carried out using the column dummy.

4.3. Theory

4.3.1. Chromatography model

A model is needed to describe the diffusional mass transfer rates for spherical porous chromatography beads:

$$\varepsilon_p \frac{\partial c}{\partial t} + \frac{\partial q}{\partial t} = \frac{1}{r^2}\frac{\partial}{\partial r}\left[r^2\left(\varepsilon_p D_p \frac{\partial c}{\partial r} + D_s \frac{\partial q}{\partial r}\right)\right] \quad (4.1)$$

With boundary conditions:

$$t = 0;\ c = 0;\ q = 0 \quad (4.1.1)$$

$$r = 0;\ \frac{\partial c}{\partial r} = 0 \quad (4.1.2)$$

$$r = \varepsilon_p D_p \frac{\partial c}{\partial r} + D_s \frac{\partial q}{\partial r} = k_f \cdot (C - c) \quad (4.1.3)$$

The concentrations *c* and *C* are the pore fluid and external bulk fluid concentrations. ε_p is the porosity of the particles, D_p is the pore diffusion coefficient and D_s is the solid diffusion coefficient, k_f is the film mass transfer coefficient. If $D_s = 0$, pore diffusion models can be employed, typically for porous particles. For column adsorption, mass transfer can be described by:

$$\varepsilon_b \frac{\partial C}{\partial t} + (1 - \varepsilon_b) \cdot \frac{\partial \bar{q}}{\partial t} + u \frac{\partial C}{\partial z} = \varepsilon_b D_L \frac{\partial^2 C}{\partial z^2} \quad (4.2)$$

With boundary conditions:

$$t = 0;\ C = 0 \quad (4.2.1)$$

$$z = 0: uC_0 = uC - \varepsilon_b D_L \frac{\partial C}{\partial z} \quad (4.2.2)$$

$$z = L: \frac{\partial C}{\partial z} = 0 \quad (4.2.3)$$

The column is described by the length of the column *L*, the axial bed length coordinate *z* and ε_b is the bed or total porosity. D_L is the axial dispersion coefficient; *u* is the superficial velocity. When binding is favorable and pore diffusion is dominant, analytical solutions based on the shrinking core model of Weber and Chackraborty [22] are available:

$$n_{pore}(1-\tau_1) = +\frac{15}{2} ln\left[1+(1-X)^{\frac{1}{3}}+(1-X)^{\frac{2}{3}}\right] - \frac{15}{\sqrt{3}} tan^{-1}\left[\frac{2}{\sqrt{3}}(1-X)^{\frac{1}{3}}+\frac{1}{\sqrt{3}}\right] - \frac{n_{pore}}{n_{film}}[\ln(X)+1] + \frac{5\pi}{2\sqrt{3}} - \frac{5}{2} \qquad (4.3)$$

$$n_{pore}\tau_1 < \frac{5}{2} + \frac{n_{pore}}{n_{film}}$$

$$\tau_1 = \left(\frac{u\cdot t}{L} - \varepsilon\right)\cdot\frac{C_0}{(1-\varepsilon)\cdot q_{max}} \qquad X = \frac{C}{C_0} \qquad (4.3.1)$$

$$n_{pore} = \frac{15\cdot(1-\varepsilon)\cdot D_e}{r_p^2}\cdot\frac{L}{u} \qquad n_{film} = \frac{3\cdot(1-\varepsilon)\cdot k_f}{r_p}\cdot\frac{L}{u} \qquad (4.3.2)$$

In case the constant pattern conditions are not met, the general solution is employed:

$$n_{pore} = \frac{15}{2} ln\left[1+(1-X)^{\frac{1}{3}}+(1-X)^{\frac{2}{3}}\right] - \frac{15}{\sqrt{3}} tan^{-1}\left[\frac{2}{\sqrt{3}}(1-X)^{\frac{1}{3}}+\frac{1}{\sqrt{3}}\right] - \frac{n_{pore}}{n_{film}}\ln X + 0.8294 \qquad n_{pore}\tau_1 > \frac{5}{2} + \frac{n_{pore}}{n_{film}} \qquad (4.3.3)$$

n_{pore} and n_{film} describe the number of transfer units for the respective diffusion mechanisms, τ_1 is the dimensionless time, C_{out} is the concentration at the outlet of the column and r_p is the radius of the beads. *L/u* is the residence time. The effective pore diffusivity, D_e, has to be fitted by an iterative process, but the first estimation can be calculated using the following expression:

$$D_e = \frac{K_p \varepsilon_p}{\tau} D_o \qquad (4.4)$$

where K_p is the hindrance parameter for pore diffusion and τ the tortuosity factor for intraparticle diffusion [23]. The diffusivity in the mobile phase D_0 was calculated using the Stokes-Einstein equation [24]:

$$D_0 = \frac{k_B T}{6\pi\mu R_h} \quad (4.5)$$

k_B is the Boltzmann constant (1.38 x 10^{-23} J.K^{-1}), T is the absolute temperature (K), μ is the dynamic viscosity and R_h is the hydrodynamic radius of the solute molecule.

4.3.2. Inverse size exclusion chromatography

iSEC was used to measure the pore dimensions of CaptureSelect resins with dextrane standards. To determine the porosities of the packed columns, pDNA and acetone were injected under non-binding conditions. The different porosities can be calculated from the response signals:

$$\varepsilon_p = \frac{(\varepsilon_p - \varepsilon)}{(1 - \varepsilon)} \quad (4.6)$$

Where:

$$\varepsilon_b = \frac{V_{R,acetone}}{V_C}\ ;\ \varepsilon = \frac{V_{R,pDNA}}{V_C};\ V_{R,pDNA} = V_0 \quad (4.6.1)$$

ε is the void fraction of a packed column, V_R describes a retention volume of a molecule migrating through the column, which is known as the void volume V_0 in case of very large molecules. V_C is the column volume. The distribution coefficient K_D for the differently sized standards is calculated according to:

$$K_D = \frac{V_R - V_0}{V_C - V_0} = \frac{\frac{V_R}{V_T} - \varepsilon}{(1 - \varepsilon)} \quad (4.7)$$

For this case we assume cylindrical pores for the particle. With known hydrodynamic radius of the molecules, the average pore radius, r_{pore}, can be determined:

$$K_D = \varepsilon_p \left(1 - \frac{R_h}{r_{pore}}\right)^2 \quad (4.8)$$

$$R_h = 0.027 \cdot {M_W}^{0.498} \text{ [11]} \quad (4.8.1)$$

r_m is the radius of the injected molecule, in case of globular proteins it can be calculated with the correlation in Equation 4.8.1: The resulting pore radius is further used to estimate the hindrance parameter and the tortuosity, where λ_m is the ratio of the solute molecule radius to the pore radius.

$$K_p = 0.865 \left(1 - 2.1\,\lambda_m + 2.09\,{\lambda_m}^3 - 0.984\,{\lambda_m}^5\right) \quad (4.9)$$

$$\lambda_m = \frac{r_m}{r_p} \quad (4.9.1)$$

4.3.3. Productivity and resin utilization

Economic factors like resin utilization and productivity are used compare different chromatographic processes [25]. They are described by:

$$Pr = \frac{DBC_{10\%}}{\left(t_{load_{10\%}} + t_{rest}\right) V_c\,(1-\varepsilon)} \quad (4.10)$$

$$RU = \frac{DBC_{10\%}}{EBC} = \frac{\int_0^{V_{10\%}} (C_F - C)dv}{V_c\,(1-\varepsilon)\,q_m} \quad (4.11)$$

Pr is the productivity, *EBC* is the equilibrium and $DBC_{10\%}$ is the dynamic binding capacity, given at 10% breakthrough. $t_{load10\%}$ is the required time to reach 10% breakthrough, while t_{rest} combines all other process time intervals. *RU* is the resin utilization and q_m is the maximum binding capacity.

4.4. Results and Discussion

4.4.1. Recovery and characterization of the sIgA

Affinity chromatography was performed as a capture step to recover secretory IgA directly from clarified cell culture supernatant. 40 column volumes (CV) of clarified cell culture supernatant were loaded to either Capture Select IgA (CSA) or Capture Select IgA-CH1 (CSH) at a superficial velocity of 200 cm/h, corresponding to 9 mg sIgA per mL column. Figure 4.2. A and B show the chromatograms for Capture Select IgA or Capture Select IgA-CH1, respectively. Both elution peaks present shoulders, suggesting that more than one molecule is eluting. The product elutes in a considerably broader peak in CSA (Figure 4.2.A) compared to CSH (Figure 4.2.B). Only low concentrations of sIgA can be seen in the clarified cell culture supernatant (Figure .C, lane 1) and no product can be detected in the flow-through and wash fractions (lanes 1-3 and 6-8), suggesting that the column was not overloaded. Several bands can be detected in the eluate fractions from either column, corresponding to sIgA and mIgA with molecular mass of 410 kDa and 160 kDa respectively [26]. Additional bands with molecular mass of, approximately, 250 kDa and, approximately, 117 kDa of unknown identity were also detected. Since these impurity bands are present in both CSA and CSH eluates, they are likely to be molecules comprising both Fc domain – bound by CSA – and the CH1 domain – bound by CSH. Since mIgA, as well as sIgA, present both domains, the recovery of both molecules was expected, but it is unknown if mIgA was already present in the feed material or if its presence resulted from the degradation of sIgA. Even though dIgA can also be co-purified by both resins, no corresponding band was observed in SDS-PAGE.

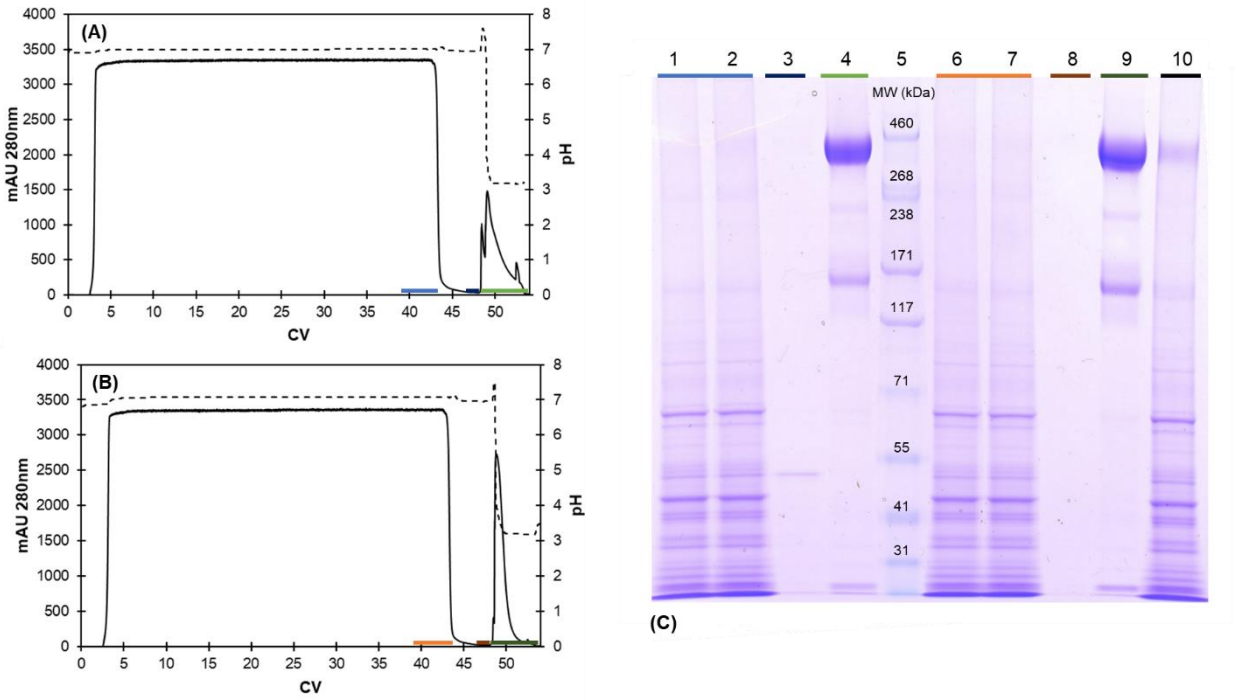

Figure 4.2. Chromatograms for sIgA capture on Capture Select IgA (panel A) and Capture Select IgA-CH1 (panel B). Solid traces represent the absorbance at 280 nm, dashed traces represent the pH. Panel C: SDS-PAGE under non-reducing conditions with Coomassie staining of load, flowthrough, washing and elution fractions of captures shown in panels A and B. Capture Select IgA: Lane 1-2 represent last flowthrough fractions (light blue); Lane 3 represents last wash fraction (dark blue); Lane 4 represents the eluate fraction (light green). Lane 5: molecular weight marker HiMark™ Pre-stained Protein Standard. Capture Select IgA-CH1: Lane 6-7 represent last flowthrough fractions (orange); Lane 8 represents last wash fraction (brown); Lane 9 represents the eluate fraction (dark green). Lane 10 clarified cell culture supernatant/load containing sIgA (black). It is noteworthy that sIgA and mIgA have molecular weights of 410 and 160 kDa, respectively.

4.4.2. Breakthrough curves

Capture Select IgA and Capture Select IgA-CH1 were overloaded at two residence times 1.6 and 5 min, and breakthrough curves (BTC) were established (Figure 4.3.). The pore diffusion model was used to determine the unknown parameters q_m and D_e by a global fit of the breakthrough curves (Table 4.1.). Normally, only the *De* is obtained by fitting the model, but q_m could not be determined experimentally because the purified protein precipitated when the eluate at pH 3 was increased to 7.

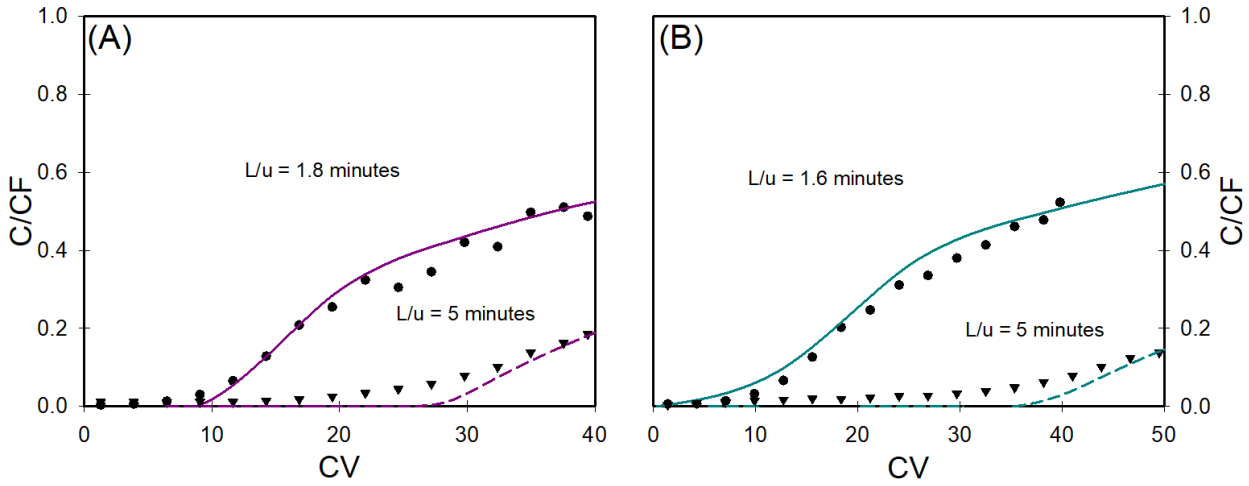

Figure 4.3. Comparison of sIgA breakthrough during the loading phase on CSA (Panel A) and CSH (Panel B) at different residence times. Measured values are plotted as circles and triangles for the low and intermediate residence times, respectively. Solid traces represent the model fit.

The dynamic binding capacity ($DBC_{10\%}$) was also calculated experimentally and estimated with the fitted model for both columns at the different residence times (Table 4.2.). D_e of sIgA in Capture Select IgA and Capture Select IgA-CH1 is more than 48 times lower than the theoretical D_0 of sIgA, indicating that both loading processes are highly mass transfer limited. This large difference between D_0 and D_e is explained that the pore size of the chromatography media is not large enough to accommodate the large protein. The protein to pore size ratio should not be below 0.2 in order to prevent severe hindered diffusion [19, 23]. The resin utilization – defined as

the ratio between $DBC_{10\%}$ and EBC – is below 30% for CSA and CSH, even when the residence time is 5 min. Low resin utilization even at high residence times implies severe mass transfer limitations, requiring very long process times to efficiently utilize the resin.

Table 4.1. Pore diffusion model parameters determined by global fit of the breakthrough curves.

Resin	**CSA**	**CSH**
q_m	38 mg/mL	44 mg/mL
D_e	3.7 x 10^{-9} cm^2/s	3.6 x 10^{-9} cm^2/s

Table 4.2. Dynamic binding capacities observed during breakthrough curve experiments.

	DBC10% (mg/mL)			
	CSA		**CSH**	
L/u (min)	**Experimental**	**Model**	**Experimental**	**Model**
1.8	4.6	4.6	n/a	n/a
1.6	n/a	n/a	5	4.1
5	10	10.9	10.7	11.6

Dynamic and electrophoretic light scattering was used to determine hydrodynamic radius (R_h) and isoelectric point (pI) respectively. Figure 4.4.A shows the distribution of the molecular diameters in the eluates of chromatographic runs from both columns used. The two graphs are very similar,

which was expected because it is the same molecule purified by different methods, and the mean hydrodynamic radius obtained was 10.2 ± 0.9 nm. This value can be compared with the radius of gyration (R_g) present in the literature for sIgA – 8.3 ± 0.2 nm [6]. For proteins, R_g/R_h is between 0.75 – 1.75, which matches 0.81 obtained by comparing our measured R_h with literature R_g [27].

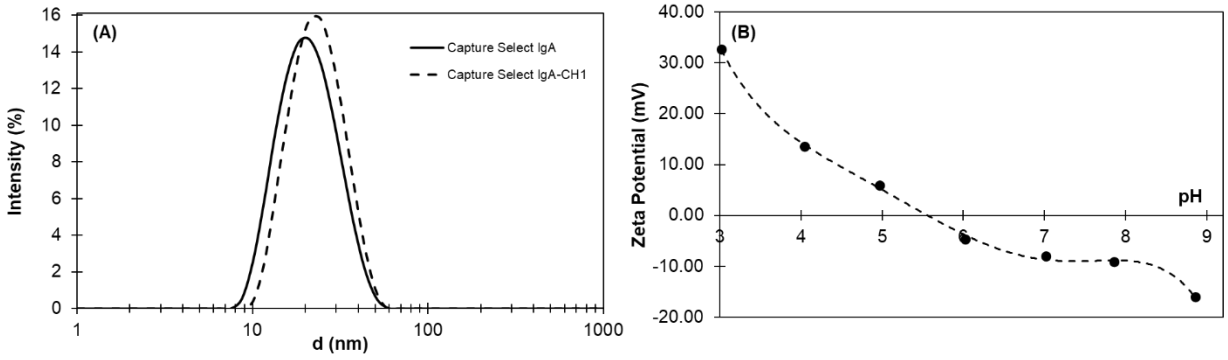

Figure 4.4. Panel A: Determination of the hydrodynamic radius of sIgA from CSA and CSH eluates using DLS. CSA is shown as a solid line and CSH as a dashed line. Panel B shows the Zeta potential of a pool of sIgA eluates in a range of pH 3 to 9.

Figure 4.4.B shows the zeta potential of the concentrated pool of the eluates from both columns at different pH. Applying a linear regression between the value at pH 5 and pH 6, it was possible to find the pI of the sIgA – 5.5 – value in accordance with the range found in the literature – between 5.4 and 6.2 [28]. The determination of the isoelectric point of sIgA is important for two reasons: i) at this pH value, the electrical repulsion between the proteins is minimal, increasing the risk of precipitation, which is very problematic in the chromatography process; ii) the monomeric IgA is the main impurity recovered (Figure 4.2.C), using the same procedure, in future work, to measure its charge at different pH and its pI, the possible difference between the charges of the two molecules can be used in a further ion exchange chromatography to successfully separate them.

4.4.3. Inverse size exclusion chromatography (iSEC)

The average pore size of Capture Select IgA and Capture Select IgA-CH1 columns were analyzed by iSEC (Table 4.3.) with 18.1 and 21.8 nm pore radius. This is in agreement with observations for agarose-based chromatography material [29]. The void fraction (ε) was determined by retention of pDNA, which is unable to enter the pores due to its large hydrodynamic radius of 110 nm [30]. The observed ε values of 0.37 and 0.38 were within the expected range of 0.3 to 0.4 [31]. Acetone, with its high diffusivity and small size, fully penetrated the pores and was employed to measure bed porosities (Equation 4.6.1). The bed porosities (ε_b) determined by acetone retention was 0.95 and 0.93 for Capture Select IgA and Capture Select IgA-CH1, respectively. These results are considered reasonable since agarose resins usually have a high bed porosity of over 0.9. Since the beads in both columns are agarose-based with similar ligands, comparable results were anticipated, which was also true for the particle porosities ε_p which were calculated.

Five dextran probes, ranging from 5 to 670 kDa, were employed to determine the average pore size based on the K_D values. The sIgA molecular radius obtained from DLS measurements and ε_p values facilitated the calculation of the pore size radii for CSA and CSH. For each dextran probe, the pore radius was individually calculated, resulting in an average pore radius of 18.1 ± 3.4 nm for Capture Select IgA and 21.8 ± 3.4 nm for Capture Select IgA-CH1 . Difference between the two resins may be explained by differences in the ε_p values of the respective columns. Previous studies have reported pore size values of 19.4 nm for the base agarose resin at 0M NaCl [12]. The values for λ_m (Equation 4.9.1), representing the ratio of the hydrodynamic radius (R_h) of the solute molecule to the average pore size, ranged from 0.48 to 0.57. It is important to note that this calculation does not account for pore size distribution but focuses solely on the average pore radius.

It is likely that the first sIgA molecule to enter the pore space will restrict further molecules from accessing it. This hinders the diffusion process, leading to a significant reduction in pore diffusion and imposing severe constraints on process economics, especially in below average pores. The tortuosity factor (τ) considers the random orientation of intraparticle pores and characterizes the effective diffusion path of solutes. A small τ suggests unhindered diffusion, typically falling within

the range of 1.5 to 4 for chromatographic matrices. Values exceeding 4 indicate a severe limitation in diffusion. In the case Capture Select IgA and Capture Select IgA-CH1 matrices, the calculated τ values ranged from 5.2 to 7.5. The combination of small pores and high tortuosity contributes to a diminished efficiency in the purification of sIgA using Capture Select IgA and Capture Select IgA-CH1 media primarily due to restricted diffusion.

Table 4.3. Extra particle-, bed- and particle porosities of the CSA and CSH columns. Calculated R_h values of injected dextran standards, molecular weights of the probes were taken from the supplier. K_D values from the dextran probe retention data and the resulting calculated pore sizes for CSA and CSH.

	Porosities		**Dextran probes**	***K_D* values**		**Pore size radius *r_{pore}* (nm)**	
	CSA	**CSH**	**R_h (nm)**	**CSA**	**CSH**	**CSA**	**CSH**
ε	0.37	0.38	1.78	0.74	0.74	18.5	22.1
ε_b	0.95	0.93	3.74	0.50	0.54	14.5	17.2
ε_p	0.91	0.88	6.81	0.31	0.43	16.3	22.4
			12.34	0.06	0.11	16.8	19.1
			19.11	0.04	0.09	24.4	28.4
			Average *r_{pore}* (nm)			18.1	21.8
			Standard deviation (nm)			3.4	3.8

4.4.4. Productivity

A steep drop in $DBC_{10\%}$ at with decreasing residence times can be observed for both resins, as shown in Figure 4.5.A. Capture Select IgA-CH1 performed better at all residence times used, possibly due to its slightly larger pores (see Table 4.3.). Resin utilization and productivity were further calculated, shown and plotted in Figure 4.5.B. The maximum resin utilization achieved was 32.5% for Capture Select IgA-CH1 at 10 minutes residence time. Productivity decreases with increasing resin utilization, indicating that the process should be run at 10-11% *RU* with *Pr* between 0.022 and 0.027 g L^{-1} min^{-1}. If diffusion is not hindered in the process, a bell-shaped relationship is expected. At low resin loadings, the process is inefficient but fast. High resin utilization can only be achieved at the expense of productivity. Optimal operating conditions are at the apex of the curve where productivity is highest [25]. Figure 4.5.B shows that both resins are missing this apex, therefore no optimal conditions are observable.

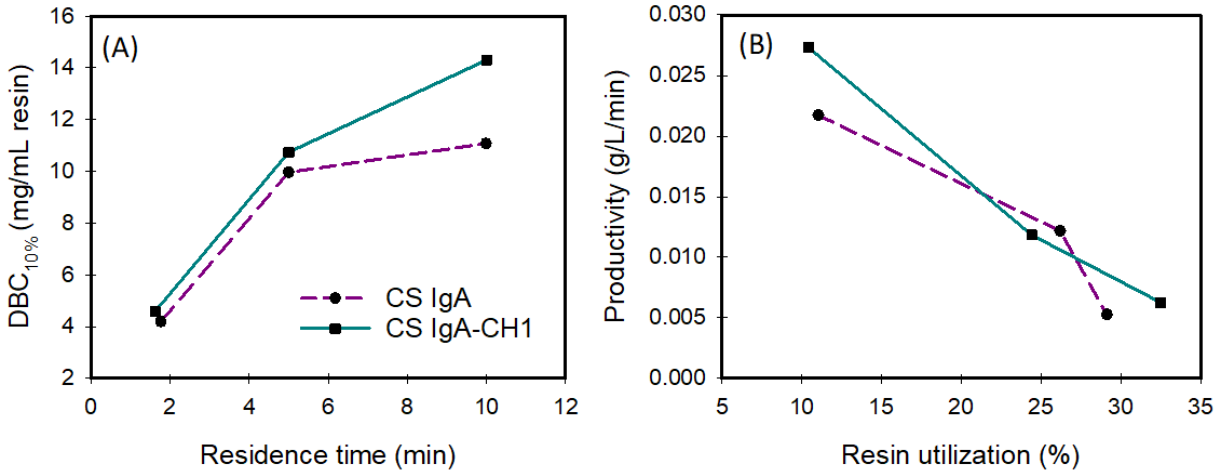

Figure 4.5. Panel A: Experimental data of dynamic binding capacities of CSA and CSH at three residence times. CSA is visualized as a dashed purple line, CSH is the solid dark cyan line. Panel B shows the six data points from Panel A and the corresponding productivity and resin utilization of each experiment.

Productivity was compared with those obtained in protein A chromatography for IgG, where three extreme cases were investigated. Optimal productivity at constant flow rates was 0.71 g L^{-1} min^{-1}

with resin utilization of approximately 38%, which is 26 times lower than the observed values for either affinity resin. This resin would be a prime example to improve productivity either by counter current loading or a velocity gradient during loading [18], because the most gain of productivity and resin utilization is obtained with columns exerting a shallow breakthrough [32].

4.4.5. Theoretical optimization of the resin

While the interaction between ligand and solute molecules is shown to be selective enough to act as an affinity capture step, hindered diffusion is the limiting factor for the chromatographic capture of sIgA in Capture Select IgA and Capture Select IgA-CH1. Adapting the resin structure to a macroporous backbone would result in improved mass transfer and allow for better process performance. We simulated two scenarios of a resin with identical experimental setup. EBC was estimated to be 40 mg sIgA/mL column, around the same capacity as Capture Select IgA and Capture Select IgA-CH1. Increasing the pore size results in a trade-off with the resin surface area. Lower ligand densities are probable, however for this simulation we assumed similar ligand densities and EBC. The effective pore diffusivity of sIgA in the resin was increased, resulting in a better ratio of D_e/D_0.

The apparent D_e/D_0 was 0.02 for Capture Select IgA and Capture Select IgA-CH1, the simulation employed ratios of 0.2 and 0.1 respectively. Ratios of 0.2 have been reported for IgG in MabSelect Protein A resin [33]. We included a ratio of 0.1 to demonstrate the effect of an intermediate increase. Figure 4.6.A shows the breakthrough during loading of CSH at 5 minutes residence time and the simulated resins. The BTCs were calculated utilizing the constant-pattern solution for pore diffusion. Both simulated resins exhibit a steeper breakthrough, improving the DBC by 3-fold in comparison to CSH.

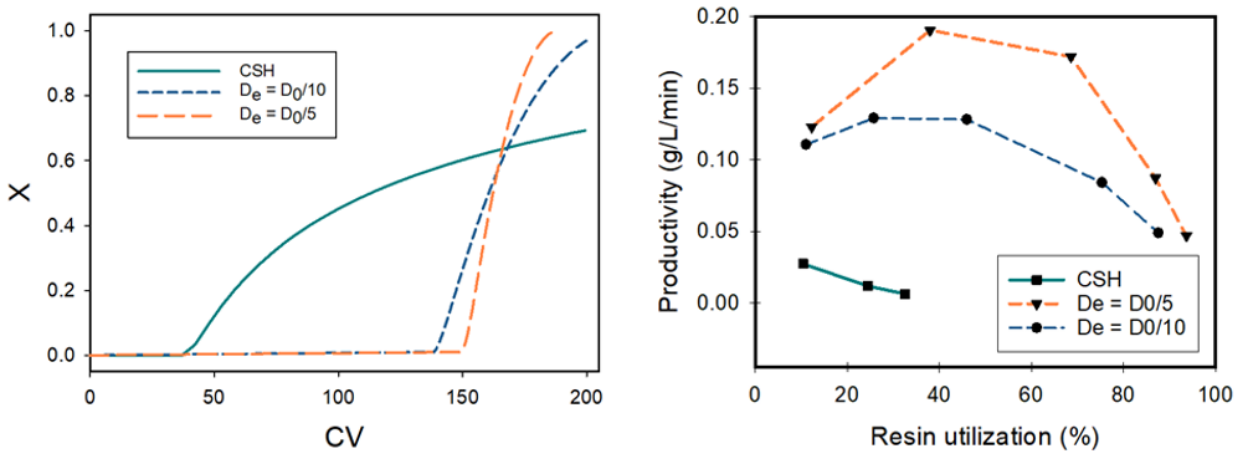

Figure 4.6. Panel A: Comparison of experimental breakthrough behavior of CSH (dark cyan line) with theoretical resins with improved mass transfer. The blue short-dashed line shows the BTC at an effective pore diffusivity at one tenth of the free diffusivity, while the orange dashed line is one fifth of D_0. Panel B: Productivity curve of CSH from Figure 4.5.B plotted with the productivity of the simulated improved resins. 5 different residence times were used in the calculation.

Figure 4.6.B shows the potential improvement in productivity and resin utilization compared to CSH. Calculations were carried out for 5 residence times: 0.5, 1, 2, 5 and 10 minutes. The resulting curves show the expected bell shape for both resins with optimum operating conditions. The apex shifts to lower residence times and resin utilization with increased effective pore diffusivity. At D_e/D_0 ratio of 0.1, the highest productivity observed was 0.129 g L^{-1} min^{-1}, an almost 5-fold increase. When the ratio is 0.2, a theoretical 7-fold improvement in productivity at 0.191 g L^{-1} min^{-1} could be achieved at 1-minute residence time. Adapting the process conditions for the purification of sIgA could further improve the productivity of the capture step.

4.5. Conclusion

It was observed severe mass transfer limitation during immuno-affinity chromatography of secretory immunoglobulin A from CHO cell culture supernatant. This resulted in very low resin

utilization and volumetric productivity. It was assumed that the average pore diameter of the agarose-based affinity resins is very close to the hydrodynamic diameter of the protein of interest. Dynamic light scattering of the protein and inverse size exclusion of the resin confirmed that the average pore diameter was approximately twice the hydrodynamic diameter of sIgA. We compared resin utilization and productivity to a typical protein A process for IgG and propose a resin architecture that would be more suitable for capture of sIgA. A macroporous backbone as alternative could improve process efficiency and productivity. Simulating the capture step of two macroporous resins showed a potential 7-fold increase of volumetric productivity with unhindered diffusion.

4.6. References

[1] P.N. Boyaka, Inducing Mucosal IgA: A Challenge for Vaccine Adjuvants and Delivery Systems, J Immunol, 199 (2017) 9-16.

[2] H.A. Parray, S. Shukla, R. Perween, R. Khatri, T. Shrivastava, V. Singh, P. Murugavelu, S. Ahmed, S. Samal, C. Sharma, S. Sinha, K. Luthra, R. Kumar, Inhalation monoclonal antibody therapy: a new way to treat and manage respiratory infections, Appl Microbiol Biotechnol, 105 (2021) 6315-6332.

[3] A. Richards, D. Baranova, N.J. Mantis, The prospect of orally administered monoclonal secretory IgA (SIgA) antibodies to prevent enteric bacterial infections, Hum Vaccin Immunother, 18 (2022) 1964317.

[4] C. de Fays, F.M. Carlier, S. Gohy, C. Pilette, Secretory Immunoglobulin A Immunity in Chronic Obstructive Respiratory Diseases, Cells, 11 (2022) 1324.

[5] A. Hockenberry, E. Slack, B.M. Stadtmueller, License to Clump: Secretory IgA Structure-Function Relationships Across Scales, Annu Rev Microbiol, 77 (2023) 645-668.

[6] A. Bonner, A. Almogren, P.B. Furtado, M.A. Kerr, S.J. Perkins, Location of secretory component on the Fc edge of dimeric IgA1 reveals insight into the role of secretory IgA1 in mucosal immunity, Mucosal Immunol, 2 (2009) 74-84.

[7] A. Matlschweiger, H. Engelmaier, G. Himmler, R. Hahn, Secretory immunoglobulin purification from whey by chromatographic techniques, J Chromatogr B Analyt Technol Biomed Life Sci, 1060 (2017) 53-62.

[8] B. Moldt, K. Saye-Francisco, N. Schultz, D.R. Burton, A.J. Hessell, Simplifying the synthesis of SIgA: combination of dIgA and rhSC using affinity chromatography, Methods, 65 (2014) 127-132.

[9] M.R. Gittings, D.A. Saville, The determination of hydrodynamic size and zeta potential from electrophoretic mobility and light scattering measurements, Colloids and Surfaces a-Physicochemical and Engineering Aspects, 141 (1998) 111-117.

[10] P. DePhillips, A.M. Lenhoff, Pore size distributions of cation-exchange adsorbents determined by inverse size-exclusion chromatography, J Chromatogr A, 883 (2000) 39-54.

[11] L. Hagel, M. Ostberg, T. Andersson, Apparent pore size distributions of chromatography media, Journal of Chromatography A, 743 (1996) 33-42.

[12] M.C. Stone, G. Carta, Protein adsorption and transport in agarose and dextran-grafted agarose media for ion exchange chromatography, J Chromatogr A, 1146 (2007) 202-215.

[13] Y. Yao, A.M. Lenhoff, Pore size distributions of ion exchangers and relation to protein binding capacity, J Chromatogr A, 1126 (2006) 107-119.

[14] J.F. Langford, M.R. Schure, Y. Yao, S.F. Maloney, A.M. Lenhoff, Effects of pore structure and molecular size on diffusion in chromatographic adsorbents, J Chromatogr A, 1126 (2006) 95-106.

[15] P. Brandtzaeg, H. Prydz, Direct evidence for an integrated function of J chain and secretory component in epithelial transport of immunoglobulins, Nature, 311 (1984) 71-73.

[16] J.M. Woof, M.W. Russell, Structure and function relationships in IgA, Mucosal Immunol, 4 (2011) 590-597.

[17] C.K. Ng, H. Osuna-Sanchez, E. Valery, E. Sorensen, D.G. Bracewell, Design of high productivity antibody capture by protein A chromatography using an integrated experimental and modeling approach, J Chromatogr B Analyt Technol Biomed Life Sci, 899 (2012) 116-126.

[18] T. Eslami, M. Steinberger, C. Csizmazia, A. Jungbauer, N. Lingg, Online optimization of dynamic binding capacity and productivity by model predictive control, J Chromatogr A, 1680 (2022) 463420.

[19] G. Carta, A. Jungbauer, Protein Chromatography, 2010.

[20] Y. Wang, G. Wang, Y. Li, Q. Zhu, H. Shen, N. Gao, J. Xiao, Structural insights into secretory immunoglobulin A and its interaction with a pneumococcal adhesin, Cell Res, 30 (2020) 602-609.

[21] S. Hammerschmidt, S.R. Talay, P. Brandtzaeg, G.S. Chhatwal, SpsA, a novel pneumococcal surface protein with specific binding to secretory immunoglobulin A and secretory component, Mol Microbiol, 25 (1997) 1113-1124.

[22] T.W. Weber, R.K. Chakravorti, Pore and Solid Diffusion Models for Fixed-Bed Adsorbers, Aiche Journal, 20 (1974) 228-238.

[23] J.L. Anderson, J.A. Quinn, Restricted transport in small pores. A model for steric exclusion and hindered particle motion, Biophys J, 14 (1974) 130-150.

[24] J.T. Edward, Molecular volumes and the Stokes-Einstein equation, Journal of Chemical Education, 47 (1970) 261.

[25] S. Ghose, D. Nagrath, B. Hubbard, C. Brooks, S.M. Cramer, Use and optimization of a dual-flowrate loading strategy to maximize throughput in protein-a affinity chromatography, Biotechnol Prog, 20 (2004) 830-840.

[26] L. Sun, S. Kallolimath, R. Palt, K. Stiasny, P. Mayrhofer, D. Maresch, L. Eidenberger, H. Steinkellner, Increased in vitro neutralizing activity of SARS-CoV-2 IgA1 dimers compared to monomers and IgG, Proc Natl Acad Sci U S A, 118 (2021) e2107148118.

[27] M. Nygaard, B.B. Kragelund, E. Papaleo, K. Lindorff-Larsen, An Efficient Method for Estimating the Hydrodynamic Radius of Disordered Protein Conformations, Biophys J, 113 (2017) 550-557.

[28] K.B. Elkon, Isoelectric focusing of human IgA and secretory proteins using thin layer agarose gels and nitrocellulose capillary blotting, J Immunol Methods, 66 (1984) 313-321.

[29] M.C. Nweke, R.G. McCartney, D.G. Bracewell, Mechanical characterisation of agarose-based chromatography resins for biopharmaceutical manufacture, J Chromatogr A, 1530 (2017) 129-137.

[30] A. Zochling, R. Hahn, K. Ahrer, J. Urthaler, A. Jungbauer, Mass transfer characteristics of plasmids in monoliths, J Sep Sci, 27 (2004) 819-827.

[31] R.F. Benenati, C.B. Brosilow, Void Fraction Distribution in Beds of Spheres, Aiche Journal, 8 (1962) 359-361.

[32] G. Carta, E.X. Perez-Almodovar, Productivity Considerations and Design Charts for Biomolecule Capture with Periodic Countercurrent Adsorption Systems, Separation Science and Technology, 45 (2010) 149-154.

[33] T.E. Bankston, M.C. Stone, G. Carta, Theory and applications of refractive index-based optical microscopy to measure protein mass transfer in spherical adsorbent particles, J Chromatogr A, 1188 (2008) 242-254.

Chapter 5 – Conclusions and Future Challenges

This work demonstrated that continuous processing of biologics can be effectively implemented with the aid of an oscillatory flow reactor (OFR), with two distinct unit operations successfully carried out in the OFR, namely continuous aqueous two-phase extraction (ATPE) and continuous precipitation.

ATPE performed in an OFR was shown to be a viable technique for the initial purification of biological products, exemplified by partition the of commercial enzyme, α-amylase. Indeed, a recovery of over 94% and a partition coefficient of 4.7 were obtained, representing an considerable improvement from the results obtained in batch (85% and 1.6, respectively), and suggesting that the flow regime inside the OFR increases the performance of the ATPE. It was also proved that a full continuous ATPE (extraction and separation of the phases) can be performed in this type of reactor, as well as the clarification of the α-amylase from a cell broth of *S. cerevisiae*. However, when the collection of the top phase was done using just valve, that seemed to disturb somehow the system of two phases, leading to a higher partition of the protein to the top phase. This problem should be solved in the future by using a pump to control the flow and the pressure of extraction. In the case of the clarification from the cell broth, the partition of the enzyme was not significantly affected by the presence of the cells and, once more, the flow regime inside the OFR was able to increase the performance of the ATPE comparing with the batch assay.

This continuous ATPE using OFR sets the foundations that can contribute to the implementation of this process in the downstream processing of, for example, food enzyme from a cell broth as capture step, although further research is still needed, particularly to build a continuous downstream bioprocessing, beginning right after the cell broth containing the product of interest and using continuous operations after the OFR, as membrane processes.

OFR was also proven as a viable technique for the initial purification of human antibodies, exemplified by the purification of IgG from an artificial IgG and FBS mixture, enabling to recover over 99% of antibodies with 90% purity. The combination of different precipitants, namely PEG/NaCl and PEG/$ZnCl_2$, was successfully evaluated in batch under different pH, with

precipitation proven to be the most efficient when performed with 14% (w/v) PEG6000 and 4 mM $ZnCl_2$ at pH 7. Transferring precipitation to continuous operation mode was demonstrated in an OFR with the sequential addition of $ZnCl_2$ and PEG. The influence of the operating variables of the reactor, namely the total flow rate, the frequency and the amplitude of oscillations were studied and optimized through DoE construction with regards to yield and purity. Higher yields were obtained under high turbulence (high flow rate, high frequency and medium amplitude), contrarily to purity, suggesting that high turbulence may lead to a partial loss of selectivity.

Circular dichroism spectroscopy did not reveal any changes in the secondary structure of antibodies after precipitation, centrifugation and resolubilization. Unlike resolubilization of the precipitate using a low-pH buffer which proved to be an efficient approach, recovery of the precipitate by centrifugation after continuous precipitation caused a partial loss of IgG due to the visible detachment of the precipitate when removing the supernatant.

The process herein described showed results comparable to the continuous precipitation studies in the literature using tubular reactors, with the advantage of the OFR operation allowing higher yields. Besides, additional units can be added in series to increase its volume capacity, making OFR promising to integrate precipitation into a large-scale purification sequence.

As in the case of continuous ATPE, the continuous precipitation using OFR sets foundations that can contribute to the implementation of this process in downstream processing of therapeutic antibodies as a single capture step. In the future, other complex feedstocks must be used, namely cell culture supernatants and animal serum, since real feedstocks have a lower initial IgG purity (typically around 30%) than the artificial feed tested (50% purity).

As future work, it would be interesting to combine these two processes, in two different OFRs: a fully continuous ATPE for a clarification of the bioproduct (for example, an antibody), followed by a continuous precipitation for the further purification of the molecule. This would be possible, since the top phase would not only contain the product of interest but also the PEG, only requiring the addition of the $ZnCl_2$. After continuous precipitation, the collection and washing of the precipitate could be further achived through single-pass tangential flow filtration.

Lastly, the purification of a non-conventional immunoglobulin, secretory immunoglobulin A (sIgA), from CHO cell culture supernatant, was attempted by immuno-affinity chromatography. Severe mass transfer limitation were observed during the affinity chromatography of sIgA, which resulted in very low resin utilization and volumetric productivity. It was assumed that the average pore diameter of the agarose-based affinity resins is very close to the hydrodynamic diameter of the sIgA protein. Dynamic light scattering of the protein and inverse size exclusion of the resin confirmed that the average pore diameter was approximately twice the hydrodynamic diameter of sIgA. The resin utilization and productivity were compared to a typical protein A process for IgG and propose a resin architecture that would be more suitable for capture of sIgA. A macroporous backbone as alternative could improve process efficiency and productivity. Simulating the capture step of two macroporous resins showed a potential 7-fold increase of volumetric productivity with unhindered diffusion.

The determination of some physical properties of sIgA allows to hypothesize possible next chromatography processes for a further purification of this molecule: i) the difference of molecular weights between sIgA and the impurities present suggest a size exclusion chromatography (SEC); ii) the calculated isoelectric point of sIgA (5.5) indicates that a cation exchange chromatography could be an excellent next purification step, since the pH of the eluate from the affinity chromatography is lower than the pI of this protein.